PREPARATION AND CHARACTERIZATION OF MULTI-LAYER BIODEGRADABLE NANOFIBERS BY COAXIAL ELECTROSPINNING AND THEIR POTENTIAL FOR TISSUE ENGINEERING

by

Wenwen Liu

A dissertation submitted to the Faculty of the University of Delaware in partial fulfillment of the requirements for the degree of Doctor of Philosophy in Materials Science and Engineering

Fall 2015

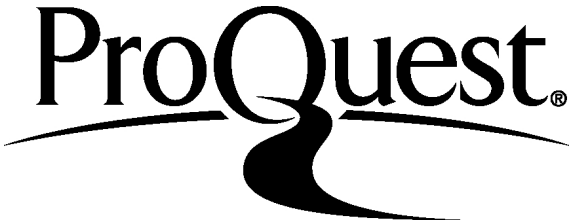

PREPARATION AND CHARACTERIZATION OF MULTI-LAYER BIODEGRADABLE NANOFIBERS BY COAXIAL ELECTROSPINNING AND THEIR POTENTIAL FOR TISSUE ENGINEERING

by

Wenwen Liu

Approved: _____
Darrin Pochan, Ph.D.
Chair of Department of Materials Science and Engineering

Approved: _____
Babatunde A. Ogunnaike, Ph.D.
Dean of the College of Engineering

Approved: _____
Ann L. Ardis, Ph.D.
Interim Vice Provost for Graduate and Professional Education

I certify that I have read this dissertation and that in my opinion it meets the academic and professional standard required by the University as a dissertation for the degree of Doctor of Philosophy.

Signed: _____

John F. Rabolt, Ph.D.
Professor in charge of dissertation

I certify that I have read this dissertation and that in my opinion it meets the academic and professional standard required by the University as a dissertation for the degree of Doctor of Philosophy.

Signed: _____

D. Bruce Chase, Ph.D.
Member of dissertation committee

I certify that I have read this dissertation and that in my opinion it meets the academic and professional standard required by the University as a dissertation for the degree of Doctor of Philosophy.

Signed: _____

Xinqiao Jia, Ph.D.
Member of dissertation committee

I certify that I have read this dissertation and that in my opinion it meets the academic and professional standard required by the University as a dissertation for the degree of Doctor of Philosophy.

Signed: _____

Joseph Deitzel, Ph.D.
Member of dissertation committee

ACKNOWLEDGMENTS

I would like to start by sincerely thanking my advisor, Dr. John F. Rabolt and co-advisor Dr. D. Bruce Chase, for their constant inspiration, encouragement, guidance and support during my graduate study. I learn and benefit a lot not only from their knowledge but also their personalities. I also want to express my thanks to the National Science Foundation under DMR (Polymers), and Delaware EPSCoR for their financial support.

I would like to thank my committee member, Dr. Xinqiao Jia, who gave me the opportunity to work with her group. The cooperation and discussion have been of great value in this study. I would also like to thank my committee member Dr. Joseph Deitzel, for his time, valuable discussion and suggestion to this research study.

In addition, I would like to thank Dr. Chaoying Ni, Dr. Fei Deng and Mr. Frank Kriss for their help and assistance with TEM and FIB-SEM. I would like to thank Dr. Jeffrey Caplan for his help with the super resolution microscopy measurements. I am thankful to Dr. Zhixiang Tong, Dr. Xian Xu, and Dr. Tugba Ozdemir for their help, discussion and cooperation. I also want to thank the members of the Rabolt research group, Dr. Carl Giller, Dr. Xiaoqian Ma, Dr. Wenqiong Tang and Liang Gong, for the help, support and friendship in the past years. Many thanks to the department of Materials Science and Engineering for providing exciting study and research environment.

Finally, I wish to express my gratitude to my family, my parents and younger brother, for the love and encouragement throughout my life. I am blessed to have family like them and their stained love will support me to pursue the dream in the future.

TABLE OF CONTENTS

LIST OF TABLES

LIST OF FIGURES

ABSTRACT

As an evolution of conventional electrospinning, coaxial electrospinning became popular soon after its debut as a novel way to develop nanofibers with special structures, such as core-shell and hollow interior. In recent years, there has been an increasing interest in a modified coaxial electrospinning, tri-layer coaxial electrospinning, to develop more complex structures, such as multi-layer and nanowire-in-microtube. Previous studies have primarily concentrated on the fabrication of tri-layered inorganic fibers while studies on tri-layered coaxial polymeric fibers has not been reported until very recently. Our research focuses on the fabrication of core-shell and tri-layer structured biodegradable polymeric nanofibers with coaxial electrospinning. Different characterization methods have been applied to observe the internal structure in single nanofibers and the potential application of tri-layer coaxial electrospinning has been discussed.

The material system consists of biodegradable natural polymer gelatin, synthetic polymers poly (ε-caprolactone) (PCL) and poly (lactic-co-glycolic acid) (PLGA). A uniquely designed three-needle concentric spinneret is developed to perform tri-layer coaxial electrospinning. Different kinds of core-shell structured nanofibers, including gelatin/PCL, PCL/gelatin, gelatin/PLGA and PCL/PLGA, have been fabricated with a customized coaxial electrospinning apparatus. Two kinds of tri-layer coaxial nanofibers, two-component ABA structured gelatin/PCL/gelatin biodegradable nanofibers and tri-

recomponent ABC structured gelatin/PCL/PLGA biodegradable nanofibers, have been developed with the customized three needle coaxial electrospinning setup.

The core-shell and tri-layered structures of electrospun nanofibers have been characterized by several commonly used techniques, such as laser scanning confocal microscopy (LSCM) and transmission electron microscopy (TEM). Besides the conventional methods, other newer techniques, including focused ion beam-scanning electron microscopy (FIB-SEM), super-resolution structured illumination microscopy (SR-SIM) and nanoscale-infrared spectroscopy (nano-IR), have been explored to investigate the internal structure in singles fibers.

Additionally, the potential application of coaxial electrospinning in the fabrication of bioactive scaffolds for tissue engineering has been studied. Different kinds of coaxial nanofibers were fabricated and studied to determine the potential for BSA and growth factor release and some preliminary results were obtained.

Chapter 1

INTRODUCTION

1.1 Introduction of Electrospinning and Coaxial Electrospinning

1.1.1 Background of Electrospinning

The electrospinning process was first patented by JF Cooley and WJ Morton in 1900[1] and 1902[2, 3]. About ten years later, John Zeleny[4] described, for the first time, the behavior of fluid droplets at the end of metal capillaries. Then, during 1934-1944, Anton Formhals[5-7] tried to commercialize this technique and he described the process and apparatus of electrospinning in series of patents. From 1964 to 1969, Taylor[8, 9] developed a further fundamental understanding on the jet forming process during electrospinning. He described the formation of a cone (known as the Taylor cone) from the charged fluid droplet under the influence of an electric field. Despite a long history covering over 100 years, it has only been during the last twenty years that electrospinning gained tremendous attention due to an increasing demand for nanomaterials and developing nanotechnologies. In the early 1990s, Reneker[10, 11] re-energized the field of electrospinning and demonstrated that many organic polymers could be electrospun into nanofibers. Since then, thousands of papers on the fundamentals and applications of electrospinning have been published. Currently, electrospinning is being used industrially as a simple and scalable technique to produce continuous fibers with diameters ranging from tens of nanometers to micrometers.

Fig. 1.1 shows a typical electrospinning setup. The system consists of four components: 1) a pair of power supplies with positive or negative polarity, 2) a syringe with needle through which the solution is forced, 3) a syringe pump to control the flow rate of the solution and 4) a collector for the deposition of fibers. A positive electrode is connected with the needle and a negative or grounded electrode is connected with the collector. In the electrospinning process, the solution forms a hemispherical droplet at the tip of the needle. Under an electric field, the droplet is charged and deforms into a suspended conical shape (called Taylor cone[8]) as a result of the balance between electrical repulsive forces due to the accumulated surface charges and surface tension of the liquid droplet. When the repulsive force overcomes the surface tension, an electrically charged jet is emitted from the apex of the Taylor cone and accelerated toward the collector. During the propagation to the collector, the fiber jet experiences a chaotic bending instability, whipping motion, solvent evaporation, and finally deposition on the collector as dry fibers with diameters ranging from tens of nanometers to tens of microns[12].

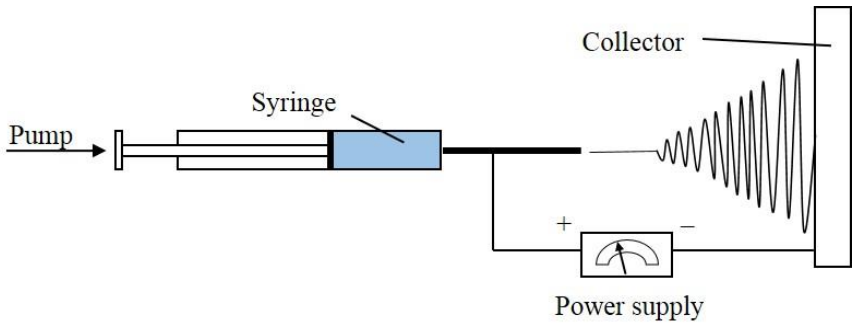

Figure 1.1 Schematic diagram of electrospinning setup

Electrospinning has been applied to process many varieties of materials into nanofibers, including natural polymers, synthetic polymers, synthetic biodegradable polymers and ceramic precursors. Since electrospun nanofibers have a high surface-to-volume ratio, tunable porosity, tailored composition and properties, they have been applied in a wide range of fields, such as filtration[13], catalysis[14], sensors[15], and especially in the biomedical area[16].

1.1.2 Introduction of Coaxial Electrospinning

As an evolution of conventional electrospinning, coaxial electrospinning became popular soon after its debut as a novel way to develop nanofibers with core-shell or hollow structures[17, 18]. The coaxial electrospinning setup is similar to an ordinary electrospinning system except that two concentric needles form the spinneret (Fig. 1.2). The outer needle is connected to a syringe containing the shell or sheath solution and the inner needle is attached to a syringe containing the core solution. The flow rates of the two different solutions are controlled by two syringe pumps independently. The delivered solutions converge at the tip of the concentric spinneret and form a core-shell droplet.

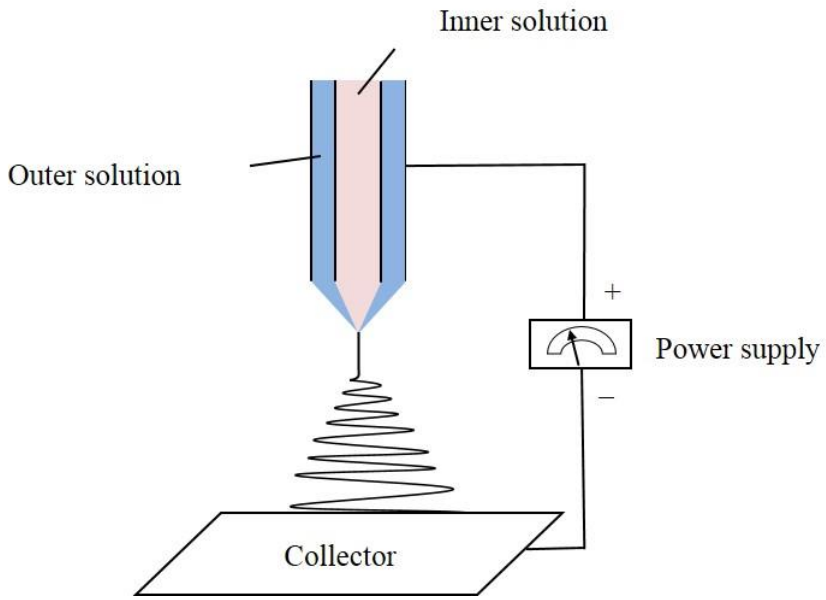

Figure 1.2 Schematic diagram of coaxial electrospinning setup

The formation of a stable core-shell compound Taylor cone at the nozzle tip is necessary for a successful coaxial electrospinning process. Figure 1.3 is the schematic illustration of how a compound Taylor cone forms in coaxial electrospinning[19]. Under the influence of the electric field, the charges accumulate on the surface of the sheath solution, and then the sheath solution will be elongated and stretched into a cone due to the surface repulsive force. If the shell solution is sufficiently viscous and the viscous stress overcomes the interfacial tension between the two solutions, the core solution is also stretched into a cone and a compound Taylor cone is formed. Figure 1.4 shows a stable, compound Taylor cone in which the core solution is well wrapped by the shell solution. With a strong electric field, a coaxial jet emerges from the compound Taylor cone and undergoes similar

stretching and bending instability as in ordinary electrospinning. After solvent evaporation on the path toward the collector, the coaxial jet solidifies and deposits on the collector as dry fibers with a core-shell structure.

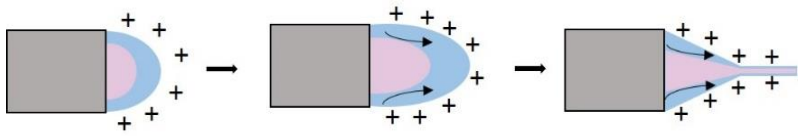

Figure 1.3 Schematic illustration of compound Taylor cone formation

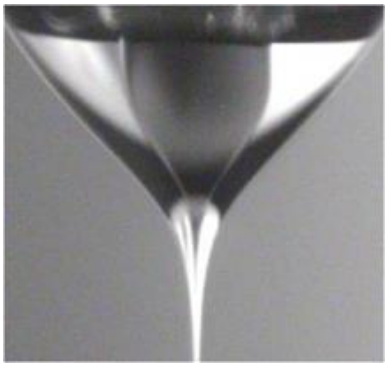

Figure 1.4 Photograph of a stable compound Taylor cone

Coaxial electrospinning has been utilized to fabricate various complex structures. A core-sheath structure was the most common structure that coaxial electrospinning could develop and it was first reported by Sun et al.[17] in 2003. To fabricate

hollow nanofibers or nanotubes, a core-sheath configuration was obtained using an inorganic precursor and polymer as the shell phase and mineral oil as the core phase. After that, post-treatment, such as extraction of mineral oil and annealing, was performed to create a hollow structure[20]. Coaxial electrospinning has also been utilized to fabricate nanofibers with nanoparticles incorporated[21-23] and fibers with unique periodic structures[24]. In addition, coaxial electrospinning has been used to fabricate fibers from nonelectrospinnable materials by incorporating these materials into the shell and then removing the shell with proper solvents[17, 25]. Additionally, by combining different materials, coaxial electrospinning could allow one to tailor the mechanical and surface properties[26, 27] to be different from those of the pure polymer fibers. The ability to fabricate specific structures and tailor composition and properties makes coaxial electrospinning a promising technique in many areas, including energy storage[28] and tissue engineering[29].

1.1.3 Introduction of Tri-layer Coaxial Electrospinning

A modified coaxial electrospinning setup using a spinneret with three concentric needles is illustrated schematically in Figure1.5. Three different solutions are delivered independently into the three needles in the concentric spinneret with flow rates controlled by three different syringe pumps. The solutions converge at the tip of the spinneret and form a coaxial droplet. Under a strong electrostatic field, the droplet deforms into a Taylor cone. The formation of a stable compound Taylor cone with tri-layer structure is similar to the description in Figure 1.3. A tri-layer concentric jet is pulled out of the apex of the compound Taylor cone when the electrostatic force overcomes the surface tension of the shell solution. The solvents gradually evaporate from the jet before reaching

the collector and finally multi-layer structured fibers are collected as a nonwoven mat. Generally, this advanced electrospinning technique was described as "triaxial electrospinning"[30-32] or "triple coaxial electrospinning"[33]. However, based on our understanding, this electrospinning technique is based on coaxial electrospinning with a three needle concentric configuration. Since it is a modification of coaxial electrospinning, we describe this process as coaxial electrospinning or tri-layer coaxial electrospinning.

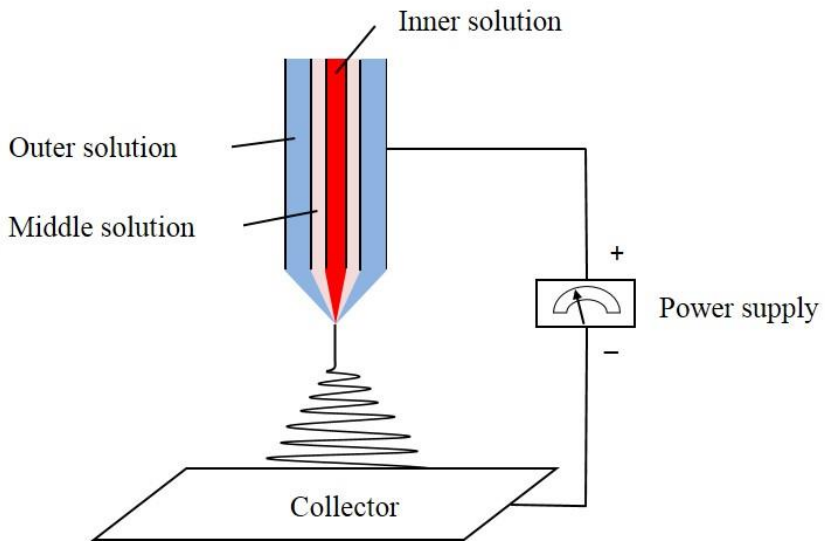

Figure 1.5 Schematic diagram of tri-layer coaxial electrospinning setup

This modified coaxial electrospinning was first reported[34] in 2007 in which the outer needle was used to deliver solvent rather than polymer solution. By using a sheath flow of ethanol to avoid solidification of the Taylor cone, Lallave et al.[34] obtained the smooth lignin hollow nanofibers. Although some studies on tri-layer coaxial

electrospinning have been performed in recent years, in most of the reported studies, the addition of a third channel was employed to assist the formation of core/shell or hollow structures. Chen et al.[35] developed nanowire-in-microtube structured nanofibers by using inner most and outer most needles to deliver a targeted solution, with the middle needle delivering mineral oil. The oil was then removed from the middle layer of the fiber. With mineral oil as the inner solution, Chen et al.[36] prepared amorphous carbon nanotubes with hollow graphitic carbon nanospheres for high-performance Li ion batteries. Joo et al.[37] first reported the fabrication of tri-layered coaxial solid fibers with silica as the shell and core layers and a self-assembling polymeric material as the intermediate layer. Although tri-layer coaxial electrospinning has received much attention as a novel electrospinning technique, most studies focus on the fabrication of multi-layer inorganic fibers and research on tri-layered coaxial polymeric fibers has not been published until very recently. Jiang et al. published their study on fabrication of highly tough, flexible, and strong polystyrene (PS) fibers using tri-layer coaxial electrospinning with elastomeric thermoplastic polyurethane (TPU) as the middle layer to reinforce and toughen the brittle PS.[31] The stress-strain curves for different kinds of single fibers (PS, TPU-PS, PS-TPU-PS) showed that the PS-TPU-PS structured fiber has highest toughness and largest strain at break. The great advantage offered by a tri-layer concentric structure in comparison to the bi-layer coaxial structure came from a better interface with the sandwich structure. In addition, the study of potential applications of tri-layer coaxial electrospinning in tissue engineering has been initiated recently by D. Han et al.[30] A novel dual drug delivery system was fabricated by loading two model drugs into different layers of PCL (polycaprolactone) /PCL/PVP

(polyvinylpyrrolidone) coaxial electrospun nanofibers. Both burst release of molecules from the sheath and controlled release of molecules from the core were observed. It was also claimed that tri-layer coaxial structured nanofibers offered a degree of freedom in the selection of the polymers and drug molecules.

1.2 Important Parameters in Coaxial Electrospinning

There are two kinds of parameters which are important in electrospinning: solution parameters and processing parameters. Generally, the solution parameters include solution concentration and viscosity, conductivity, and solvent volatility. The processing parameters include applied voltage, flow rate of solution, working distance (capillary-collector distance), temperature and humidity. All these parameters play important roles in fiber formation, morphology and structure. Many efforts have contributed to the fundamental study of the electrospinning process and relationships between individual parameters and morphology of electrospun fibers[38-40]. As a modified electrospinning technique, coaxial electrospinning has similar jet forming and travel processes to conventional mono-axial electrospinning and thus depends on similar parameters as does ordinary electrospinning. However, the addition of the second and third solutions will introduce interfacial interactions between different solutions and this makes the electrospinning process more complicated. According to the review by Moghe and Gupta[19], there are some particular rules which one needs to consider in polymer and solvent selection processes to get acceptable coaxial electrospinning. A systematic solution selection model based on Hansen solubility parameters was proposed by Z. Kurban et al. to predict the properties of solvent mixtures[41]. With this model, it is possible to create

optimum solution sets for given core and shell materials. Besides the solution parameters, processing variables also dominate the morphology of nanofibers and formation of core-shell or hollow structures. A successful coaxial electrospinning process is the result of the correct balance between various solution parameters and processing parameters.

1.2.1 Solution Parameters

1.2.1.1 Solution Incompatibility

The addition of the second and third solutions introduces interfacial interactions between different solutions in coaxial electrospinning and thus the compatibility between solutions will be the first and foremost issue in polymer and solvent system selection. The solubility of polymers in different solvents needs to be considered so that the polymers in either of the solutions will not be precipitated by the solvent of the other solution when the solutions converge at the tip of the spinneret[19]. This is a critical issue in coaxial electrospinning of hydrophobic polymers (organic solvents preferred) and hydrophilic polymers or water soluble bioactive agents (polar organic solvents or water preferred). If solutions are incompatible with each other, there will be precipitation at the tip of the spinneret and little chance for a successful coaxial electrospinning process.

1.2.1.2 Solution Viscosities

Solution viscosity plays a crucial role in electrospinning since it controls the degree of chain entanglement and determines surface tension of the solution. The viscosity is mainly determined by solute type, molecular weight, and concentration. The optimal viscosity of solutions in electrospinning ranges from 800 to 4000 centipoise[10]. It would be

difficult to electrospin a solution with a viscosity out of this range because of the break-up of jet and formation of beads (below range) as well as large surface tension (over range). In coaxial electrospinning, the shell solution serves as a guide and drives the elongation of the core solution by viscous stress. The viscosity of the shell solution has to reach a certain value so that it could be electrospun by itself. This provides sufficient viscous stress on the core solution to maintain the coaxial structure. The requirements on the spinnability and viscosity of the core solution are less important since the jet break-up of the core could be prevented by the shell because of a lower surface force on the core than the shell and strain hardening of the interface between shell and core[25]. However, the core solution still requires some level of viscosity to make sure it is incorporated continuously without break-up.

1.2.1.3 Solvent Miscibility

As mentioned previously, in the formation of a stable compound Taylor cone and compound jet, the elongation of core solution happens when the viscous stress on the core solution overcomes the interfacial tension between the two solutions. If the interfacial tension between solutions is low, it would be easier to generate a stable compound Taylor cone. Poor miscibility between core/shell solutions (e.g. water and chloroform) requires higher field strengths to overcome the solution surface tension. Improving the solution miscibility (using binary solvents) not only reduces the necessary applied voltage but also improves the fiber size uniformity. Although many studies have been performed on the miscibility of different solutions in coaxial electrospinning, it is still difficult to quantify the effect of miscibility on the coaxial electrospinning process and the

opinions of researchers diverge on the issue of miscibility of core and shell solution[42]. Li et al. demonstrated that the evaporation and diffusion of the solvents could drive polymers to mix together if the two polymer solutions contain miscible solvents[42]. However, Sun et al.[17] claimed that the characteristic time of the diffusion spreading of a sharp boundary between two identical polymers is great compared to the fast stretching and solidification processes, so that a sharp boundary should survive in coaxial electrospinning. Additionally, Z. Kurban et al.[41] reported their study on the effect of solution miscibility on fiber morphology by coaxial electrospinning of miscible, semimiscible and immiscible solutions. They built a model based on the azimuthal capillary wave to analyze their experimental results and claimed that the more miscible the solutions, the more unstable the azimuthal capillary wave. Hence the core solution would penetrate into the shell to leave a regular pattern of porous inclusion. This claim is in contrast to many reported studies. For a better understanding of coaxial electrospinning, further study is needed on the effect of miscibility between different solutions.

1.2.1.4 Solvent Volatility

Solvent volatility is critical in determining the diameter, surface morphology and inner structure of electrospun nanofibers. In coaxial electrospinning, it would be beneficial to use solvents with similar volatility for shell and core solutions. Otherwise the difference in volatility between solvents will introduce extra difficulties for the formation of fibers with specific structures[43]. From the previous research, solvents with high volatility may not be used in the shell solution because high volatility leads to unstable Taylor cones and multiple jets due to fast evaporation. Also, in our experience, solvents

with high volatility in the shell solution could cause the development of a hard shell of the cone and result in clogging of the spinneret. The solvent vapor pressure for the core should not be higher than that for shell because evaporation of core solvent will create a thin layer at the interface between shell and core[42]. This layer would be a barrier and slow down the evaporation of interior solvent. A vacuum in the core is created when the fiber is completely dried and the core will collapse resulting in a transition from a round to ribbon shaped cross-section under atmospheric pressure. This process is similar to the formation of flat ribbon shaped fibers in conventional mono-axial electrospinning[44].

1.2.1.5 Solution Conductivities.

Solution conductivity plays an important role in the electrospinning process. It determines surface charge density as well as the repulsive force due to the surface charges. Generally, the conductivity could be controlled by the addition of ionic salts or by using a binary or ternary solvent system to get the required dielectric constant. In coaxial electrospinning, conductivity of the shell solution is more important than that of the core solution because elongation of the core is driven by elongation of the shell. It is claimed that higher shell solution conductivity would induce higher shear stress on the core and result in the formation of a thinner core, while higher core solution conductivity would result in a discontinuity in the core or separated core and shell fibers. In addition, non-conductive or less conductive solution has been successfully incorporated as the core into a higher conducting shell. However, coaxial electrospinning was performed successfully with nonspinable material as the shell and highly conducting material as the core and the driving force was induced by the charges collected on the interface between the core and

shell[41]. This result is not consistent with the conventional wisdom about the effects of solution conductivities and formation of a compound Taylor cone in coaxial electrospinning. Further studies are required on this issue.

1.2.2 Processing Parameters

1.2.2.1 Applied Voltage

In coaxial electrospinning, the required voltage lies in a small, specified range. Within this range, the system could tolerate a specific combination of polymers and solvents to generate a stable compound Taylor cone and uniform fibers. Outside of this range there could be some problems: poor jet formation and dripping of the solutions will happen if the applied voltage is below this range. If the applied voltage is above this range, the Taylor cone will recede, resulting in separate jets from the shell and core solutions.

1.2.2.2 Flow Rate Ratio

The core solution to shell solution flow rate ratio is an additional processing parameter in coaxial electrospinning. According to previous work, a flow rate ratio ranging between 1:3 and 1:6 is ideal for generating a stable compound Taylor cone and a consistent core-shell structure. At a high core-shell ratio value, there is insufficient shell solution to surround the core and the viscous drag induced by the shell solution is not high enough to confine the core solution resulting in fibers with an incomplete shell or mixture of shell and core. In contrast, at a low core-shell ratio value, the incorporated core may be discontinuous. However, from our study, the best flow rate ratio range also depends on other solution and solvent parameters, such as solvent miscibility and surface tension. For

example, if the solvents are miscible and the interfacial tension is low enough, a core-shell structure could be fabricated with a flow rate ratio of 1:1 or even lower.

1.2.2.3 Other Processing Parameters

A successful coaxial electrospinning process also depends on some other parameters, such as working distance and humidity. These parameters play similar roles with respect to the formation and morphology of fibers in coaxial electrospinning as well as in conventional electrospinning.

1.3 Application of Coaxial Electrospinning

As mentioned in 1.1.2 and1.1.3, coaxial electrospinning could be used to fabricate fibers with special structures, such as core-shell, hollow interior, unique periodic structures at the molecular level and multilayer structures, as well as incorporation of non-spinable material or bioactive agents into nanofibers. As a convenient and scalable way to develop nanofibers with special structure and properties, coaxial electrospinning holds great promise for unique applications in different fields, especially in the biomedical area[29, 43, 45], and for use in energy storage[28, 46, 47].

1.3.1 Tissue Engineering

Design of polymeric scaffolds with specific mechanical and biological properties to mimic the extracellular matrix (ECM) is one aspect of tissue engineering. An ideal scaffold should be porous, biocompatible, biodegradable, and exhibit suitable mechanical properties as well as possess the ability to deliver bioactive growth factors[48]. An electrospun nonwoven mat is an excellent candidate for a tissue engineering scaffold

considering its high surface area to volume ratio, its 3D interconnected porous network, and its versatility in modifying the mechanical and surface properties. Many kinds of polymers have been electrospun into nanofibers to mimic the ECM and support cell proliferation, including biodegradable synthetic polymers, such as poly(glycolic acid) (PGA)[49], poly(ε-caprolactone) (PCL)[50], and natural polymers, such as collagen[51], chitosan[52] and silk[53]. Due to the flexibility in selecting materials and tuning properties, electrospinning has been widely studied in bone[54], cartilage[51], and nerve[55] tissue engineering.

Compared with mono-axial electrospinning, one of the great advantages of coaxial electrospinning is the ability to modify the surface properties (biocompatibility and hydrophilicity) of nanofibers and to encapsulate drugs or bioactive agents, such as growth factors, peptides and plasmid DNA, into the fiber core in one-step. Although mono-axial electrospinning of polymer/drug blends shows the ability to incorporate and release drugs or bioactive agents, the initial burst release and the loss of bioactivity due to harsh solvents are drawbacks that constrain the application of ordinary electrospinning to bioactive tissue substrates. With encapsulation of bioactive agents in the core, coaxial electrospinning overcomes these limitations by preventing the contact between bioactive agents and harsh solvents, mitigating the initial burst release and providing sustained release. A variety of studies have been reported with regard to using coaxial electrospun nanofibers as a scaffold for release control, including therapeutic agents[56, 57] (antibiotics, anticancer drugs) and bioactive agents (proteins, DNA)[55, 58]. Most of the current studies on delivery systems developed with coaxial electrospinning focus on core-shell structured nanofibers. Recently,

a novel dual drug delivery system with tri-layer structured nanofibers has been reported by D. Han et al., in which two model drugs were loaded into different layers of tri-layer structured coaxial nanofibers. Compared with core-shell structured nanofibers, the tri-layer structured nanofibers provide greater possibility and flexibility for dual or triple drug loading and controlled release.

1.3.2 Other Applications

Besides tissue engineering, coaxial electrospinning has attracted much interest for its potential in other fields, including luminescence, photocatalysis, solar cell formation, lithium ion batteries and microelectronics. Below are highlighted some potential applications in the energy field.

1.3.2.1 Light Emitting

Fiber-based electroluminescent devices, such as organic light-emitting devices, have been widely studied for their high efficiency, mechanical flexibility and low costs. In order to fabricate multiple layers of conductors, semiconductors and insulators in a single fiber, various techniques, including template-assisted synthesis and dip-pen nanolithography, have been employed. However, the efficiency and throughput of these fabrication techniques are lower than required for the application. As a simple and scalable technique for nanofiber fabrication, electrospinning has already been applied to develop photoluminescent nanofibers of conjugated polymers and copolymers at a relatively large scale. Recently, coaxial electrospinning has shown potential application in this area due to its ability to develop core-shell structures and other complex structures. Yang et al.[59] has

designed a novel electro-luminescent fiber with three coaxial layers in a single fiber, in which a conductive liquid metal, Galinstan, served as the inner core, an organic electroluminescent material served as the middle layer and a high conductive and transparent indium-thin oxide (ITO) served as the outmost layer. This design was achieved by coaxial electrospinning to encapsulate the liquid core into the polymer shell and then coating an ITO layer on the shell. This novel electroluminescent fiber fabrication technique is very interesting for many research areas, including optoelectronic textiles, bioimaging and flexible panel displays. In addition, similar design and fabrication procedures have been reported in many studies with different materials for various applications.

1.3.2.2 Energy Storage Devices

Among the various energy storage devices, lithium ion batteries are the most popular research topic due to the high gravimetric specific energy, long duration, and wide operational temperature range. Coaxial electrospinning has exhibited significant potential in fabrication of novel high-performance anodes[47], cathodes, and separators for lithium-ion batteries. The study of anodes mainly focused on hollow structured carbon nanofibers because it could buffer the volume expansion during the lithiation process and core-shell structured silicon/carbon nanofibers for high lithium-storage capacity due to superior capacity of silicon itself. In addition, coaxial electrospun hollow TiO_2 nanofibers are another option for anodes in lithium ion batteries with their high capacity and stability[60]. Similar to anodes, coaxial electrospinning could also be used to develop high-performance cathodes. Core-shell structured $LiCoO_2$-MgO nanofibers showed excellent reversibility and preferable electrochemical properties with an obvious improvement of cycling

compared to bare $LiCoO_2$ fiber cathodes[61]. The application of coaxial nanofibers in separators is very promising due to their tunable mechanical strength, high thermal stability and preferable rate capability[62]. Other than serving as electrodes for lithium ion batteries, coaxial electrospun nanofibers have other applications in energy fields such as hydrogen storage devices. Kurban et al.[41] developed coaxial electrospun AB-PS nanofibers with different porous structures by using polystyrene (PS) as a protective sheath and hydride ammonia borane (AB) as the incorporated core. The dehydrogenation properties of various AB-PS nanofibers was investigated to evaluate the performance of AB-PS fibers as a potential hydrogen storage device. This study has demonstrated that coaxial electrospinning could be utilized as a scalable, one-step production process for a lightweight nanostructured hydrogen storage device by incorporating hydride that can be dissolved or suspended in compatible solvents.

1.4 Research Motivation and Objectives

As mentioned above, although coaxial electrospinning of tri-layer structured nanofibers has received much attention, most studies focus on the fabrication of tri-layer inorganic fibers. There are few studies on developing tri-layer structured polymeric fibers by coaxial electrospinning. One of our motivations to study coaxial electrospinning is to fabricate a tri-component, tri-layer structured biodegradable polymeric nanofiber. In addition, coaxial electrospinning expands the application of electrospinning in the biotechnology area by fabricating fibers with a core-shell structure. Many studies have been performed on the preparation of core-sheath biodegradable nanofibers with applications in tissue engineering and drug delivery. Among these studies,

three main objectives have been summarized as follows : 1) increasing the mechanical properties of fibers by using a stronger core; 2) incorporating drugs or bioactive agents into the sheath for controlled release; and, 3) increasing the biocompatibility of fibers by using a more natural polymer as the sheath. Most coaxial electrospun fibers could satisfy one or two of the issues mentioned, however, it is difficult to realize all three objectives with a two-layer structure. Thus another motivation is to fabricate tri-layer structured biodegradable nanofibers and study their potential applications in the biomedical area.

To approach these goals, we fabricated core-shell structured nanofibers with biodegradable polymers and characterized their core-shell structure in a single nanofiber. Then, fabrication of a bi-component tri-layer structured nanofibers with biodegradable polymers through coaxial electrospinning was performed. Finally, we fabricated a tri-component, tri-layer structured nanofiber with biodegradable polymers and characterized the tri-layer structure in a single nanofiber. As an example, a controlled BSA release using a coaxial electrospun nanofibrous scaffold was developed for tissue engineering applications.

1.5 Dissertation Overview

This dissertation is divided into seven chapters. Chapter 1 introduces the background, motivation and research design of this study. Chapter 2 discusses the coaxial electrospinning setup and various characterization methods. Chapters 3 to 6 are the major body of this dissertation and each one consists of an introduction, an experimental section, results and conclusions. Chapter 3 describes the fabrication of different kinds of PCL/gelatin nanofibers with coaxial electrospinning and how to prove the existence of

core-shell and the tri-layered structure in a single nanofiber. Chapter 4 describes the fabrication of a different kind of PCL/PLGA/gelatin nanofibers with coaxial electrospinning and also the characterization of core-shell and tri-layered structure in single nanofiber. Chapter 5 discusses a new IR technique-Nano IR and the application of Nano IR in characterization of coaxial electrospun nanofibers. Chapter 6 discusses potential applications of coaxial electrospinning on tissue engineering. Finally, chapter 7 summarizes the work in this dissertation and discusses future work.

REFERENCES

1. Cooley, J. F. Improved methods of and apparatus for electrically separating the relatively volatile liquid component from the component of relatively fixed substances of composite fluids. GB 06385, May 19, 1900.
2. Morton, W. J. Method of dispersing fluids. 0705691, July 19, 1902.
3. Cooley, J. F. Apparatus for electrically dispersing fluids. 692631, February 4, 1902.
4. Zeleny, J. *Physical Review* **1914,** 3, (2), 69.
5. Formhals, A. Process and apparatus for preparing artificial threads. 1975504, October 2, 1934.
6. Formhals, A. Method and apparatus for spinning. 2160962, Jun 6, 1939.
7. Formhals, A. Method and apparatus for spinning. 2349950, May 30, 1944.
8. Taylor, G. I. *Proceedings of the Royal Society of London* **1964,** 280, 383-397.
9. Taylor, G. I. *Proceedings of the Royal Society A* **1969,** 313, (1515), 453.
10. Doshi, J.; Reneker, D. H. *Journal of Electrostatics* **1995,** 35, (2-3), 151-160.
11. Reneker, D. H.; Chun, I. *Nanotechnology* **1996,** 7, (3), 216-223.
12. Greiner, A.; Wendorff, J. H. *Angewandte Chemie-International Edition* **2007,** 46, (30), 5670-5703.
13. Qin, X. H.; Wang, S. Y. *Journal of Applied Polymer Science* **2006,** 102, (2), 1285-1290.
14. Roben, C.; Stasiak, M.; Janza, B.; Greiner, A.; Wendorff, J. H.; Studer, A. *Synthesis-Stuttgart* **2008**, (14), 2163-2168.

15. Landau, O.; Rothschild, A.; Zussman, E. *Chemistry of Materials* **2009,** 21, (1), 9-11.

16. Pham, Q. P.; Sharma, U.; Mikos, A. G. *Tissue Engineering* **2006,** 12, (5), 1197-1211.

17. Sun, Z. C.; Zussman, E.; Yarin, A. L.; Wendorff, J. H.; Greiner, A. *Advanced Materials* **2003,** 15, (22), 1929-1932.

18. Yarin, A. L. *Polymers for Advanced Technologies* **2011,** 22, (3), 310-317.

19. Moghe, A. K.; Gupta, B. S. *Polymer Reviews* **2008,** 48, (2), 353-377.

20. Li, D.; Xia, Y. N. *Nano Letters* **2004,** 4, (5), 933-938.

21. Graeser, M.; Pippel, E.; Greiner, A.; Wendorff, J. H. *Macromolecules* **2007,** 40, (17), 6032-6039.

22. Song, T.; Zhang, Y. Z.; Zhou, T. J.; Lim, C. T.; Ramakrishna, S.; Liu, B. *Chemical Physics Letters* **2005,** 415, (4-6), 317-322.

23. Zhang, Y. Z.; Ouyang, H. W.; Lim, C. T.; Ramakrishna, S.; Huang, Z. M. *Journal of Biomedical Materials Research Part B-Applied Biomaterials* **2005,** 72B, (1), 156-165.

24. Ma, M. L.; Krikorian, V.; Yu, J. H.; Thomas, E. L.; Rutledge, G. C. *Nano Letters* **2006,** 6, (12), 2969-2972.

25. Yu, J. H.; Fridrikh, S. V.; Rutledge, G. C. *Advanced Materials* **2004,** 16, (17), 1562-1566.

26. Huang, Z. M.; Zhang, Y. Z.; Ramakrishna, S. *Journal of Polymer Science Part B-Polymer Physics* **2005,** 43, (20), 2852-2861.

27. Han, D. W.; Steckl, A. J. *Langmuir* **2009,** 25, (16), 9454-9462.

28. Qu, H. L.; Wei, S. Y.; Guo, Z. H. *Journal of Materials Chemistry A* **2013,** 1, (38), 11513-11528.

29. Zhang, H.; Zhao, C. G.; Zhao, Y. H.; Tang, G. W.; Yuan, X. Y. *Science China-Chemistry* **2010,** 53, (6), 1246-1254.

30. Han, D.; Steckl, A. J. *ACS Applied Materials & Interfaces* **2013,** 5, (16), 8241-8245.

31. Jiang, S. H.; Duan, G. G.; Zussman, E.; Greiner, A.; Agarwal, S. *ACS Applied Materials & Interfaces* **2014,** 6, (8), 5918-5923.

32. Liu, W.; Ni, C. Y.; Chase, D. B.; Rabolt, J. F. *ACS Macro Letters* **2013,** 2, (6), 466-468.

33. Chen, Y. M.; Lu, Z. G.; Zhou, L. M.; Mai, Y. W.; Huang, H. T. *Energy & Environmental Science* **2012,** 5, (7), 7898-7902.

34. Lallave, M.; Bedia, J.; Ruiz-Rosas, R.; Rodriguez-Mirasol, J.; Cordero, T.; Otero, J. C.; Marquez, M.; Barrero, A.; Loscertales, I. G. *Advanced Materials* **2007,** 19, (23), 4292-4296.

35. Chen, H. Y.; Wang, N.; Di, J. C.; Zhao, Y.; Song, Y. L.; Jiang, L. *Langmuir* **2010,** 26, (13), 11291-11296.

36. Chen, Y.; Lu, Z.; Zhou, L.; Mai, Y.-W.; Huang, H. *Energy & Environmental Science* **2012,** 5, (7), 7898-7902.

37. Kalra, V.; Lee, J. H.; Park, J. H.; Marquez, M.; Joo, Y. L. *Small* **2009,** 5, (20), 2323-2332.

38. Deitzel, J. M.; Kleinmeyer, J.; Harris, D.; Tan, N. C. B. *Polymer* **2001,** 42, (1), 261-272.

39. Reneker, D. H.; Yarin, A. L. *Polymer* **2008,** 49, (10), 2387-2425.

40. Theron, S. A.; Zussman, E.; Yarin, A. L. *Polymer* **2004,** 45, (6), 2017-2030.

41. Kurban, Z.; Lovell, A.; Bennington, S. M.; Jenkins, D. W. K.; Ryan, K. R.; Jones, M. O.; Skipper, N. T.; David, W. I. F. *Journal of Physical Chemistry C* **2010,** 114, (49), 21201-21213.

42. Li, D.; Babel, A.; Jenekhe, S. A.; Xia, Y. N. *Advanced Materials* **2004,** 16, (22), 2062-2066.

43. Chakraborty, S.; Liao, I. C.; Adler, A.; Leong, K. W. *Advanced Drug Delivery Reviews* **2009,** 61, (12), 1043-1054.

44. Koombhongse, S.; Liu, W. X.; Reneker, D. H. *Journal of Polymer Science Part B-Polymer Physics* **2001,** 39, (21), 2598-2606.

45. Wang, C.; Yan, K. W.; Lin, Y. D.; Hsieh, P. C. H. *Macromolecules* **2010,** 43, (15), 6389-6397.

46. Yuan, T.; Zhao, B. T.; Cai, R.; Zhou, Y. K.; Shao, Z. P. *Journal of Materials Chemistry* **2011,** 21, (38), 15041-15048.

47. Raza, A.; Yu, J. Y.; Zhai, Y. Y.; Sun, G.; Ding, B., *Applications of Electrospinning in Design and Fabrication of Electrodes for Lithium-Ion Batteries*. Springer: New York, 2014; p 69-89.

48. Armentano, I.; Dottori, M.; Fortunati, E.; Mattioli, S.; Kenny, J. M. *Polymer Degradation and Stability* **2010,** 95, (11), 2126-2146.

49. Boland, E. D.; Wnek, G. E.; Simpson, D. G.; Pawlowski, K. J.; Bowlin, G. L. *Journal of Macromolecular Science-Pure and Applied Chemistry* **2001,** 38, (12), 1231-1243.

50. Cipitria, A.; Skelton, A.; Dargaville, T. R.; Dalton, P. D.; Hutmacher, D. W. *Journal of Materials Chemistry* **2011,** 21, (26), 9419-9453.

51. Matthews, J. A.; Boland, E. D.; Wnek, G. E.; Simpson, D. G.; Bowlin, G. L. *Journal of Bioactive and Compatible Polymers* **2003,** 18, (2), 125-134.

52. Ohkawa, K.; Cha, D. I.; Kim, H.; Nishida, A.; Yamamoto, H. *Macromolecular Rapid Communications* **2004,** 25, (18), 1600-1605.

53. Kim, S. H.; Nam, Y. S.; Lee, T. S.; Park, W. H. *Polymer Journal* **2003,** 35, (2), 185-190.

54. Ramachandran, K.; Gouma, P. I. *Recent Patents on Nanotechnology* **2008,** 2, (1), 1-7.

55. Su, Y.; Li, X.; Tan, L.; Huang, C.; Mo, X. *Polymer* **2009,** 50, (17), 4212-4219.

56. Mourino, V.; Boccaccini, A. R. *Journal of the Royal Society Interface* **2010,** 7, (43), 209-227.

57. Nie, H. R.; Li, J. X.; He, A. H.; Xu, S. S.; Jiang, Q. S.; Han, C. C. *Biomacromolecules* **2010,** 11, (8), 2190-2194.

58. Young, S.; Wong, M.; Tabata, Y.; Mikos, A. G. *Journal of Controlled Release* **2005,** 109, (1-3), 256-274.

59. Yang, H. F.; Lightner, C. R.; Dong, L. *ACS Nano* **2012,** 6, (1), 622-628.

60. Han, H.; Song, T.; Bae, J. Y.; Nazar, L. F.; Kim, H.; Paik, U. *Energy & Environmental Science* **2011,** 4, (11), 4532-4536.

61. Gu, Y. X.; Chen, D. R.; Jiao, X. L.; Liu, F. F. *Journal of Materials Chemistry* **2007,** 17, (18), 1769-1776.

62. Liu, Z. H.; Jiang, W.; Kong, Q. S.; Zhang, C. J.; Han, P. X.; Wang, X. J.; Yao, J. H.; Cui, G. L. *Macromolecular Materials and Engineering* **2013,** 298, (7), 806-813.

Chapter 2

EXPERIMENTAL METHODS AND CHARACTERIZATION TECHNIQUES

2.1 Coaxial Electrospinning Instrumentation

2.1.1 1st Generation of Coaxial Setup

The 1st generation coaxial nozzle (Figure 2.1a) was designed and fabricated in our laboratory using N_2 gas (Figure 2.1b) to control the flow of the solution. This design worked; however, there were some problems in the nozzle and experimental processing protocol that needed to be solved. Initially, copper was used for the first spinneret. In electrospinning, acid solvents are often used and the acid would corrode the copper and destroy the spinneret. In addition, there was concern that Cu^{2+} could contaminate the solution and have an effect on the electrospinning process. Secondly, it was very difficult to control the flow of multiple solutions accurately by controlling the N_2 gas pressure. In coaxial electrospinning, the flow rate of the core solution is relatively small (0.05-0.2 ml/h, depending on the material and desired fiber diameter), and using the N_2 gas to control flow at these low levels was difficult. Finally, the solution chamber of this setup was very large (5 cm^3) so that a large quantity of solution was needed and most of solution (around 80%) was actually wasted. Hence this was not a very efficient coaxial setup.

Figure 2.1 Photograph of 1st generation coaxial setup. a: 1st coaxial electrospinning nozzle; **b**: solution flow control device

2.1.2 2nd Generation of Coaxial Setup

The 2nd generation was an improvement, and, as shown in Figure 2.2a, stainless steel served as the main body of this nozzle rather than copper so that this setup was resistant to most corrosive solvents. Instead of connecting to N_2 gas to control the flow of solution, the needles were connected to different syringes with small diameter tubing. Finally, syringe pumps (Figure 2.2b) were used to control the flow of the solution in each syringe. Unfortunately, one of the problems encountered with this 2nd generation coaxial setup was that the solution reservoir was still large and a lot of solution was required for one experiment. In addition, the concentricity of the three needles was still difficult to control due to their small diameters and the length of the individual needles.

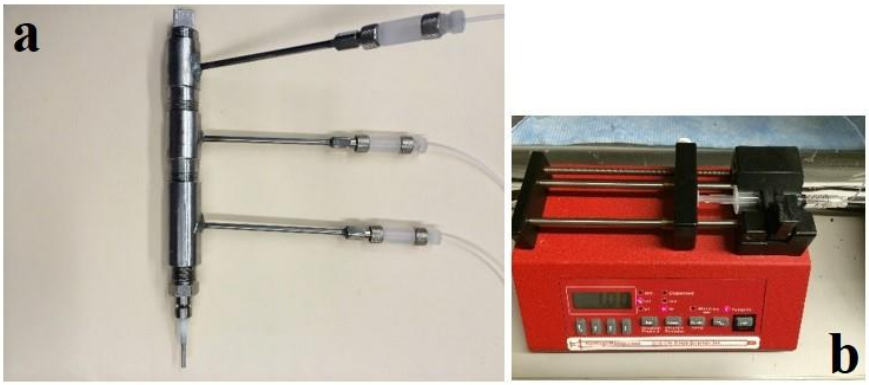

Figure 2.2 Photograph of 2nd generation coaxial setup. a: 2nd coaxial electrospinning nozzle; **b**: solution flow control device

2.1.3 3rd Generation of Coaxial Setup

The 3rd generation (Figure 2.3a) was a customized product from Rame-Hart Instrument Company. The flow of solution was controlled by pumps (Figure 2.3b) in the same fashion as the second generation setup. However, as shown in Figure 2.3a, the spinneret is actually assembled from three needles directly and there is no large chamber, so that there was less spin solution wasted in the electrospinning process than that used in the first 2 generations. Meanwhile, this spinneret was much easier to assemble, disassemble and clean. The most significant improvement in this design was that the concentricity of the three needles within this nozzle was much improved due to the short length of the needles and their adjustability.

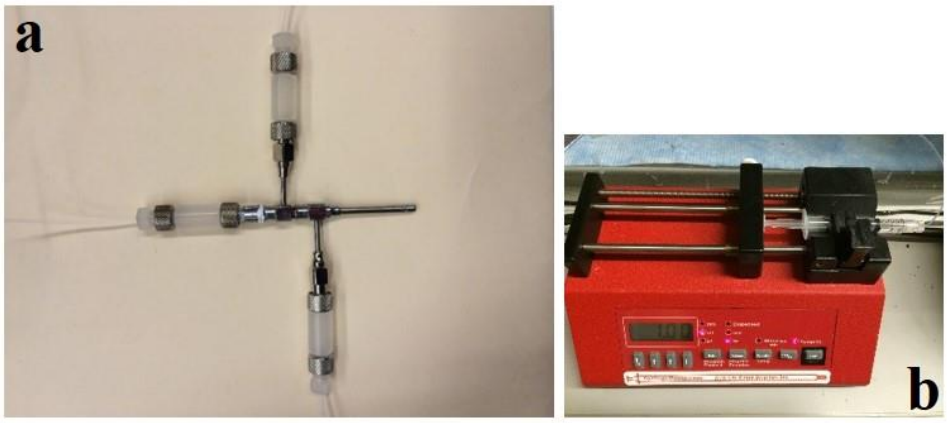

Figure 2.3 Photograph of 3rd generation coaxial setup. a: 3rd generation coaxial electrospinning nozzle; **b**: solution flow control device

In this most recent generation device, the spinneret could be placed parallel to the ground to allow horizontal electrospinning. However, due to gravity, the horizontal setup could have an effect on the distribution[1] of polymer in the core of the fibers. In our study, a vertical coaxial electrospinning configuration was utilized in which the needle was placed perpendicular to the benchtop and the collector was placed parallel to the benchtop (Fig 2.4).

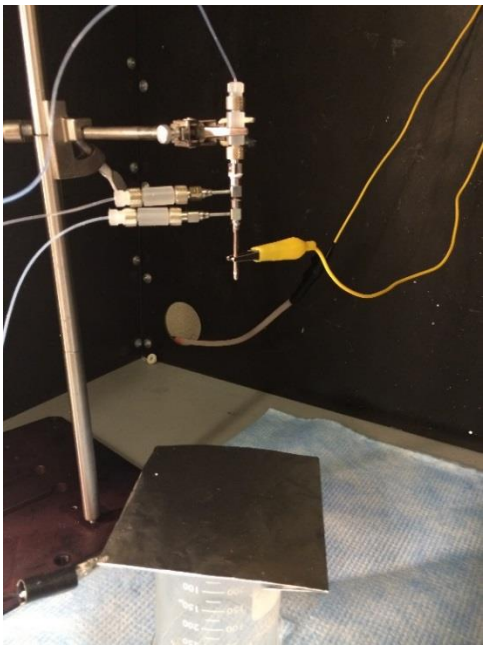

Figure 2.4 Vertical tri-layer, coaxial electrospinning configuration

2.1.4 Accessories

The temperature and humidity were recorded with a digital thermal and humidity gauge. To study Taylor cone formation and liquid jet behavior, a high resolution camera (Aven 26700-300 Zipscope USB digital microscope, Figure 2.5a) was connected with a laptop for recording and observing the electrospinning process. Figure 2.5b shows the core-shell structured Taylor cone captured with the camera during the coaxial electrospinning process.

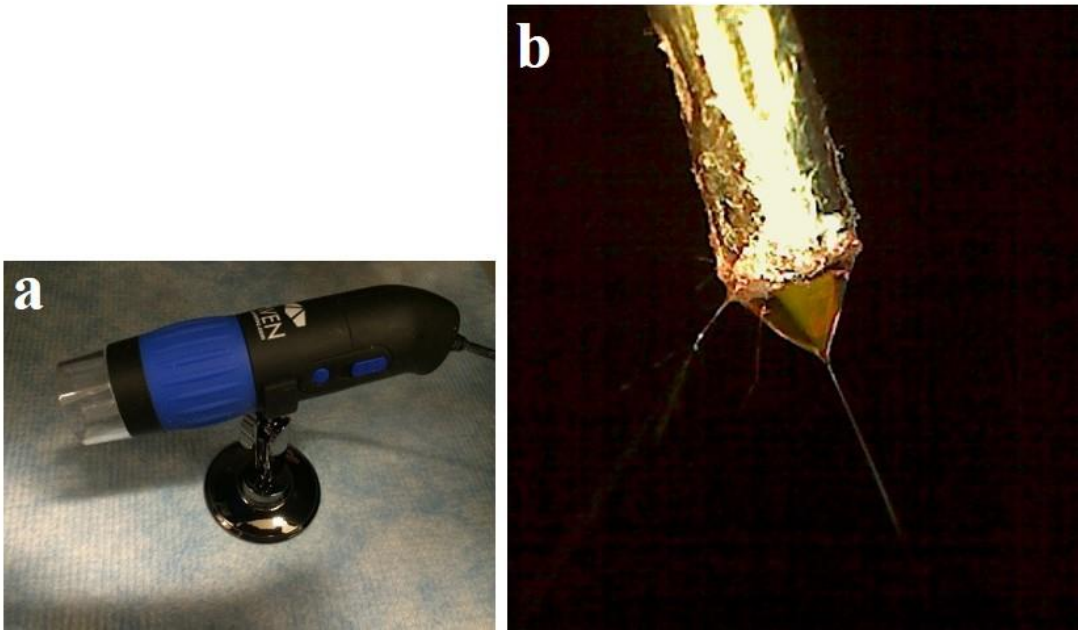

Figure 2.5 Photograph of camera and stable compound Taylor cone. a: high speed camera; **b**: stable core-shell Taylor cone with continuous fiber drawing

As shown in Figure 2.6, two different collectors were used in this study: an aluminum foil covered cardboard sheet without an air gap (collector I) and aluminum foil covered cardboard sheet with a rectangular air gap (collector II). Collector I is a configuration that is widely used for collecting randomly oriented non-woven fibrous mats. With collector II, the fibers accumulated in the gap are macroscopically aligned and fibers accumulated off the gap are randomly oriented (Figure 2.6c). In our study, collector I was used in most of our electrospinning experiments, while collector II was used to fabricate aligned fibers for preparation of cross section samples.

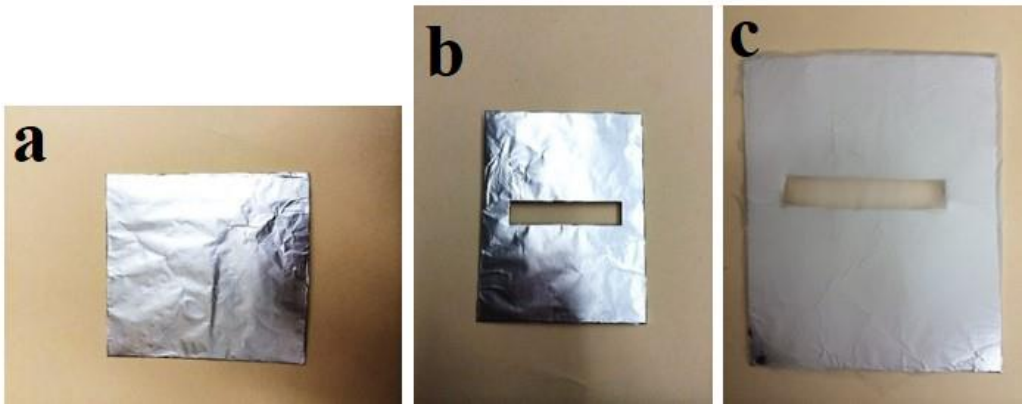

Figure 2.6 Photograph of different collectors. a: aluminum foil covered cardboard sheet (collector I); **b**: aluminum foil covered cardboard sheet with a rectangular air gap (collector II); **c**: photograph of fibers on collector II

2.2 Characterization Techniques

The morphology of electrospun nanofibers is easy to observe with scanning electron microscopy (SEM). Besides of fiber morphology, our studies mainly focus on the characterization of internal structure in a single fiber. Although many studies of core-shell structured or hollow nanofibers have been reported, characterization of a core-shell structure within a single fiber is still challenging. The commonly used characterization methods are SEM, transmission electron microscopy (TEM) and confocal fluorescence microscopy. The characterization of a tri-layered, coaxial structure within polymer fibers is much more difficult due to the low contrast of electron densities between polymer phases and the overlapping of layers under TEM examination. Besides the conventional methods, we explored other newer techniques for the characterization of core-shell and tri-layered,

coaxial morphology. These were focused ion beam-scanning electron microscopy (FIB-SEM) super-resolution structured illumination microscopy (SR-SIM), and nanoscale-infrared spectroscopy (nano-IR).

2.2.1 Scanning Electron Microscopy (SEM)

SEM is an important technique used to obtain high resolution images of a sample surface[1]. In our current study, a JEOL 7400F SEM was used to observe and measure the fiber diameters, diameter distribution, porosity, fiber orientation and fiber surface roughness. To prepare samples for SEM, the electrospun mat was mounted on the aluminum stub using carbon tape and then sputtered with gold for 45 sec. The gold coated sample was observed under the SEM. An accelerating voltage of 3 kV and a current of 10 μA were used to generate high resolution images without damaging the samples.

2.2.2 Attenuated Total Reflectance-Fourier Transform Infrared Spectroscopy (ATR-FTIR)

FTIR is a widely used analytical tool for studying the chemical structure of sample. Attenuated total reflection (ATR) is a sampling technique that simplifies sample preparation. The IR beam enters into the ATR crystal and is totally internally reflected at the interface between the crystal and the sample. Due to the wave like properties, the reflection induces an evanescent field that penetrates into the sample. The penetration depth of the evanescent wave is typically on the order of a few microns (0.5-3 μm) depending on the wavelength, the refractive indices of the ATR crystal and the sample, and the angle that IR beam enters the crystal[2]. In our study, a NEXUS-670 FTIR was utilized to obtain the

IR spectra and to characterize molecular orientation in the electrospun nanofibers. The film samples were placed on the top of ATR crystals and pressed with a stylus to insure intimate contact with it. The spectral range utilized extended from 400 to 4000 cm^{-1} and measurements were made by averaging 64 scans at a resolution of 4 cm^{-1}. The observed absorption peaks were compared with known compounds to make assignments.

2.2.3 Transmission Electron Microscopy (TEM)

TEM is a technique in which a beam of electrons are transmitted through an ultra-thin specimen and interact with it. A TEM image is generated from the interaction of the electrons as they pass through the specimen[3]. Samples for TEM have to be thin and there must be a contrast between phases in order to image them effectively. The image contrast in TEM is due to differences in electron density which are determined via the thickness and composition of the material. In our study, a JEOL JEM 2000FX was used to obtain images of core-shell structured gelatin/PCL fibers. The voltage of the 2000FX is 200 kV, which is large enough for the observation of polymeric nanofibers with a diameters in the 400-800 nm range. To prepare fiber samples for TEM, carbon–coated copper TEM grids were used to collect the fibers directly from the electrospinning jet. The contrast of the different layers in our fibers was weak since the polymers used are mainly composed of the same light elements. To increase the contrast, a chemical staining procedure was applied to selectively stain the cross sections of the fibers. The cross section sample preparation and staining will be discussed separately in the results for each individual fiber sample since the procedure varies for each. The instrument used for characterization of

cross section samples was the Cryo-TEM (Tecnai-12), which has an accelerating voltage of 120 kV.

2.2.4. Laser Scanning Confocal Microscopy (LSCM)

Fluorescence microscopy has been widely applied in the characterization of the internal structure of electrospun fibers[4, 5]. As an optical imaging microscopic technique, LSCM uses a scanning focused laser beam to illuminate different spots within the sample, a fixed detector to detect the light from illuminated spots and a fixed pinhole at an optically conjugate plane in front of the detector to suppress out of focus signal. With LSCM, the images are actually captured point by point at various depths within the sample and reconstructed in the software to obtain the three-dimensional (3D) image[6]. In our study, a Confocal LSM 5LIVE Highspeed microscope was used to acquire 2D and 3D images of the core-shell structured nanofibers. The florescent agent was Rhodamine B. The excitation and emission wavelengths of Rhodamine B are 550 nm and 580 nm, respectively.

2.2.5. Focused Ion Beam-Scanning Electron Microscopy (FIB-SEM)

FIB-SEM is a technique that combines FIB (focused ion beam) and SEM together[1, 7, 8]. In this system, a beam of Ga+ ions is generated to create specific cross section samples, which are effectively machined by the beam. These cross sections can be imaged directly without transferring the sample itself. Also, ion milling could be used to prepare lamella samples (under 100 nm) for TEM or STEM. Additionally, FIB can be used to image a sample directly, detecting emitted electrons. In our study, the samples are soft polymer nanofibers, which are very difficult to cross section without creating defects. The

FIB prepared cross sections are relatively ideal since no mechanical stress or contaminants are introduced into the samples during the ion milling process. We mainly used FIB-SEM in two ways, to create cross sections of nanofibers followed by imaging them with an SEM, and, to prepare lamella samples of fibers for TEM study. The preparation of nanofiber samples for FIB-SEM is similar to SEM except that a low fiber density was required for creating cross sections with the FIB. To prepare low density samples, we used a double sided carbon tape covered aluminum stub to touch the fibrous mats and stick several fibers on the stub. For the preparation of TEM lamella, a special grid was used to transfer the lamella sample as shown in Figure 2.7. The milling current and imaging current in the FIB was 50 pA without effecting or damaging the samples, while the accelerating voltage in the SEM was 2 kV and 3 kV.

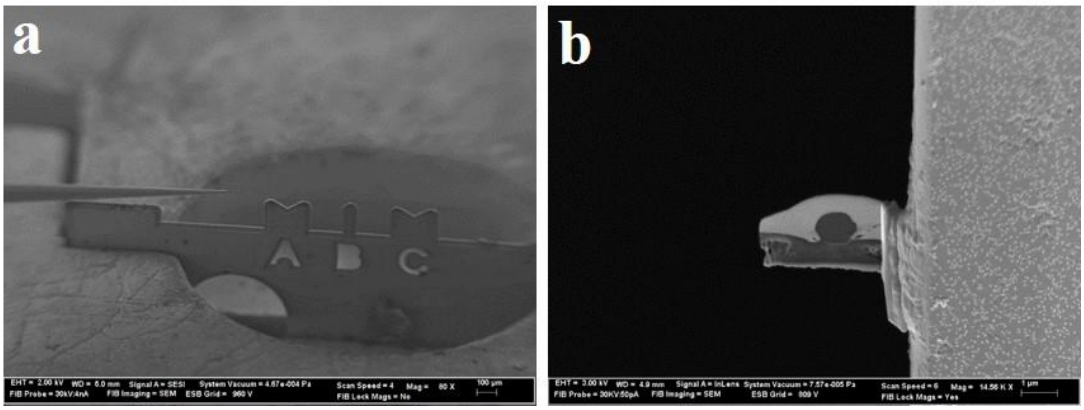

Figure 2.7 Photograph of FIB-SEM chamber and sample. a: working chamber; **b**: lamella sample

2.2.6. Super-Resolution Structured Illumination Microscopy (SR-SIM)

Although confocal microscopy was used to observe the core-shell structure of nanofibers, it was limited when characterizing the tri-layer structure due to the resolution limitation. SR-SIM, on the other hand, is based on a structured illumination technique in which a grid pattern is generated through interference of diffraction orders and superimposed on the specimen while capturing images. The grid is rotated in steps by specific degrees and the images are captured after each rotation of the grid. Thus, the image set is actually a collection of individual image subsets. The image collection is the raw data and can be processed with a specialized algorithm to reconstruct a final high-resolution image with a lateral resolution improvement approximately twice that of the diffraction-limit[9]. Hence, the resolution could be enhanced simply by increasing the rotation number (decreasing the rotation degree) of the grid. The SR-SIM used in our current study has a lateral resolution (XY) of 120 nm and an axial resolution (Z) of 300 nm[10]. To prepare the samples for SR-SIM, Rhodamine B was used as the florescent agent and added into the shell and core solutions before electrospinning. The excitation and emission wavelengths of Rhodamine B are 550 nm and 580 nm, respectively.

2.2.7. Nanoscale-Infrared Spectroscopy (Nano-IR)

Nano-IR is a technique that combines AFM and infrared spectroscopy[11, 12]. Although IR spectroscopy has wide applications in chemical analysis, the resolution when studying heterogeneous sample is generally constrained to a spatial resolution which is three times the wavelength of the IR radiation. By using an AFM cantilever as the detector

for measuring IR absorption, the nano-IR system breaks through resolution limits in conventional IR spectroscopy. In another words, the key feature of nano-IR is the ability to identify the chemistry and structure of material under the tip of an AFM. Additionally, the nano-IR instrument can also be equipped with nanothermal analysis as an optional feature to provide additional dimensions of analytical information. The details about the science behind this system will be discussed in detail in Chapter 5. The primary challenge of using nano-IR to characterize the core-shell or tri-layered structure of nanofibers is sample preparation. The optimum sample thickness for the nano-IR system is approximately 200-500 nm. To prepare cross sectioned fiber samples for nano-IR, a cryo-microtome process was used, the details of which will be described in the following section.

2.3 Sample Preparation and Treatment

2.3.1 Microtome and Cryo-microtome

To prepare the cross section samples, the nanofibrous mat was embedded in a mold, which was subsequently filled with liquid resin (LR). After 48 hrs of curing, the resin reached the required hardness and the embedded sample was first trimmed at room temperature with the regular microtome (R.J.) to produce the cutting stub. Then the stub was transferred to the cryo-microtome (Leica). In order to obtain thin and large cross section samples, multiple parameters needed to be set properly before cutting, including temperature, thickness and cutting speed[13]. The applied temperatures in the cryo-microtome depend on the glass transition temperature (T_g) of the polymer samples. For example, the T_g of PCL is close to -60 ℃ so the temperature of the diamond knife would be set at a lower value, approximately -65 ℃ with the actual cutting temperature a bit lower

than that of knife, so approximately -70 ℃. The cutting speed would be adjusted based on the required thickness and the size of stub. These parameters are partially based on experimental experience and vary depending on the hardness of resin, the required thickness of the samples, the condition of the diamond knife and the method used to collect the cross section samples.

2.3.2 Selective Chemical Staining

It is generally difficult to differentiate polymer layers in an electrospun polymer nanofiber with TEM since the difference in electron densities between polymer phases is small and leads to little contrast under TEM, which is very weak. Thus, contrast enhancement is induced by performing chemical staining, which is widely practiced in polymer research. OsO_4, which stains the gelatin selectively, was applied to increase the contrast of polymer layers in TEM[14]. To prepare staining samples for TEM, the cross sections of the nanofibers were first prepared with a microtome or FIB-SEM and then loaded on a TEM grid. The grid with sample attached was left in a staining jar overnight. Then, finally, the stained cross sections were investigated with TEM to view their internal structure.

REFERENCES

1. Jim Mabon, W. S. *Scanning Electron Microscopy (SEM) and Focused Ion Beams* of Illinois at Urbana-Champaign: 2012.
2. *FT-IR Spectroscopy—Attenuated Total Reflectance (ATR)*; Perkin Elmer Life and Analytical Sciences: 2007.
3. Zaluzec, N. J. *Introduction to Transmission/Scanning Transmission Electron Microscopy and Microanalysis*; Electron Microscopy Center, Materials Science Division, Argonne National Laboratory.
4. Saraf, A.; Lozier, G.; Haesslein, A.; Kasper, F. K.; Raphael, R. M.; Baggett, L. S.; Mikos, A. G. *Tissue Engineering Part C-Methods* **2009,** 15, (3), 333-344.
5. Tomczak, N.; van Hulst, N. F.; Vancso, G. J. *Macromolecules* **2005,** 38, (18), 7863-7866.
6. Claxton, N. S.; Fellers, T. J.; Davidson, M. W. *Laser Scanning Confocal Microscopy*; Florida State University.
7. Materials Analysis: Focused Ion Beam. *Philips Innovation Services* 2012.
8. Reuteler, J. *Introduction to FIB-SEM: Basic Physics and Applications*; Swiss Federal Institute of Technology Zurich.
9. Huang, B.; Bates, M.; Zhuang, X. W., Super-Resolution Fluorescence Microscopy. In *Annual Review of Biochemistry*, Annual Reviews: Palo Alto, 2009; Vol. 78, pp 993-1016.
10. Schermelleh, L.; Heintzmann, R.; Leonhardt, H. *The Journal of Cell Biology* **2010,** 190, (2), 165-175.

11. Marcott, C.; Kjoller, K.; Lo, M.; Prater, C.; Shetty, R.; Dazzi, A. *Spectroscopy* **2012,** 27, (2), 60-65.

12. Dazzi, A.; Prater, C. B.; Hu, Q. C.; Chase, D. B.; Rabolt, J. F.; Marcott, C. *Applied Spectroscopy* **2012,** 66, (12), 1365-1384.

13. Leica UC7/FC7 Cryo-Ultramicrotome Manual; Leica-Microsystems.

14. Li, Z., Industrial Applications of Electron Microscopy. CRC Press: 2003; p 80-81.

Chapter 3

COAXIAL ELECTROSPINNING OF PCL AND GELATIN BIODEGRADABLE NANOFIBERS

3.1 Introduction

Electrospinning of polymeric materials has attracted great attention in the past ten years for potential applications in tissue engineering[1, 2]. Generally, the physical and biological properties of electrospun fibers depend on the base materials' chemical compositions. Both synthetic and natural electrospun polymers have been widely studied for tissue engineering and their corresponding advantages and disadvantages have been clarified[1]. Compared to naturally occurring biopolymers, synthetic polymers are less expensive, more commonly available and easier to electrospin into fibers because of their generally higher molecular weight. Also synthetic polymers usually provide better mechanical performance thereby better mimicking the properties of the native extracellular matrix (ECM). Many synthetic polymers have been electrospun into nanofibrous scaffolds for tissue engineering, including poly(ε-caprolactone) (PCL), polyglycolide (PGA), polylactide (PLA), polyurethane, and poly(vinyl alcohol) (PVA) among others[1, 3, 4]. However, in contrast, natural polymers offer better biocompatibility and lower immunogenicity. Most research on the electrospinning of natural polymers has been focused on gelatin[5], collagen, elastin[6], chitosan, fibrins and silk[7]. In order to combine the advantages of synthetic and natural polymers to create composite scaffolds with desirable

properties, blend electrospinning of polymer mixtures has been developed and applied to the production of tissue engineering scaffolds. However, electrospinning of polymer blends is constrained with respect to solvent choices and thermodynamic compatibility issues. An alternative effective method that combines the advantages of synthetic and natural polymers in the fabrication of composite scaffolds is coaxial electrospinning. Coaxial electrospinning is a modification of traditional electrospinning involving co-electrospinning without direct mixing of the two or more different solutions. This technique is very attractive for tissue engineering since it produces core-shell or multi-layer structured fibers. In contrast to blend electrospinning, coaxial electrospinning not only enhances the polymer properties by electrospinning different polymers together but also provides an effective way to protect the bioactive elements (such as growth factors, DNA, etc.) during the electrospinning process[8-10].

Initially, our studies on coaxial electrospinning started with a selection of the most appropriate polymer systems for experiments. Physical and biological properties, such as biodegradability, biocompatibility, mechanical properties, hydrophilicity and cell interactions were specially considered in this process. The first polymer system studied was gelatin and PCL, both of which are popular in the construction of tissue engineering scaffolds. Gelatin is produced from the triple-helix structured collagen by treating the collagen with dilute alkaline, or acid and heating to denature the collagen. As a natural biodegradable polymer, gelatin has excellent cell biocompatibility and allows for cell adhesion and proliferation[5]. One critical drawback of electrospun gelatin fibers for tissue engineering applications is that gelatin is water soluble at room temperature. This problem

is usually addressed by chemically cross linking electrospun gelatin fibers to decrease their water solubility so that electrospun fibers maintain their nanofibrous morphology after water exposure[11]. Another disadvantage of gelatin in tissue engineering is its low mechanical strength, lower than that of many other synthetic polymers. PCL, on the other hand, is the most commonly used synthetic biodegradable polymer for tissue engineering. It is a semi-crystalline polymer with a very low melting point (around 55-60 ℃). The good mechanical properties and low degradation rate (2-4 years) allow PCL to be suitable for various applications in tissue engineering[3]. However, biocompatibility of PCL is not as good as that of natural polymers and its hydrophobicity results in poor wettability and poor cell attachment. Core-shell structured gelatin/PCL nanofibers combine the advantages of PCL and gelatin and avoid the limitations of each individual polymer. Besides, gelatin serves well as a drug carrier[12] and electrospun nanofibers with gelatin as the core would have potential for controlled drug release. In addition, electrospinning of pure gelatin[13], pure PCL[14] and core-shell structured PCL/gelatin fibers have been reported previously in the literatures[15, 16], providing a basis for our study on coaxial electrospinning of tri-layer structured gelatin/PCL/gelatin nanofibers.

3.2 Experimental Section

3.2.1 Materials

The materials and their sources are listed as following: PCL pellets (Mn=45,000) were purchased from Sigma-Aldrich. Gelatin B was obtained from Eastman Kodak Co., NY. Rhodamine B solution (0.2% in isopropanol) and OsO_4 (solid state) were purchased from Sigma-Aldrich. 2,2,2-Trifluoroethanol (TFE) solvent was purchased from

Fisher Scientific. All materials were used as received. Three kinds of solutions were made in this study: 11 wt% gelatin in 80/20 w/w TFE/ deionized water, 17 wt% gelatin in 80/20 w/w TFE/ deionized water and 11 wt% PCL in TFE. All solutions were stirred overnight before use. To prepare fluorescent samples, Rhodamine B was used to dye the gelatin solution (1 drop of Rhodamine B solution for 10 ml gelatin solution). For staining, 5% OsO_4 in H_2O was made and 1 ml of OsO_4 solution was added for each staining experiment. Table 3.1 and Table 3.2 list the solution and solvent parameters used in the experiments.

Table 3.1 Polymer solution parameters

solution	composition	Viscosity at 20 °C (cp)
Gelatin	17% Gelatin in TFE/H_2O	63.08
PCL	11% PCL in TFE	98.97
Gelatin	11% Gelatin in TFE/H_2O	10.46

Table 3.2 Solvent parameters

solvent	Boiling point (℃)	Vapor pressure at 20 ℃ (atm)	Electrical conductivity at 25 ℃ (s/cm)	Dielectric constant
TFE	73.5	9.86×10^{-2}	3.9×10^{-7}	26.14
H_2O	100	2.75×10^{-2}	5.5×10^{-3}	78.54

3.2.2 Coaxial Electrospinning Process

As described in Chapter 2, there are two sets of parameters to be considered in electrospinning. In our study, electrospinning solution parameters, such as solution concentrations and feeding rates, are partially referenced from the literature and partially determined based on the experiments; while electrospinning processing parameters, such as working distances and voltages, are optimized experimentally until spinning resulted in uniform fibers with consistent diameters.

3.2.2.1 Coaxial Electrospinning of Gelatin/PCL Core-shell Structured Nanofibers

An 11 wt% gelatin solution (as the core solution) and an 11 wt% PCL solution (as the shell solution) were loaded independently into the coaxial nozzle. Two pumps (NE-300, New Era Pump Systems Inc) were applied to keep the flow rate at 0.15 ml/h and 0.5 ml/h, core and shell respectively. An aluminum foil covered cardboard sheet served as the collector in the experiments. The distance between the nozzle and collector was 18 cm. A high voltage power supply was used to produce a potential difference across the coaxial spinneret and the collector. When the electric field was applied across the spinneret and the collector (+16 kV, -1 kV), a fluid jet was emitted, and as it travelled to the collector, the solvent evaporated. Eventually the dry fibers accumulated randomly on the collector in the form of a non-woven mat.

3.2.2.2 Coaxial Electrospinning of PCL/Gelatin Core-shell Structured Nanofibers

The electrospinning apparatus and experimental setup were similar to that described in 3.2.2.1. An 11 wt% PCL solution (as the core solution) and a 17 wt% gelatin solution (as shell solution) were loaded independently into the coaxial concentric nozzle. Two pumps were applied to keep the flow rates at 0.15 ml/h and 0.5 ml/h, core and shell respectively. The distance between the nozzle and collector was held at 15 cm. The applied voltage was 10 kV for the nozzle and -2 kV for the collector. The dry fibers were collected randomly on the collector plate in the form of a non-woven mat.

3.2.2.3 Coaxial Electrospinning of Gelatin/PCL/Gelatin Tri-layer Structured Nanofibers

A three-needle concentric nozzle was fabricated and used to electrospin tri-layer, coaxial nanofibers. The shell and core solutions were 17 wt% and 10 wt% gelatin, respectively, in 80/20 w/w TFE/ deionized water. The middle layer solution was 11 wt% PCL in TFE. Three solutions were loaded independently into the concentric nozzle. Three pumps were applied to keep the flow rates at approximately 1.0, 0.4 and 0.15 ml/h, from shell solution to core solution. An aluminum foil covered cardboard sheet was used as the collector with a high voltage applied between the nozzle and the collector (+13 kV, -1 kV). The working distance was set as 17 cm. Fibers were accumulated with random orientation on the collector plate.

3.2.3 Characterization

To observe the morphology of electrospun nanofibers, a sample (0.5 cm x 0.5 cm) was cut from the fibrous membrane, mounted on the aluminum stub with carbon tape and then sputtered with gold for 45 sec. The coated sample was investigated with a JEOL JSE 7400F SEM. The ATR-FTIR spectra were obtained with a NEXUS-670. To characterize the core-shell structure, confocal microscopy (LSM 25LIVE) was employed to take the florescence images of the fibers. TEM images of single fibers and cross-sections of fibers were captured with a JEOL 2000FX TEM. The three-layer structure in a single electrospun fiber was characterized with three different techniques. First, a JEOL 2000FX TEM was employed to observe the three-layer structure within the cross section of fibers. Secondly, super-resolution structured illumination microscopy (SR-SIM) was employed to characterize the three-layer structure in a single fiber by taking florescence images. Finally, focused ion beam-scanning electron microscopy (FIB-SEM) was utilized to investigate the interior structure of the fibers. To avoid degradation in the sample, the milling current and imaging current in the FIB was 50 pA while the accelerating voltage in the SEM was 3 kV.

3.3 Results and Discussion

3.3.1 Coaxial Electrospinning of Gelatin/PCL Core-shell Structured Nanofibers

SEM images of coaxial electrospun nanofibers were obtained to investigate the nanofiber morphology. The accelerating voltage used in SEM was 3.0 kV and the current was 10 μA. The diameter of the fibers was measured using Image J software. As shown in Figure 3.1a, the coaxial electrospun gelatin/PCL nanofibers are uniform and free

of bead defects. The average diameter of the gelatin/PCL nanofibers is 334 nm. Figure 3.1b shows aligned nanofibers accumulated in a gap with collector II. Comparing Figure 3.1a with Figure 3.1b, there is not much difference in morphology between random gelatin/PCL nanofibers and aligned gelatin/PCL nanofibers.

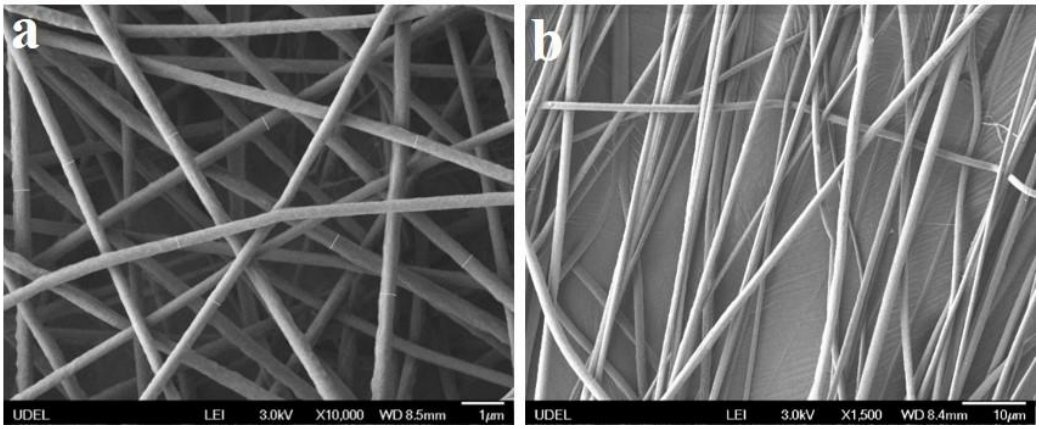

Figure 3.1 SEM images of coaxial electrospun gelatin/PCL nanofibers. a: random nanofibers collected with collector I; **b**: nanofibers with alignment collected with collector II

To characterize the core-shell structure in single fibers, the coaxial electrospun fibers were investigated with TEM. A carbon-coated TEM grid was used to collect a few nanofibers and then loaded into the TEM. Due to the difference in electron densities between polymer phases, there will be a slight contrast between different polymer layers in the TEM image. Figure 3.2 shows TEM images of gelatin/PCL nanofibers. For each nanofiber, there is a light shaded part in the center. The contrast between the center

part and outer part of the nanofiber indicates the existence of two layers and the lighter section inside the nanofibers results from the gelatin core. Although the difference in electron densities as well as the contrast between core and shell layer is slight, since the PCL and gelatin are mainly composed of the same light elements (C, H, O, N), the TEM images did suggest the existence of a core-shell structure in coaxial electrospun gelatin/PCL nanofibers.

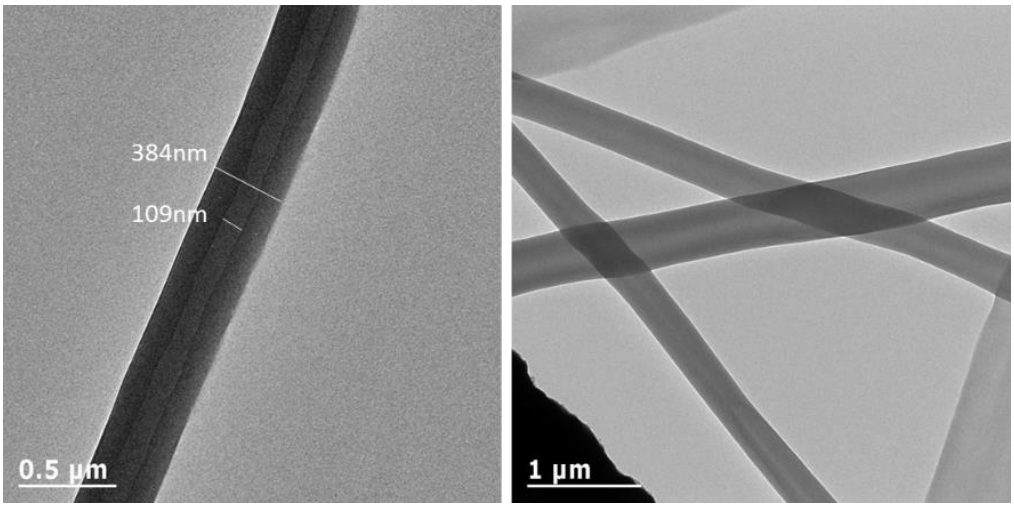

Figure 3.2 TEM images of core-shell structured gelatin/PCL nanofibers.

3.3.2 Coaxial Electrospinning of PCL/Gelatin Core-shell Structured Nanofibers

Coaxial electrospun PCL/gelatin nanofibers were also fabricated using PCL as the core material and gelatin as the shell material. Figure 3.3a is an SEM image showing the random nanofibers collected with collector I. As can be seen, the coaxial electrospun

PCL/gelatin nanofibers have a smooth fiber surface and uniform fiber diameter distribution. Using Image J software, the average diameter of PCL/gelatin nanofibers was determined to be 860 nm. Figure 3.3b shows aligned nanofibers accumulated in a gap with collector II. The alignment of the fibers in the gap is driven by the attractive forces between the residual positive charges on the fiber and the negative charge on the collector and in the alignment process, the fibers are stretched and elongated. As observed in Fig. 3.3b, the shell of the nanofiber is broken when stretched across the gap because gelatin is more brittle than PCL.

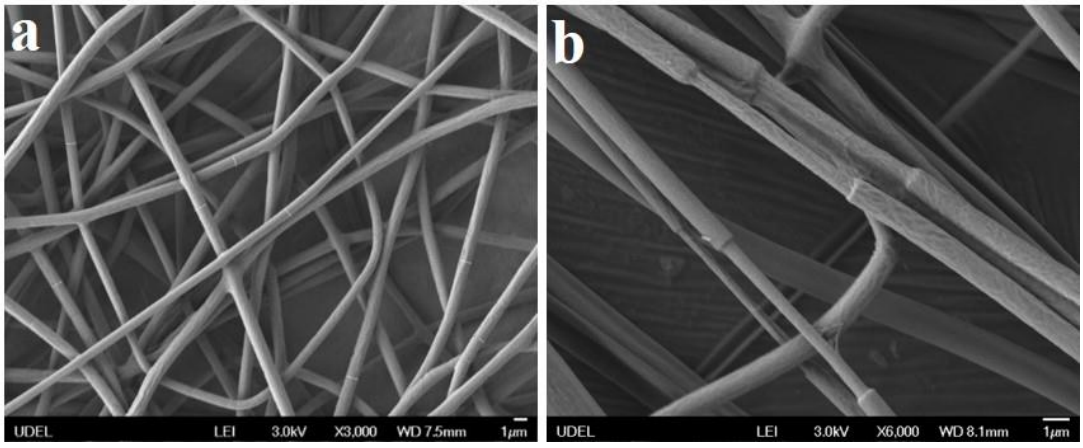

Figure 3.3 SEM images of coaxial electrospun PCL/gelatin nanofibers. a: random nanofibers collected with collector I; **b**: nanofibers with alignment and stretching collected with collector II

TEM is only useful for characterization of ultra-thin samples (at most hundreds of nanometers thick) because the electron beam is not able to transmit through the thicker samples resulting in dark images not showing any interior structure. Although

the core-shell structure of gelatin/PCL nanofibers (average diameter 334 nm) was demonstrated using TEM, coaxial electrospun PCL/gelatin nanofibers could not be characterized with TEM directly because the average diameter of PCL/gelatin nanofibers is 860 nm which is too thick for TEM. In order to overcome this problem, we carried out TEM studies of nanofiber thin cross sections.

As mentioned previously, the contrast between polymer phases under the electron beam of the TEM is weak due to the similar elemental composition of the polymers. In order to increase the contrast of core and shell layers in TEM, we used a chemical staining procedure to deposit high density metal compounds into the polymer nanofibers. The staining agent used in our study is OsO_4, which stains the gelatin layer and does not affect the PCL layer. To prepare samples for TEM, the aligned nanofibers were embedded into resin and sliced into 70 nm thick sections perpendicular to the axis using a Microtome-R.J. Then the cross sections of nanofibers were stained with OsO_4. Finally, the stained cross sections were investigated with TEM to view the internal structure. From Figure 3.4, it is obvious that the outer part of the cross section is darkly shaded indicating the successful staining of gelatin shell. The inner portion of the cross section is lightly shaded as a result of the unstained PCL core. The clear interface and contrast between two layers provides a convincing evidence for the existence of a core-shell structure in coaxial electrospun PCL/gelatin nanofibers.

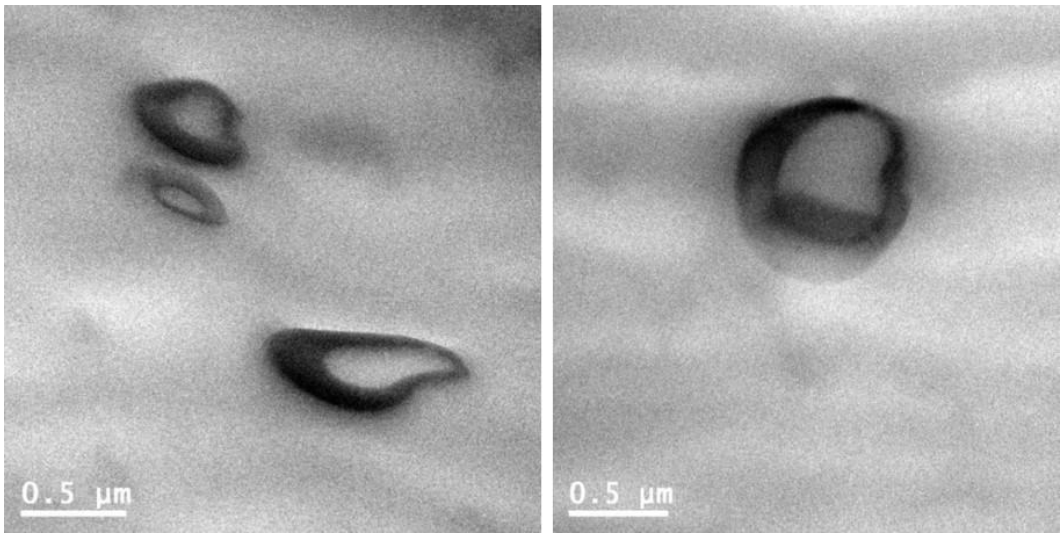

Figure 3.4 TEM images of stained cross section of coaxial electrospun PCL/gelatin nanofibers

Another method, laser scanning confocal microscopy (LSCM), was also used to investigate the core-shell structure of the PCL/gelatin nanofibers. To prepare LSCM samples, an 11 wt% PCL solution was doped with the fluorescent dye, Rhodamine B, and stirred for 1 hr so it was uniformly distributed. The electrospinning process was similar to that described in 3.2.2.2 except for the collection of nanofibers. A No.1.5 glass coverslip was attached to the aluminum foil collector to gather some nanofibers and then the coverslip with fibers was transferred to the LSCM for further studies. The results clearly demonstrated the core-shell structure of coaxial PCL/gelatin nanofibers. In Figure 3.5, the Rhodamine B doped PCL core is in red and is surrounded by a green sheath layer which is result of the auto-fluorescence of the gelatin shell. The LSCM images also show continuity of the core in the fiber.

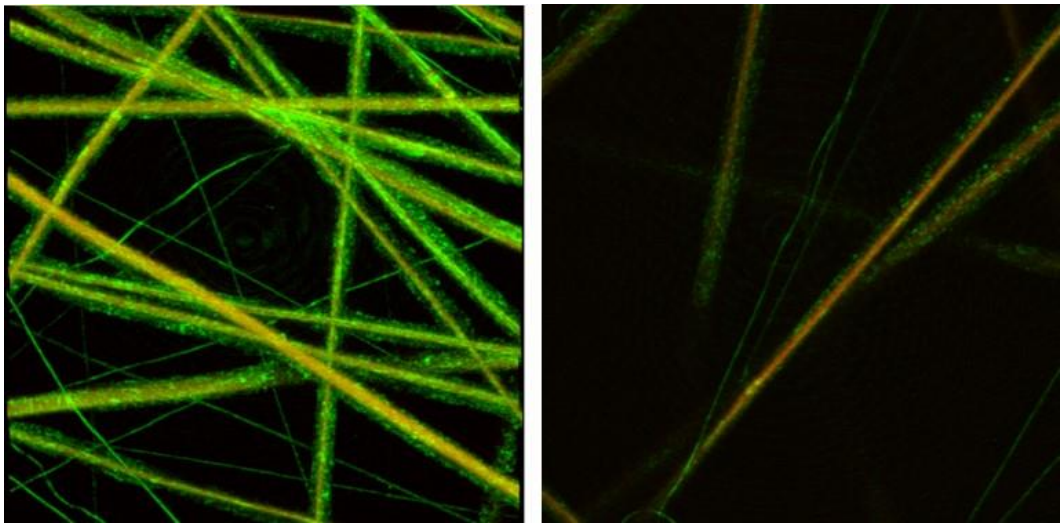

Figure 3.5 LSCM images of coaxial electrospun PCL/gelatin nanofibers

3.3.3 Coaxial Electrospinning of Gelatin/PCL/Gelatin Tri-layer Structured Nanofibers

Tri-layered coaxial electrospun gelatin/PCL/gelatin nanofibers were also investigated with SEM. As seen in Figure 3.6, the morphology of tri-layered coaxial gelatin/PCL/gelatin fibers is very similar to the previously discussed core-shell structured gelatin/PCL and PCL/gelatin fibers except for the fiber diameter. The diameter of the tri-layered coaxial electrospun gelatin/PCL/gelatin fiber is more uniform and larger, with an average value of 1.4 μm.

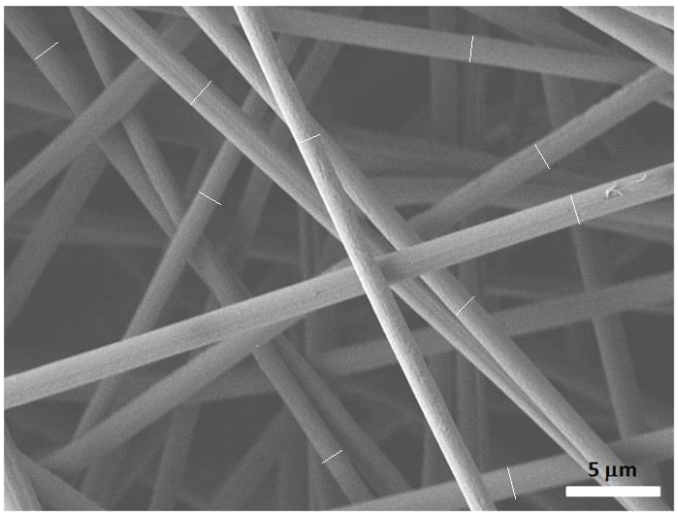

Figure 3.6 SEM image of coaxial electrospun gelatin/PCL/gelatin fibers

The chemical composition of the electrospun fibers was characterized by ATR-FTIR and the infrared spectra of the single, bi-layered and tri-layered nanofibers are shown in Figure 3.7. There are four different electrospun nanofibers: pure gelatin nanofibers, pure PCL nanofibers, coaxial electrospun gelatin/PCL nanofibers and tri-layered coaxial electrospun gelatin/PCL/gelatin nanofibers. The main absorption bands for gelatin (1540 and 1650 cm^{-1}) and PCL (1730 cm^{-1}) are listed in Table 3.3[17, 18]. The spectrum of pure gelatin nanofibers shows all the characteristic peaks of amide groups, respectively, 3310 cm^{-1} due to N-H stretching, 1650 cm^{-1} due to amide I band and 1540 cm^{-1} due to amide II band. The spectrum of PCL nanofibers has a specific peak at 1727 cm^{-1} corresponding to the carbonyl stretch. The FTIR spectra demonstrate the existence of PCL and gelatin in both coaxial electrospun gelatin/PCL and tri-layered coaxial electrospun gelatin/PCL/gelatin nanofibers. Compared with the spectrum of coaxial

electrospun gelatin/PCL nanofibers, the spectrum of coaxial electrospun gelatin/PCL/gelatin nanofibers does show an increase in the gelatin peak intensities as the outer gelatin sheath layer is added. With these ATR-FTIR results, a qualitative composition of each kind of electrospun nanofibers is proven and confirmed.

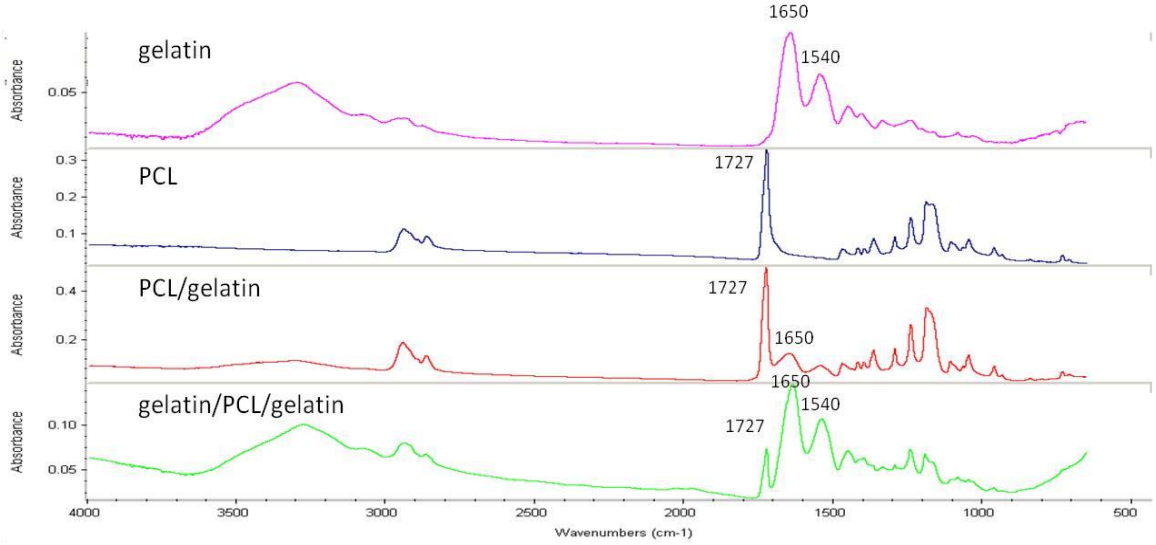

Figure 3.7 ATR-FTIR spectra of different electrospun nanofibers

Table 3.3 Main absorption bands of gelatin and PCL and their assignments

Band (cm-1)	Assignment
3310	amide A N-H stretching
1730	carbonyl group
1650	amide I C=O stretching
1540	amide II C-N stretching and N-H deformation

For a coaxial core-sheath structure, the conventional characterization methods are TEM, cross section TEM and cross section SEM. However, TEM is not the preferred choice for analyzing multilayer structure in single fibers due to the low contrast of electron densities between polymer phases and the overlapping of different layers. In our study, we applied the traditional techniques such as TEM as well as new techniques such as focused ion beam-scanning electron microscopy (FIB-SEM) and super-resolution structured illumination microscopy (SR-SIM) to analyze the three-layer structure in single nanofibers.

To characterize the three-layer structure with TEM, the contrast between polymer layers needs to be increased with chemical staining. The method we used here is similar to that described in Section 3.3.2 on core-shell structured PCL/gelatin nanofibers. As shown in Figure 3.8, the dark dot in the center of the cross section is the result of stained gelatin core. The light ring surrounding the dark gelatin is indicative of the PCL layer. There is another dark ring outside the light PCL, due to the outer gelatin layer. However, the outermost dark ring is not clear enough and may be caused by an artifact of the preparation process, such as the deformation of polymer fibers during the microtoming process making the cross section images less convincing.

The second technique applied to characterize the three-layer structure within a single fiber is SR-SIM. To prepare samples for SR-SIM, Rhodamine B was added to both shell and core gelatin solutions and mixed for 1 hr to get the dye uniformly

distributed in the solutions. The electrospinning setup and process were similar to that described in 3.2.2.3 except for the collection of fibers. A No.1.5 glass coverslip was attached to the aluminum foil collector to gather the nanofibers. Then, the coverslip with fibers was transferred to the microscope for observation. Figure 3.9 shows the SR-SIM image of a single electrospun nanofiber. The two outermost, thinner florescent red lines, although occasionally discontinuous, indicate the presence of the shell while the central, thicker florescent red line indicates the presence of the gelatin core. The nonfluorescent area between the narrow and thicker red lines is the undyed PCL middle layer, which does not fluoresce. Florescence distribution in the nanofiber is clearer in the image at the left corner. The SR-SIM result proves the continuity of the core in the fiber and makes the three-layer structure more visual and convincing.

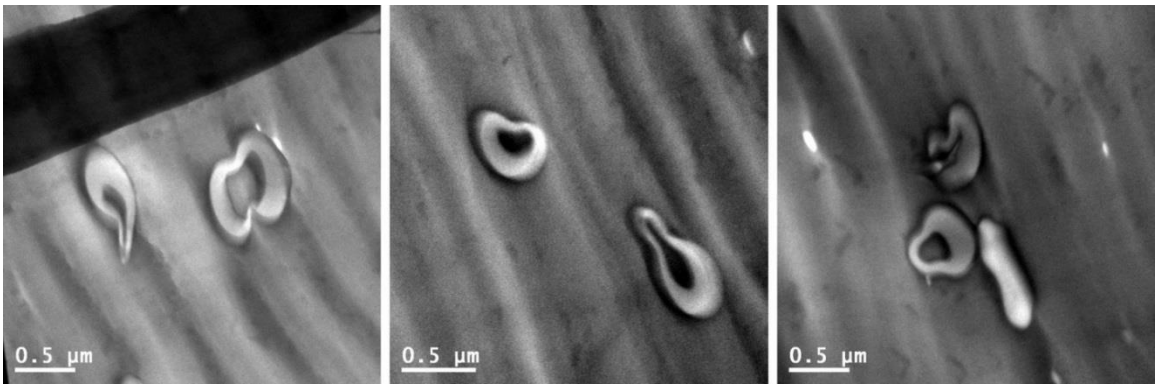

Figure 3.8 TEM images of cross sections of coaxial electrospun gelatin/PCL/gelatin fibers

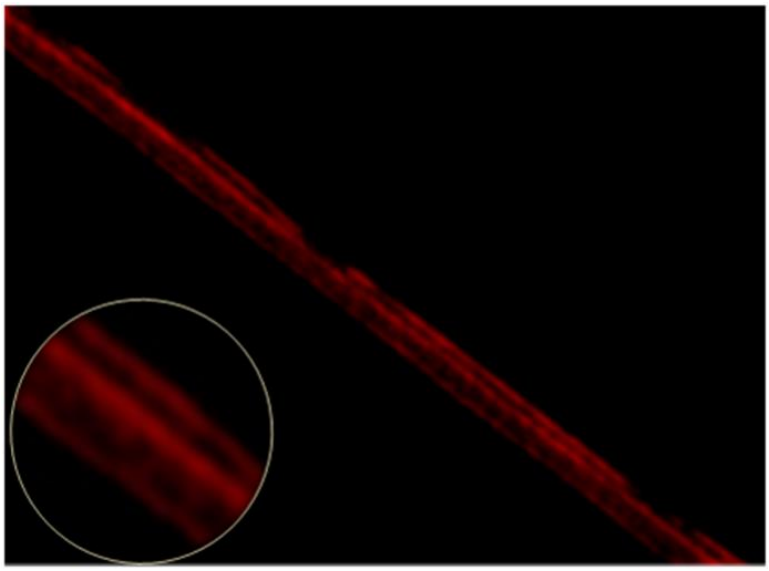

Figure 3.9 SR-SIM image of coaxial electrospun gelatin/PCL/gelatin fiber

To visually observe the three-layer structure, the fibers were then analyzed using FIB-SEM. An ion beam probe was used to cut the fiber and remove a part of the fiber through milling. Then the cross section of the fiber was imaged under the SEM (Figure 3.10). The contrast of different layers due to the difference in secondary electron densities between polymer phases clearly demonstrates the existence of three-layer structure in a single fiber. As can be seen in both the left and right images of the cut fiber cross-sections, there is a light shaded gelatin core surrounded by a dark (PCL) intermediate layer, which, in turn, is then surrounded by a thin outer sheath of gelatin. The FIB-FESEM image also indicates the specific thickness of each layer, which is 130 nm for the sheath, 240 nm for the intermediate layer, and 230 nm for the core layer. FIB-SEM images unequivocally

prove the existence of the three concentric polymer layered nanofibers produced by our unique three-layer coaxial electrospinning apparatus.

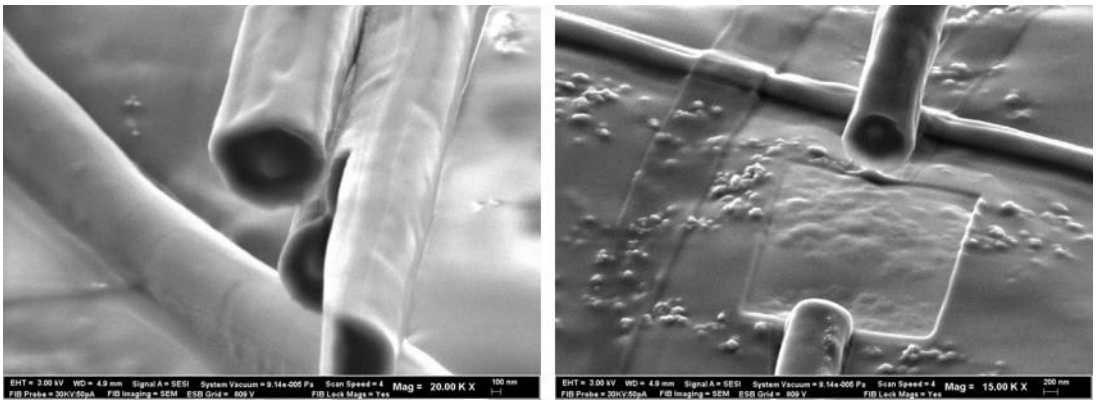

Figure 3.10 FIB-FESEM images of coaxial electrospun gelatin/PCL/gelatin nanofibers

3.4 Conclusions

Core-shell structured gelatin/PCL and PCL/gelatin nanofibers have been fabricated with a customized coaxial electrospinning apparatus. The fiber morphology was observed with SEM, while the core-shell structures were proven by TEM and LSCM. Subsequently, tri-layered coaxial gelatin/PCL/gelatin biodegradable nanofibers were successfully fabricated by electrospinning using a uniquely designed three needle concentric spinneret[19]. The tri-layer structure was initially studied with traditional TEM, but two other new techniques, SR-SIM and FIB-SEM, were employed to demonstrate the multi-layered concentric fiber structure. Compared with coaxial electrospun core-shell

structured nanofibers, the addition of the third layer in the fiber provides possibilities for the development and improvement of functional tissue scaffolds for drug delivery and wound healing. By using gelatin as both shell and core layer and PCL as middle layer, we constructed a tri-layer structured nanofiber for the applications in tissue engineering, in which a biocompatible natural polymer was used as shell layer, a synthetic polymer intermediate layer was incorporated for mechanical strength and a natural polymer layer capable of dissolving drugs and growth factors was utilized as the core layer.

REFERENCES

1. Pham, Q. P.; Sharma, U.; Mikos, A. G. *Tissue Eng.* **2006,** 12, (5), 1197-1211.
2. Sill, T. J.; von Recum, H. A. *Biomaterials* **2008,** 29, (13), 1989-2006.
3. Cipitria, A.; Skelton, A.; Dargaville, T. R.; Dalton, P. D.; Hutmacher, D. W. *Journal of Materials Chemistry* **2011,** 21, (26), 9419-9453.
4. Boland, E. D.; Wnek, G. E.; Simpson, D. G.; Pawlowski, K. J.; Bowlin, G. L. *Journal of Macromolecular Science-Pure and Applied Chemistry* **2001,** 38, (12), 1231-1243.
5. Sisson, K.; Zhang, C.; Farach-Carson, M. C.; Chase, D. B.; Rabolt, J. F. *Journal of Biomedical Materials Research Part A* **2010,** 94A, (4), 1312-1320.
6. Buttafoco, L.; Kolkman, N. G.; Engbers-Buijtenhuijs, P.; Poot, A. A.; Dijkstra, P. J.; Vermes, I.; Feijen, J. *Biomaterials* **2006,** 27, (5), 724-734.
7. Kim, S. H.; Nam, Y. S.; Lee, T. S.; Park, W. H. *Polymer Journal* **2003,** 35, (2), 185-190.
8. Amler, E.; Mickova, A.; Buzgo, M. *Nanomedicine* **2013,** 8, (4), 509-512.
9. Ji, W.; Sun, Y.; Yang, F.; van den Beucken, J. J. J. P.; Fan, M.; Chen, Z.; Jansen, J. A. *Pharmaceutical Research* **2011,** 28, (6), 1259-1272.
10. Su, Y.; Su, Q.; Liu, W.; Lim, M.; Venugopal, J. R.; Mo, X.; Ramakrishna, S.; Al-Deyab, S. S.; El-Newehy, M. *Acta Biomaterialia* **2012,** 8, (2), 763-771.
11. Sisson, K.; Zhang, C.; Farach-Carson, M. C.; Chase, D. B.; Rabolt, J. F. *Biomacromolecules* **2009,** 10, (7), 1675-1680.

12. Young, S.; Wong, M.; Tabata, Y.; Mikos, A. G. *Journal of Controlled Release* **2005,** 109, (1-3), 256-274.

13. Choktaweesap, N.; Arayanarakul, K.; Aht-Ong, D.; Meechaisue, C.; Supaphol, P. *Polymer Journal* **2007,** 39, (6), 622-631.

14. Jeun, J. P.; Lim, Y. M.; Nho, Y. C. *Journal of Industrial and Engineering Chemistry* **2005,** 11, (4), 573-578.

15. Zhang, Y. Z.; Ouyang, H. W.; Lim, C. T.; Ramakrishna, S.; Huang, Z. M. *Journal of Biomedical Materials Research Part B-Applied Biomaterials* **2005,** 72B, (1), 156-165.

16. Han, D.; Boyce, S. T.; Steckl, A. J. *Mater. Res. Soc. Symp. Proc.* **2008,** 1094, DD06-02.

17. Muyonga, J. H.; Cole, C. G. B.; Duodu, K. G. *Food Chem.* **2004,** 86, (3), 325-332.

18. Elzein, T.; Nasser-Eddine, M.; Delaite, C.; Bistac, S.; Dumas, P. *J. Colloid Interface Sci.* **2004,** 273, (2), 381-387.

19. Liu, W. W.; Ni, C. Y.; Chase, D. B.; Rabolt, J. F. *Acs Macro Letters* **2013,** 2, (6), 466-468.

Chapter 4

COAXIAL ELECTROSPINNING OF GELATIN/PCL/PLGA TRI-LAYER STRUCTURED NANOFIBERS

4.1 Introduction

One of the aims of this research is to fabricate tri-component, tri-layer (ABC, core-middle-shell) structured polymeric nanofibers using coaxial electrospinning. In Chapter 3, we described the fabrication of gelatin/PCL/gelatin tri-layered (ABA) coaxial nanofibers and demonstrated the ABA structure in single fibers using different instrumental techniques. For this study on coaxial electrospinning of ABC structured polymeric fibers, we built on the use of PCL and gelatin as two components of the material system and we added a third polymeric component. Water soluble polymers such as PEO and PVOH were excluded as choices for the third component for reasons that will be described in Chapter 6. After a thorough literature review and comparison of different synthetic polymers, PLGA (75:25) was chosen as the third component for this study on the coaxial electrospinning of ABC structured polymeric nanofibers.

PLGA is a random copolymer of lactic acid (LA) and glycolic acid (GA). It is one of the most well studied synthetic polymers for biomedical applications and is very popular for electrospinning applications involving tissue engineering due to excellent biocompatibility and controllable degradability[1-4]. The degradation rate of PLGA can be changed by adjusting the ratio of LA and GA contained in the polymer backbone. PLGA

degrades by hydrolysis of the ester linkages in the presence of water. The methyl side group in lactic acid makes it less hydrophilic than glycolic acid, and thus glycolic acid rich PLGA is more hydrophilic and degrades faster[5-7]. Table 4.1 lists the degradation rates of PLA, PGA and PLGA with different LA/GA ratios. It is obvious from this table that PLA has the slowest degradation rate. In addition, the higher the concentration of GA, the faster the degradation of PLGA[8]. However, the degradation of pure PGA is slower than any kind of PLGA because PGA is has no methyl side groups, in contrast to PLA, and thus exhibits very high crystallinity[5, 8]. PLGA (50:50) degrades faster than any of the other copolymers due to its higher percentage of GA and lowest crystallinity[9]. In addition to the ratio of LA/GA and crystallinity, the degradation rate of PLGA is also a function of M_w. Furthermore, electrospun polymeric nanofibers should degrade faster than the bulk material due to their high surface area to volume ratio and the level of water adsorption[5, 10]. Coaxial electrospun nanofibers were designed for potential applications in tissue engineering and hence polymers with appropriate degradation rate are preferred for the release of drugs or bioactive agents[11, 12]. Pure PLA was excluded due to its slow degradation rate, while pure PGA was excluded since it has poor solubility in most organic solvents. Targeting an the expected release or study period of 2 months, PLGA (75:25) with a degradation rate of approximately 4 months was chosen for the third component material for ABC structured nanofibers.

After selection of the three components, fabrication of core-shell structured gelatin/PLGA nanofibers and core-shell structured PCL/PLGA nanofibers was undertaken.

After gaining some experience with these 2-component coaxial electrospun fibers, the ABC structured gelatin/PCL/PLGA polymeric nanofibers were developed.

Table 4.1 Degradation rates of PLA, PGA, and PLGA copolymers

polymer	PLA	PGA	PLGA (85:15)	PLGA (75:25)	PLGA (65:35)	PLGA (50:50)
Degradation rate[a] (month)	>24	6-12	5-6	4-5	3-4	1-2

a: Time to complete mass loss

4.2 Experimental Section

4.2.1 Materials

The materials and their source are listed as following: PCL pellets (M_n=45,000) were purchased from Sigma-Aldrich while gelatin was obtained from Eastman Kodak Co., NY. PLGA (75:25) with a M_w of 66K-107K was purchased from Sigma-Aldrich. Rhodamine B solution (0.2% in isopropanol) and OsO_4 (solid state) was purchased from Sigma-Aldrich while the 2,2,2-Trifluoroethanol (TFE) solvent was purchased from Fisher Scientific. All materials were used as received.

Four solutions were made: 11 wt% gelatin in 80/20 w/w TFE/deionized water, 17 wt% PLGA in TFE, 11 wt% PLGA in TFE and 9 wt% PCL in TFE. All solutions were stirred overnight before use. To prepare fluorescent samples, Rhodamine B was used

to dye the gelatin and PLGA solutions (1 drop of Rhodamine B solution for 10 ml of gelatin solution or 5 ml PLGA solution). For chemical staining, 5% OsO_4 in H_2O was made and 1 ml of OsO_4 solution was added for each staining experiment.

4.2.2 Coaxial Electrospinning Process

As discussed in Chapters 2 and 3, the experimental parameters, such as working distance and voltages, were optimized experimentally until the spinning process resulted in uniform fibers with consistent diameters.

4.2.2.1 Coaxial Electrospinning of Gelatin/PLGA Core-shell Structured Nanofibers

The shell and core solutions used were 17 wt% PLGA solution and 11 wt% gelatin solutions. The two solutions were loaded independently into the coaxial nozzle. Two pumps were used to keep the flow rate at approximately 0.2 ml/h and 1.0 ml/h, core/shell respectively. An aluminum foil covered cardboard sheet was used as the collector. The working distance between the nozzle and collector was 25 cm. A high voltage was applied between the nozzle and the collector (+18 kV, -1kV). Dry fibers were accumulated with random orientation on the collector plate in the form of a non-woven mat.

4.2.2.2 Coaxial Electrospinning of PCL/PLGA Core-shell Structured Nanofibers

A 9 wt% PCL solution (as the core solution) and a 17 wt% PLGA solution (as the shell solution) were loaded independently into the coaxial nozzle. Two pumps were used to keep the flow rate at approximately 0.15 ml/h and 0.8 ml/h, for the core solution and the shell solution respectively. An aluminum foil covered cardboard sheet was used as

the collector with a distance between the nozzle and collector of 20 cm. The applied voltage was 17 kV for nozzle and -1 kV for the collector. The dry fibers were collected randomly on the collector plate in the form of a non-woven mat.

4.2.2.3 Coaxial Electrospinning of Gelatin/PCL/PLGA Tri-layer Structured Nanofibers

The three-needle concentric nozzle described in Chapter 2 was used to electrospin the ABC nanofibers. The shell and core solutions were 17 wt% PLGA and 11 wt% gelatin while the middle solution was 9 wt% PCL in TFE. Three solutions were loaded independently into the coaxial concentric nozzle. Three syringe pumps were used to keep the flow rates at approximately 0.7, 0.7 and 0.15 ml/h, for the shell/middle/core solutions. An aluminum foil covered cardboard sheet was used as the collector with a working distance between the nozzle and collector of 20 cm. In addition, a high voltage was applied between the nozzle and the collector (+17 kV, -1 kV). Dry fibers were accumulated with random orientation on the collector plate.

4.2.3 Characterization

To observe the morphology of electrospun nanofibers, a sample (0.5 cm x 0.5 cm) was cut from the fibrous membrane, mounted to an aluminum stub with carbon tape and then sputtered with gold for 45 sec. The coated sample was investigated with SEM. To characterize the core-shell structure, FIB was employed to create the cross sections from single nanofibers. The thickness of the cross section samples was 50 nm - 100 nm. Chemical staining was applied to stain the cross section samples and increase the

contrast of layers in TEM. The TEM images of cross sections of fibers were captured with a JEOL 2000FX TEM. To verify the tri-layered structure in single electrospun gelatin/PCL/PLGA fibers, the fibers were dyed with Rhodamine B and observed in super-resolution structured illumination microscopy (SR-SIM).

4.3 Results and Discussion

4.3.1 Coaxial Electrospinning of Gelatin/PLGA Core-shell Structured Nanofibers

Coaxial electrospun gelatin/PLGA nanofibers were fabricated using PLGA as the shell material and gelatin as the core material. SEM images were obtained to investigate the morphology of nanofibers collected with "collector I" described in Chapter 2. As shown in Figure 4.1, coaxial electrospun gelatin/PLGA nanofibers have a smooth fiber surface. Using Image J, the average diameter of gelatin/PLGA nanofibers was calculated to be 1.2 μm.

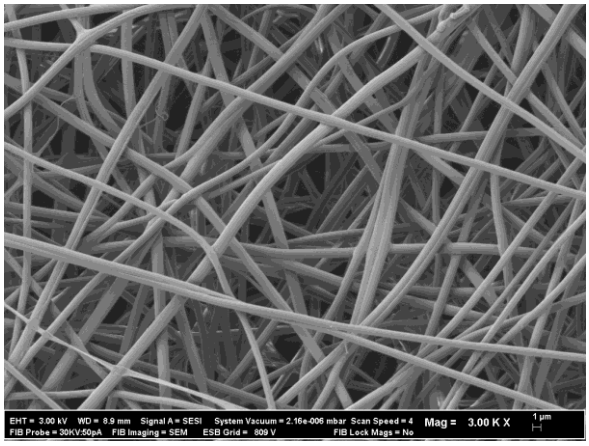

Figure 4.1 SEM image of coaxial electrospun gelatin/PLGA nanofibers

As mentioned in Chapter 3, OsO_4 selectively stains gelatin with no effects on PCL. Here, OsO_4 was used as a staining agent to increase the contrast between gelatin and PLGA layers since PLGA is not stained by OsO_4. To prepare a thin cross section of a single fiber, several gold-coated fibers were mounted onto the aluminum stub with double sided carbon tape and the stub was loaded into the FIB-SEM chamber. Palladium was used to coat a selected area on the fiber to protect the fiber during the milling process. A focused ion beam was used to cut and mill the fiber in order to get thin cross sections. A cross section was picked up and transferred with a needle, and finally attached to a special TEM grid. The cross section sample of fiber was first investigated with TEM and then stained with OsO_4 vapor overnight. After staining, we investigated the cross section sample in TEM again. Figure 4.2 shows the TEM image of a cross section sample before (Figure 4.2a) and after (Figure 4.2b) staining. The fiber cross section is marked with a red circle. The difference between the two TEM images is that the center of the sample became dark after staining with OsO_4. These results indicate that the center part of the fiber was stained by OsO_4 while the outer part was not, providing convincing evidence for the existence of a gelatin core and a PLGA shell.

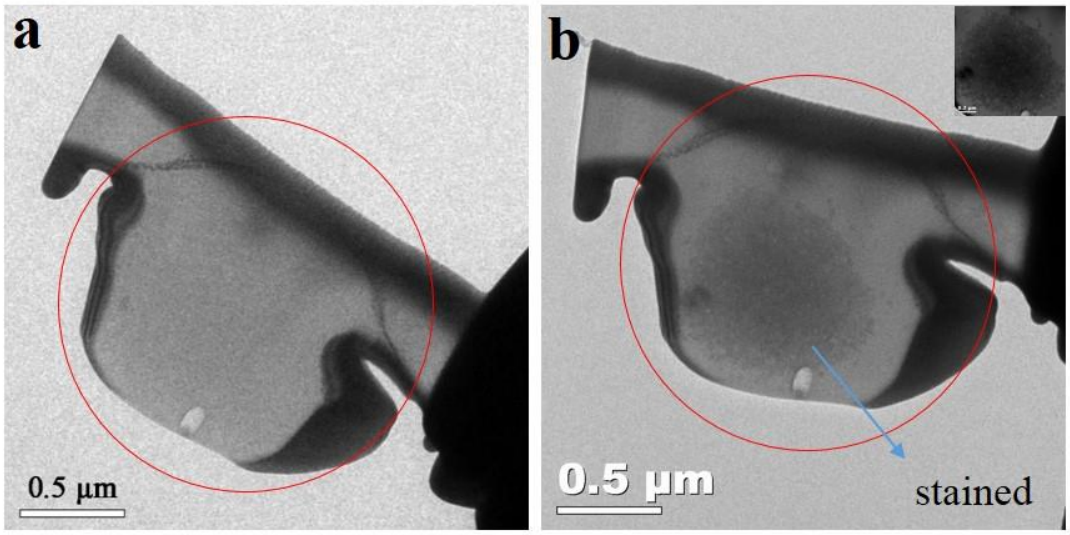

Figure 4.2 TEM images of a cross section of coaxial electrospun gelatin/PLGA nanofibers. a: before staining; **b**: after staining with OsO_4

4.3.2 Coaxial Electrospinning of PCL/PLGA Core-shell Structured Nanofibers

Coaxial electrospun PCL/PLGA nanofibers were fabricated using PLGA as the shell material and PCL as the core material. Figure 4.3 is an SEM image showing the random nanofibers collected with "collector I" previously described in Chapter 2. From the SEM image, it is clear that coaxial electrospun PCL/PLGA nanofibers have a smooth fiber surface and uniform diameter distribution. Using Image J, the average diameter of PCL/PLGA nanofibers was determined to be 1.15 µm.

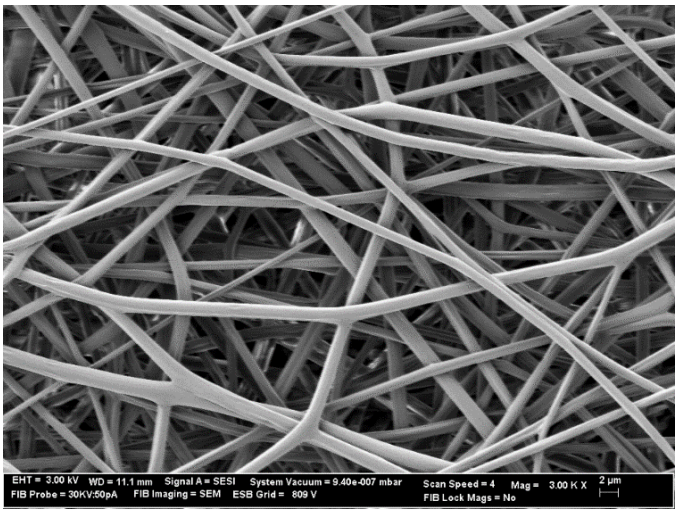

Figure 4.3 SEM image of coaxial electrospun PCL/PLGA nanofibers

It is difficult to tell the difference between PLGA and PCL layers under TEM even with chemical staining since neither PLGA nor PCL could be stained with OsO_4 or RuO_4. In order to observe the core-shell structure, we used FIB to produce a cross section of a fiber by cutting and milling and investigated it with SEM. Figure 4.4 shows the clear interface between PCL and PLGA layers. Since the polymer solutions used for PCL/PLGA coaxial electrospinning are miscible in each other, it is possible that there is diffusion between the different solutions and mixing of different polymers. However, there is currently a disagreement with respect to this issue. Sun et al.[13] claimed that no diffusion should take place between the core and shell solutions as the bending instability time was much shorter than diffusion time and fiber drawing ratio was high enough to prevent core-shell material diffusion. In our study, the interface between core and shell layers shown in

Figure 4.4 supported this claim of Sun concerning the lack of diffusion in coaxial electrospinning.

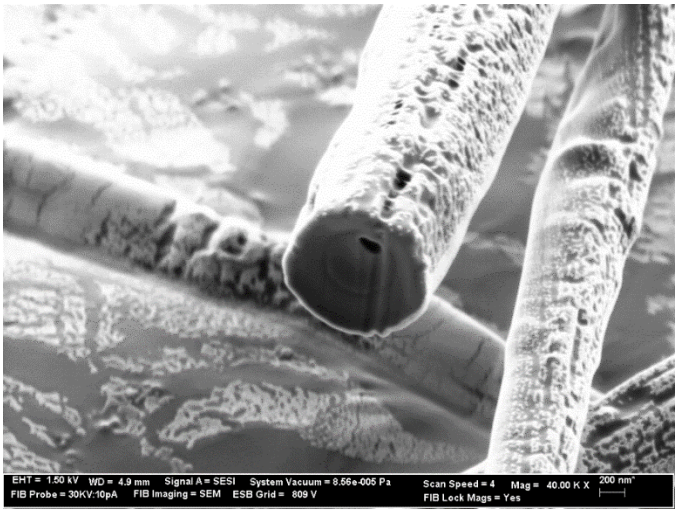

Figure 4.4 FIB-SEM image of coaxial electrospun PCL/PLGA nanofibers

4.3.3 Coaxial Electrospinning of Gelatin/PCL/PLGA Tri-layer Structured Nanofibers

Coaxial electrospun tri-component, tri-layered gelatin/PCL/PLGA nanofibers were fabricated using PLGA as the shell layer, PCL as the intermediate layer and gelatin as the core layer. The morphology of nanofibers was investigated with SEM. From Figure 4.5, the coaxial electrospun gelatin/PCL/PLGA nanofibers are uniform and free of bead defects. The average diameter of the tri-component, coaxial nanofibers is 1.5 μm.

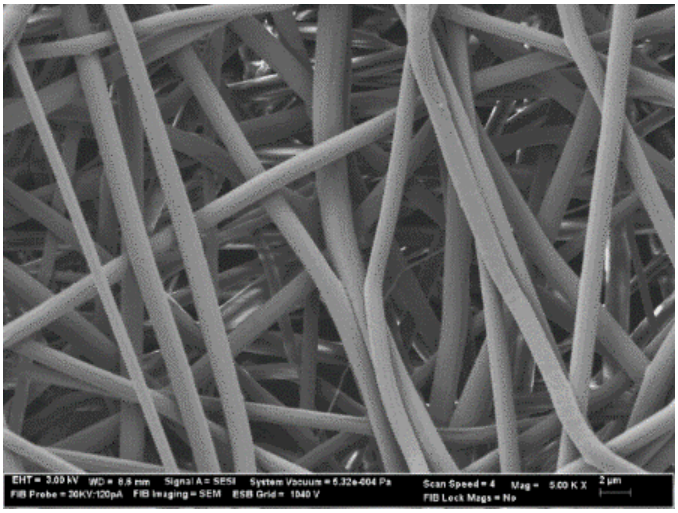

Figure 4.5 SEM image of coaxial electrospun gelatin/PCL/PLGA fibers

In Chapter 3, the difficulties of characterizing the tri-layered structure in gelatin/PCL/gelatin polymeric nanofibers were discussed. One of the difficulties encountered in the characterization of the inner structure in coaxial electrospun polymeric nanofibers is sample preparation. For TEM, cryo-microtoming is required to prepare thin cross section samples, and even with thin cross sections samples it is difficult to create contrast between PLGA and PCL layers using chemical staining agents. For FIB-SEM, effects from the ion beam during the milling process have to be avoided to get exact results. To prove the tri-layered, coaxial structure of gelatin/PCL/PLGA nanofibers, SR-SIM was employed since the preparation of a sample for SR-SIM is easy and no artifacts are induced during the sample preparation process. Rhodamine B solution was added to both shell PLGA and core gelatin solutions and mixed for 1 hr to get uniform distribution of the dye.

The coaxial electrospining process was similar to that described section in section 4.2.2.3 except for the collection of nanofibers. A No.1.5 glass coverslip was attached to the aluminum foil collector to gather some nanofibers and then the coverslip with fibers was transferred to SR-SIM for observation.

From the SR-SIM images shown in Figure 4.6b, it is obvious that there are two fibers O_1 and O_2 and each of them shows three florescent red lines. As described in 3.3.3, the two outermost florescent red lines result from the dyed PLGA shell while the central florescent line results from the dyed gelatin core. The nonfluorescent area between the red lines is the undyed PCL intermediate layer, which does not fluoresce. The florescent intensities of fiber A are high enough for observation, while the florescence intensities of fiber B are not. To confirm the tri-layer structure of fiber B, the florescence intensities were measured across the fiber (arrow E). As shown in Figure 4.6a, there are three peaks indicating the existence of three florescent lines. The red color of the florescent line was replaced with white color to increase the contrast as shown in Figure 4.6c for better visual effects. D_1 and D_2 are two points picked randomly on the fibers (D_1 was the intersection of green line and fiber O_1; D_2 was the intersection of red line and fiber O_2). The florescent results of cross sections at D_1 and D_2 were shown as D_1" and D_2" respectively. Hence, the fluorescence of these cross sections also confirms the existence of a tri-layered structure in the fiber.

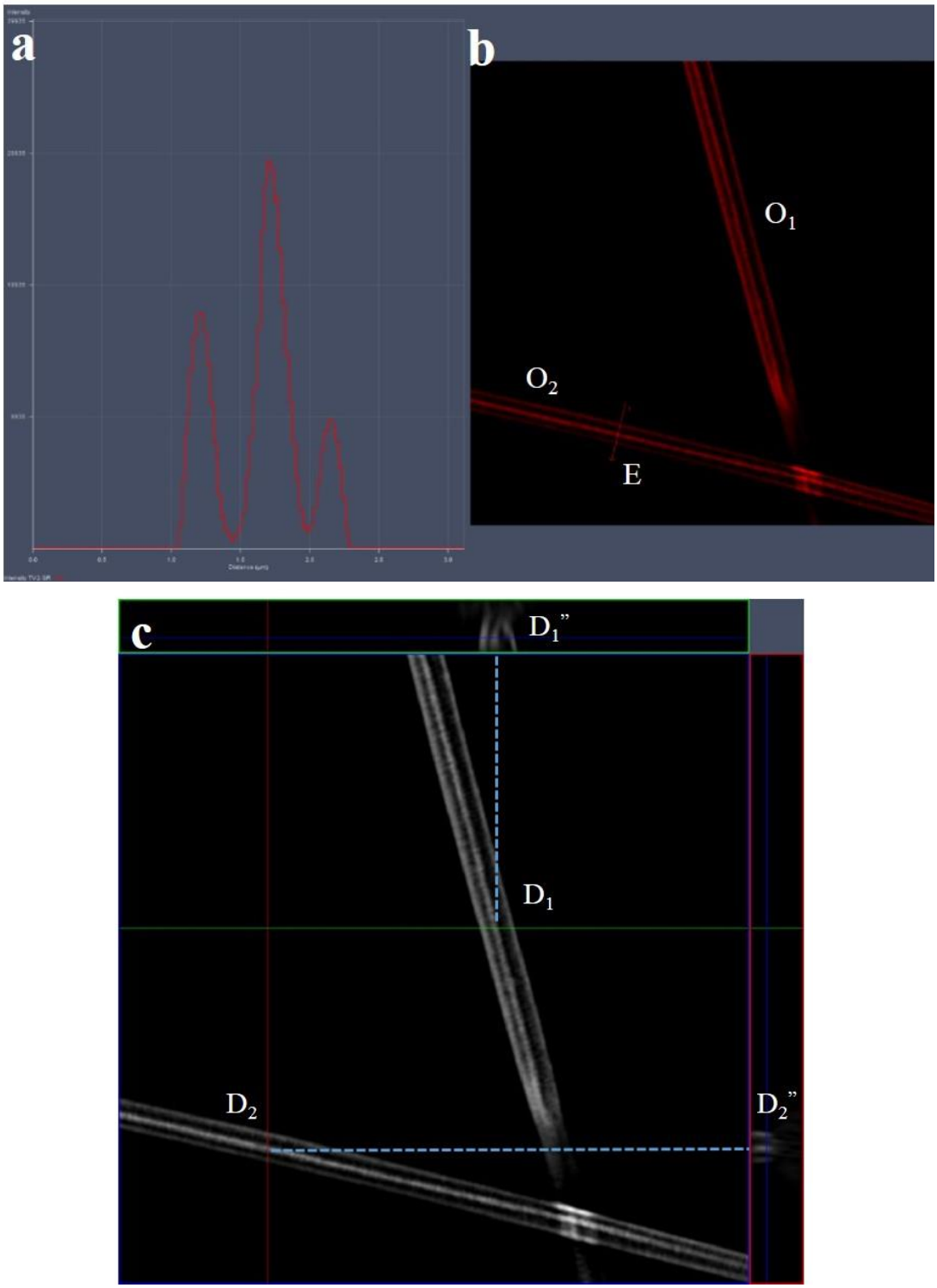

Figure 4.6 SR-SIM image of coaxial electrospun gelatin/PCL/PLGA fiber

4.4 Conclusions

To create tri-component, tri-layered polymeric ABC nanofibers with coaxial electrospinning, PLGA was selected as the third component of the material system. Initially, core-shell structured gelatin/PLGA and PCL/PLGA nanofibers were fabricated by a customized coaxial electrospinning setup. The fiber morphology was observed with SEM, while the core-shell structures were characterized by cross section TEM and FIB-SEM. Then, tri-layer structured, coaxial gelatin/PCL/PLGA biodegradable nanofibers were successfully fabricated with a three needle coaxial electrospinning setup. The smooth fiber surfaces were observed with SEM and their fiber diameters measured. Instead of characterizing the inner structure in gelatin/PCL/PLGA nanofibers with TEM or FIB-SEM, the tri-layer structure was demonstrated simply with SR-SIM. Compared to other techniques, the sample preparation for SR-SIM is much easier and this technique proved to be an efficient way to demonstrate the presence of a multi-layered structure in a single polymeric fiber. It should be pointed out that the resolution of the SR-SIM is limited (lateral resolution of 120 nm and axial resolution of 300 nm), so that SR-SIM is useful and efficient for observing multilayered fibers with layer thickness larger than 200 nm. The resolution of SR-SIM is not high enough for investigating nanofibers with very small diameters and thin multilayers.

REFERENCES

1. Bini, T. B.; Gao, S.; Wang, S.; Ramakrishna, S. *Journal of Materials Science* **2006,** 41, (19), 6453-6459.
2. Shin, H. J.; Lee, C. H.; Cho, I. H.; Kim, Y. J.; Lee, Y. J.; Kim, I. A.; Park, K. D.; Yui, N.; Shin, J. W. *Journal of Biomaterials Science-Polymer Edition* **2006,** 17, (1-2), 103-119.
3. Cantara, S. I.; Soscia, D. A.; Sequeira, S. J.; Jean-Gilles, R. P.; Castracane, J.; Larsen, M. *Biomaterials* **2012,** 33, (33), 8372-8382.
4. Liu, H.; Wang, S. D.; Qi, N. *Journal of Applied Polymer Science* **2012,** 125, E468-E476.
5. Makadia, H. K.; Siegel, S. J. *Polymers* **2011,** 3, (3), 1377-1397.
6. Dong, Y. X.; Liao, S.; Ngiam, M.; Chan, C. K.; Ramakrishna, S. *Tissue Engineering Part B-Reviews* **2009,** 15, (3), 333-351.
7. Loo, S. C. J.; Tan, Z. Y. S.; Chow, Y. J.; Lin, S. L. I. *Journal of Pharmaceutical Sciences* **2010,** 99, (7), 3060-3071.
8. Dong, Y. X.; Yong, T.; Liao, S.; Chan, C. K.; Stevens, M. M.; Ramakrishna, S. *Tissue Engineering Part A* **2010,** 16, (1), 283-298.
9. Gentile, P.; Chiono, V.; Carmagnola, I.; Hatton, P. V. *International Journal of Molecular Sciences* **2014,** 15, (3), 3640-3659.
10. Versypt, A. N. F.; Pack, D. W.; Braatz, R. D. *Journal of Controlled Release* **2013,** 165, (1), 29-37.

11. Zhang, H.; Zhao, C. G.; Zhao, Y. H.; Tang, G. W.; Yuan, X. Y. *Science China-Chemistry* **2010,** 53, (6), 1246-1254.

12. Wang, C.; Yan, K. W.; Lin, Y. D.; Hsieh, P. C. H. *Macromolecules* **2010,** 43, 6389–6397.

13. Sun, Z. C.; Zussman, E.; Yarin, A. L.; Wendorff, J. H.; Greiner, A. *Advanced Materials* **2003,** 15, (22), 1929-1932.

Chapter 5

CHARACTERIZATION OF COAXIAL ELECTROSPUN NANOFIBER WITH NANO-IR

5.1 Introduction

Although infrared (IR) spectroscopy is widely used to identify chemical species in polymer science, the application of conventional IR spectroscopy is limited at the nanoscale level since the spatial resolution is restricted due to optical diffraction limitation. Generally, the practical spatial resolution range of transmission FTIR is 10-30 μm and this value drops to 3-10 μm for attenuated total reflectance (ATR) spectroscopy. In contrast, atomic force microscopy (AFM) has wide application in nanoscale research areas, especially for measurement of surface roughness, studying mechanical and electrical properties, and evaluating interactions between molecules. However, the inability to characterize samples chemically limits applications of AFM. The invention and development of a new technique, AFM-IR or nano-IR, overcomes the spatial resolution limitation of conventional IR spectroscopy from many micrometers to 100 nm or even less and hence expands the application of both IR spectroscopy and AFM in many research areas[1-4].

Nano-IR combines AFM and IR spectroscopy together to obtain IR spectra and IR absorption images at the nanoscale. This technique is based on the photothermal induced resonance (PTIR) effect[5]. Nano-IR uses an AFM cantilever tip to detect the

thermal expansion induced by laser heating, thus measuring IR absorption below the conventional diffraction limit. Figure 5.1 is a schematic diagram of a nano-IR system with sample configuration and data transformation[2, 4]. Thin samples are placed on the top of an IR transparent subtract. A pulsed, tunable IR source is applied to illuminate the sample from the top side and excite molecular vibrations. When the sample absorbs radiation at a specific wavelength, it heats up and the heat causes a rapid thermal expansion of the material in the absorbing region. An AFM cantilever tip is in contact with the sample to detect the thermal expansion and thus the expansion signal results in resonant oscillations of the cantilever. The induced oscillations decay in a characteristic ring down which can be analyzed via fast Fourier transform (FFT) to extract the amplitudes and frequencies of the cantilever oscillations. The cantilever ring-down amplitude in the FFT spectrum is measured for each specific wavelength. The IR spectrum is obtained by plotting the amplitudes of the cantilever ring-down on the y axis as a function of the source laser wavenumber on the x axis[1, 4]. The spectra generated at the nanoscale level with nano-IR are similar to spectra collected in the bulk with conventional FTIR. In addition, by tuning and fixing the IR laser to a single wavenumber matching a specific absorption band of samples, nano-IR could be used to image or map IR absorption and contact resonance frequency of the cantilever across the sample. Another function of nano-IR is to perform thermal measurements and analyses at the nanoscale level with special probe.

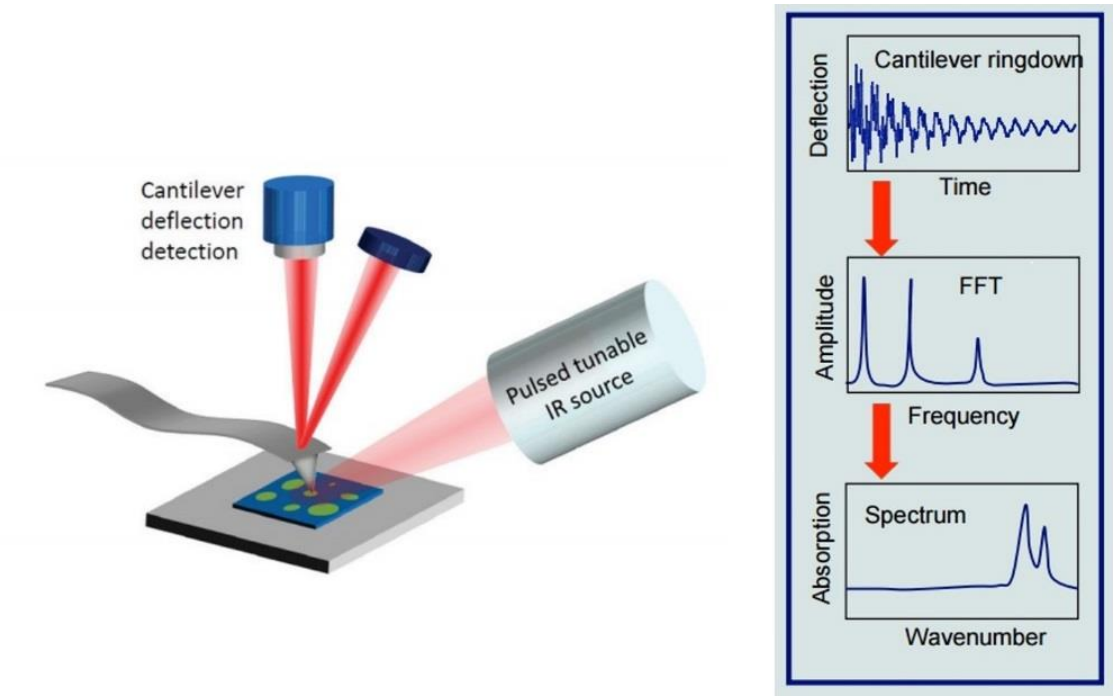

Figure 5.1 Schematic diagram of the NanoIR2 instrument.

The ability to chemically characterize specimens at nanoscale spatial resolution using the nano-IR technique has opened up various applications. It has been reported that this technique has been used to study the interface of polymer composites[2] and blends[6], the composition and structure of biological specimens[7, 8], nanostructural features in conducting polymers for photocatalysis[9] and organic photovoltaic cells[3], and molecular interactions and distributions/dispersions of drugs[10]. In these studies, the information related to interface, composition and structure in samples is acquired by performing chemical spectroscopy at different locations in the sample. The distribution and stiffness of different components or species are typically illustrated by mapping IR absorption and frequency of the cantilever resonance at a specific wavenumber. Besides

compositional analysis, the nano-IR technique has been applied to study the molecular orientation in electrospun nanofibers by polarizing the IR laser source in the two orthogonal directions[1]. Finally, with a ThermaLever self-heating AFM probe, nano-IR has been used as a nano-TA to make thermal transition measurements and analysis on polymer films and blends with nanoscale spatial resolution[11].

5.2 Experimental Section

5.2.1 Sample Preparation with Cryo-microtomy

To characterize the molecular structure in a single fiber with the top-down nano-IR, microtomy and cryo-microtomy are needed to prepare thin cross sections of fibers. The optimal thickness of samples for nano-IR is different with the sample types. The optimal thickness range for microtomed sections is between 200 nm-500 nm. To prepare cross sections of fibers, electrospun fibrous mats (0.3 cm x 0.8 cm, 0.5 mm thick) were placed into cavities (15 mm x 7 mm x 4 mm deep) of a microtome embedding mold (purchased from EMSdiasum) and liquid resin with hardener (Epo-Fix, purchased from EMSdiasum) was injected into the cavities to embed the fiber mats. After 48 hrs of curing, the resin reached the required hardness. The embedded sample was first trimmed at room temperature with the regular microtome (R.J.) to get a cutting stub. Then the stub was transferred to cryo-microtome (Leica). To get thin and large cross section samples, operational parameters such as temperature, thickness and cutting speed are needed to be set properly before cutting. After a thin cross section was generated, it was transferred with a piece of hair from the edge of the diamond knife onto the top of a nano-IR2 substrate.

5.2.2 Nano-IR Analysis

The substrate with a thin cross section sample was placed on the sample stage and loaded. An AFM probe was installed, aligned and brought down towards the sample. After laser and detector alignment, the AFM probe was engaged into controlled contact with the sample surface. Figure 5.2 shows the photograph of a thin section sample under AFM probe tip.

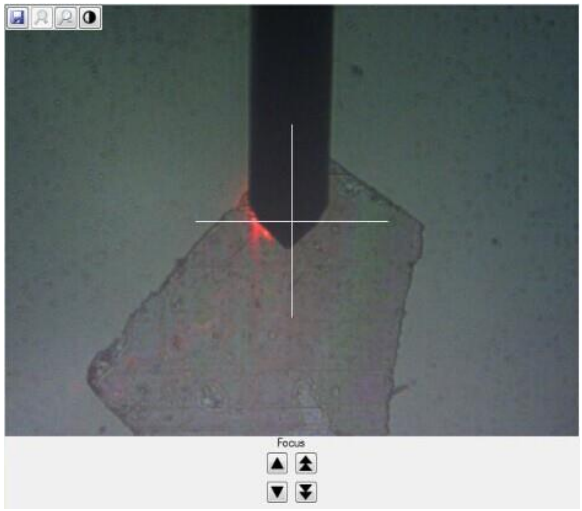

Figure 5.2 Photograph of a pierce of cryo-microtomed sample under AFM cantilever

The IR laser was aligned and the IR focus was optimized to get clear peaks in FFT mode, which shows the tip resonance frequencies. The frequency center was set based on the FFT peaks. Other general parameters, such as power, were set based on the thickness of the sample. AFM imaging was performed to look for and locate proper cross

sections of fibers on the sample. After moving the probe to the appropriate position, spectral parameters were set. In our study, nano-IR2 spectra were collected on core-shell samples over a range of 1440–1800 cm^{-1} with a resolution of 4 cm^{-1} and an accumulation of 128 scans for each designated position. Since gelatin and PCL have specific functional group absorption bands at 1650 and 1730 cm^{-1} respectively, the IR laser was tuned to 1650 cm^{-1} and then 1730 cm^{-1}. IR absorption, AFM topography and resonance frequency of the cantilever were mapped at each wavenumber with a scan rate of 0.1 Hz and an accumulation of 16 scans.

5.3 Results and Discussion

Now we will describe some results on bi-component coaxial samples with gelatin as the shell and PCL as the core. Figure 5.3a is an AFM topographical image of a fiber cross section in epoxy. Ten points on the cross section were selected and spectra taken at each position. The locations where spectra were collected are marked in different colors and named with a-e and a'-e' from inside to outside. The corresponding spectrum of each position is shown in Figure 5.3b and marked with the same color and name as the position in topographical image.

The spectral range in Figure 5.3b is between 1440 cm^{-1} to 1800 cm^{-1}. In this region, gelatin has a specific absorption peak at around 1650 cm^{-1} due to the amide I group. PCL has a specific absorption peak at around 1730 cm^{-1} corresponding to the carbonyl group. Epoxy has absorbance peaks at 1510 cm^{-1} and 1607 cm^{-1} due to the aromatic C=C stretching bands, respectively. The main absorption bands and assignments are listed in Table 5.1.

Table 5.1 Main absorption bands and their assignments

Band (cm^{-1})	Assignment
1730	PCL-carbonyl group[12]
1650	Gelatin-amide I C=O stretching[13]
1510	Epoxy- benzene C-C stretching[14]
1608	Epoxy- benzene C=C-H stretching[14]

In Figure 5.3a, positions a&a' are located in the center of sample. Spectra a&a' in Figure 5.3b have only one absorption peak, at 1730 cm^{-1}, indicating that pure PCL is located in points a&a'. In spectra b&b', there is a strong absorption at 1730 cm^{-1} and a weak absorption at 1660 cm^{-1} which indicates the existence of PCL and traces of gelatin. Hence, positons b&b' should be located on the interface of PCL and gelatin. Spectra c&c' show strong absorption peaks at 1660, 1608 and 1510 cm^{-1}, which suggest the existence of both gelatin and epoxy. Positions c&c' in Figure 5.3a should be located on the interface between the gelatin and epoxy. Spectra d&d' have a very weak peak at 1660 cm^{-1} but strong peaks at 1608 and 1510 cm^{-1}, indicating the edge of the fiber. Spectra e&e' only have peaks at 1608 and 1510 cm^{-1}, showing that pure epoxy is located in positions e&e'. Hence, the spectra generated with the nano-IR2 demonstrate not only the existence of PCL and gelatin

in the coaxial nanofibers but also prove the existence of a core-shell structure in the electrospun fiber.

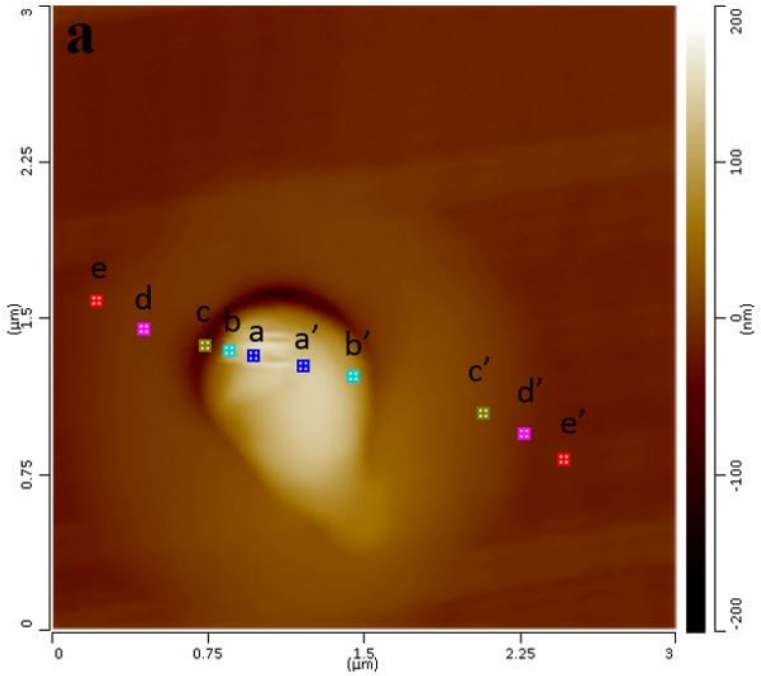

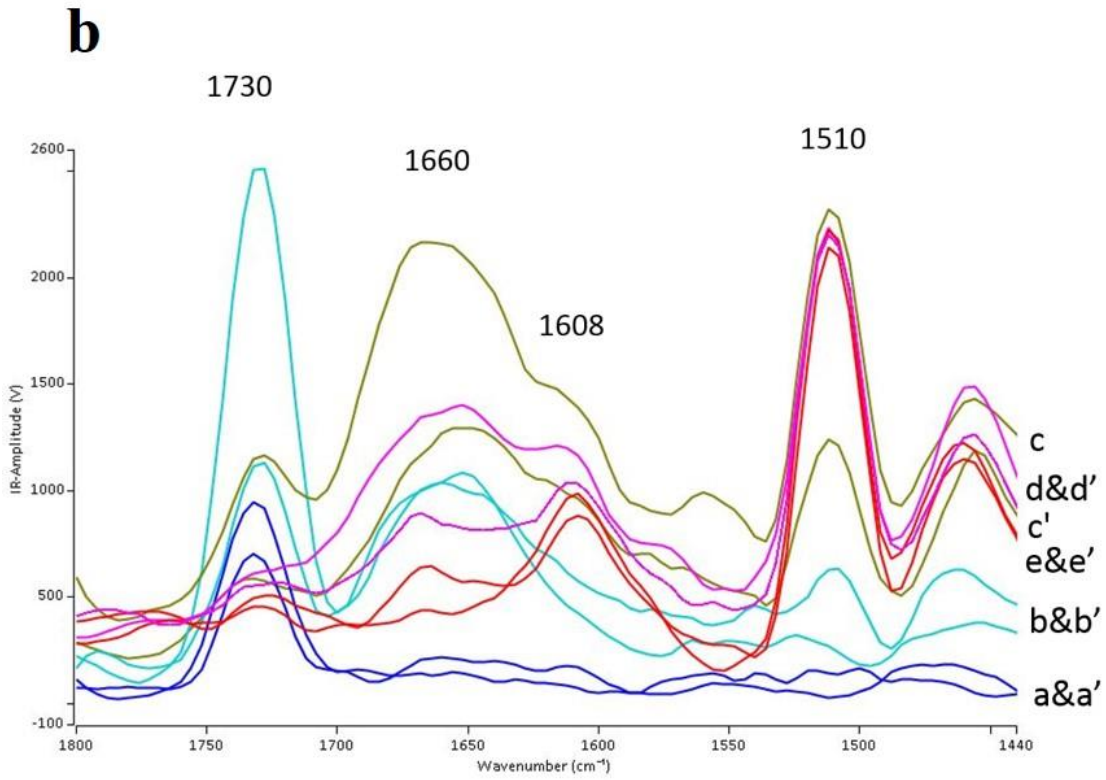

Figure 5.3 IR spectra of the cross section of a PCL/gelatin fiber. a: topographical image (3.0 x 3.0 μm^2, color scale is 200 nm); **b**: IR spectra obtained at points designated in 5.3a.

The IR laser was tuned to a single wavelength to simultaneously map surface topography, mechanical properties, and IR absorption in selected absorption bands. Figure 5.4a shows the IR absorption image with the IR laser source held at 1650 cm^{-1} where gelatin has an absorption due to the amide I group. Figure 5.4b and 5.4c are the corresponding AFM topographical image and cantilever resonant frequency image. The absorption image, AFM topography and frequency image at 1730 cm^{-1} where PCL has strong absorption are shown in Figure 5.5. In Figure 5.4a and 5.5a, the green to pink color

bar stands for the variations in absorption. The region in the pink in Figure 5.4a shows significant IR absorbance at 1650 cm^{-1}, indicating not only the existence of the gelatin component but also the ring distribution of gelatin in the fiber. The pink zone in Figure 5.5a shows maximum absorption at 1730 cm^{-1}, illustrating the existence of the PCL component and its distribution in the fiber. Comparing Figure 5.4b and 5.5b, it is obvious that all of the mapping images are collected on the same cross-sectional area. By combining IR absorption images at 1650 cm^{-1} and 1730 cm^{-1}, a bi-component core-shell structure in a single electrospun fiber is clearly observed. The variation of oscillation frequencies is related to changes of mechanical stiffness across the sample. Figure 5.4c and 5.5c shows that the PCL region is softer than the gelatin region and the surrounding epoxy.

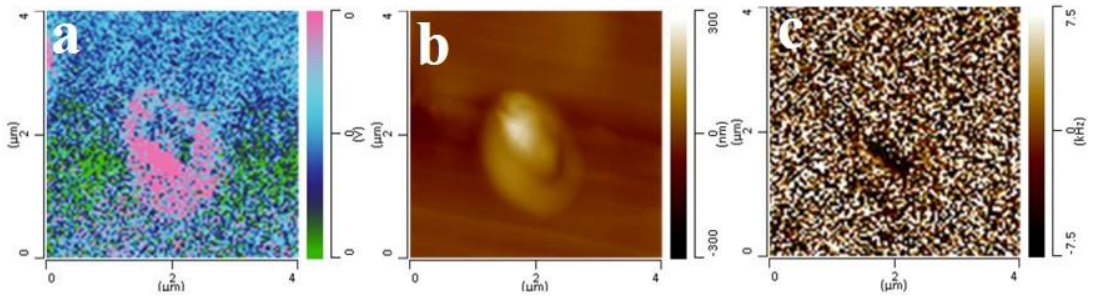

Figure 5.4 IR absorption at 1650 cm^{-1}. a: IR absorption image; **b**: AFM topographical image (4.0x4.0 μm^2, color scale is 300 nm); **c**: stiffness image.

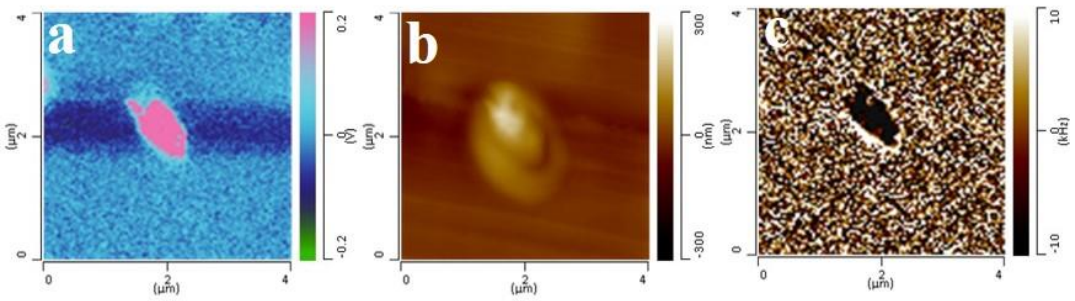

Figure 5.5 IR absorption at 1730 cm^{-1}. a: IR absorption image; **b**: AFM topographical image (4.0x4.0 μm^2， color scale is 300 nm); **c**: stiffness image.

5.4 Conclusions

We have demonstrated the application of a new technique, nano-IR, to the characterization of coaxial electrospun nanofibers. The results collected on the cross sections of samples demonstrate the bi-component core-shell structure in a single fiber spectroscopically. The IR absorption images at a fixed laser frequency demonstrates the existence of a core-shell structure in a single electrospun coaxial nanofiber. Our study suggests that the high spatial resolution of the nano-IR enables the chemical characterization of the internal structure of electrospun nanofibers. However, the preparation of cross section samples is critical for good nano-IR results. The application of nano-IR to tri-component tri-layered coaxial electrospun fibers was considerably more difficult due to the complexity of the preparation of cross section fiber samples with cryo-microtomy and further efforts are needed to overcome these obstacles.

REFERENCES

1. Dazzi, A.; Prater, C. B.; Hu, Q. C.; Chase, D. B.; Rabolt, J. F.; Marcott, C. *Applied Spectroscopy* **2012,** 66, (12), 1365-1384.
2. Marcott, C.; Lo, M.; Hu, Q. C.; Dillon, E.; Kjoller, K.; Prater, C. B. *American Laboratory* **2014,** 46, (3), 23-25.
3. Marcott, C.; Awatani, T.; Ye, J.; Gerrard, D.; Lo, M.; Kjollerd, K. *Spectroscopy Europe* **2014,** 26, (1), 19-23.
4. Marcotta, C.; Lo, M.; Kjoller, K.; Pratera, C.; Gerrard, D. P. *Microscopy Today* **2012,** 20, (06), 16-21.
5. Dazzi, A., SUB-100-Nanometer Infrared Spectroscopy and Imaging Based on a Near-Field Photothermal Technique ("PTIR"). In *Biomedical Vibrational Spectroscopy*, Lasch, P.; Kneipp, J., Eds. John Wiley & Sons, Inc.: 2007; pp 291-312.
6. Van Eerdenbrugh, B.; Lo, M.; Kjoller, K.; Marcott, C.; Taylor, L. S. *Molecular Pharmaceutics* **2012,** 9, (5), 1459-1469.
7. Dazzi, A.; Policar, C. *Biointerface Characterization by Advanced IR Spectroscopy* **2011**, 245-278.
8. Gourion-Arsiquaud, S.; Marcott, C.; Hu, Q. C.; Boskey, A. L. *Calcified Tissue International* **2014,** 95, (5), 413-418.
9. Ghosh, S.; Kouame, N. A.; Ramos, L.; Remita, S.; Dazzi, A.; Deniset-Besseau, A.; Beaunier, P.; Goubard, F.; Aubert, P. H.; Remita, H. *Nature Materials* **2015,** 14, (5), 505-511.

10. Van Eerdenbrugh, B.; Lo, M.; Kjoller, K.; Marcott, C.; Taylor, L. S. *Journal of Pharmaceutical Sciences* **2012,** 101, (6), 2066-2073.

11. Eby, T.; Gundusharma, U.; Lo, M.; Sahagian, K.; Marcott, C.; Kjoller, K. *Spectroscopy Europe* **2012,** 24, (3), 18-21.

12. Elzein, T.; Nasser-Eddine, M.; Delaite, C.; Bistac, S.; Dumas, P. *Journal of Colloid and Interface Science* **2004,** 273, (2), 381-387.

13. Muyonga, J. H.; Cole, C. G. B.; Duodu, K. G. *Food Chemistry* **2004,** 86, (3), 325-332.

14. Gonz áez, M. G.; Baselga, J.; Cabanelas, J. C., Applications of FTIR on Epoxy Resins –Identification, Monitoring the Curing, Process, Phase Separation and Water Uptake. In *Infrared Spectroscopy – Materials Science, Engineering and Technology*, INTECH Open Access Publisher: 2012; pp 266-269.

Chapter 6

APPLICATION OF COAXIAL ELECTROSPINNING TO TISSUE ENGINEERING

6.1 Introduction

6.1.1 Coaxial Electrospinning and Tissue Engineering

Biocompatible scaffolds are generally considered as one of the key elements in engineering living tissues. In the past 10-15 years, electrospinning has become a very popular method for the fabrication of nanofibrous polymeric scaffolds since electrospun polymeric mats provide the physical structure and mechanical properties necessary for cell growth[1, 2]. However, to successfully mimic the extracellular matrix (ECM), an ideal scaffold should not only provide mechanical support for cells but also provide biological signals, such as growth factors and DNA, to guide the cell regeneration process. Many efforts have contributed to the development of scaffolds with bioactive properties by combining scaffolds and fragile, water-soluble bioactive agents within the same structure[3]. Generally, surface functionalization of electrospun fibrous mats to immobilize the bioactive agents on the fibers by physical adsorption or covalent immobilization is one important method to create a bioactive scaffold[4]. However, with surface modification there are some challenges involving increasing loading efficiency and achieving accurate release control. Another way to develop a bioactive scaffold is to incorporate bioactive agents into

the scaffold directly by modified electrospinning techniques, including blend electrospinning, emulsion electrospinning and coaxial electrospinning. In particular, coaxial electrospinning has been proven to be an effective and robust technique to develop bioactive scaffolds in a one-step process[5, 6].

There are two main concerns in the fabrication of bioactive scaffolds with coaxial electrospinning: loss of bioactivity, and controlled release. Water-soluble bioactive agents, such as growth factors, are fragile and denature readily when exposed to harsh organic solvents[7, 8]. In coaxial electrospinning, the solvents for shell layer polymers are generally organic solvents, while the bioactive agents are carried by the aqueous core solution. To avoid contact between bioactive agents and harsh organics, solvents for shell solutions have to be immiscible with H_2O so that there is minimal diffusion and poor mixing between shell and core solvents. Another way to protect growth factors is to introduce heparin into the core solution. Heparin is a highly sulfated glycosaminoglycan which could bind growth factors through electrostatic interaction. The heparin binding could stabilize the growth factors, prevent early degradation and preserve bioactivity[9]. It has also been demonstrated that heparin could decrease the initial burst release and stabilize the release over a longer period of time[10].

The release mechanism of incorporated bioactive agents is generally thought to involve diffusion from the core to the aqueous media[3]. The shell polymeric layer would serve as a barrier and contribute to the control of timed release of the biomolecules. However, a lot of experimental results have suggested that the direct diffusion of encapsulated macromolecules in nanofibers is very difficult thus making it hard to realize

enough release in the required period via a diffusion mechanism[3, 11]. An efficient way to increase the release of biomolecules from the nanofiber is to create porous structures on the fiber by mixing a water soluble component, such as polyethylene glycol (PEG) or polyvinyl alcohol (PVOH), into the shell layer.[6] The biomolecules are also expected to release with the degradation of polymeric shell. It has been reported that proteins could be released from core-shell structured nanofibers with PLGA as the shell [12, 13]. The release behavior could be controlled by tuning the material composition as well as the degradation rate.

With proper design, careful material/solvent system selection and a proper release mechanism, coaxial electrospinning could be used to develop an ideal bioactive, nanofibrous scaffold by preventing the contact between bioactive agents and harsh solvents, mitigating the initial burst release and providing sustained release.

6.1.2 Research Design

Based on our assumption, coaxial tri-layer structured gelatin/PCL/gelatin nanofibers could be an ideal design for a tissue engineering scaffold with the capability to serve as the growth factor vehicle and provide the biocompatibility of the outer gelatin for cell attachment and proliferation. After successful spinning of coaxial gelatin/PCL/gelatin nanofibers, we started to study the potential of coaxial nanofibers on tissue engineering. However, these types of nanofibers suffered from some difficulties when used in an experimental study. There are two main challenges we need to overcome to increase the utility of coaxial, tri-layered nanofibers.

First, although gelatin is of great interest in tissue engineering due to its biological origin, excellent biodegradability and biocompatibility, the water solubility of gelatin will allow the outer layer of coaxial nanofibers to dissolve into the aqueous cell culture medium very quickly. As a result, the scaffold will lose the porous structure making it unsuitable for tissue scaffold applications.

Second, PCL, which degrades very slowly, serves as an intact barrier so that the molecules incorporated inside the PCL cannot be released via diffusion.

To improve the water resistance of gelatin and maintain the biomimetic nanofibrous morphology after water exposure, cross-linking of the gelatin outer layer of coaxial electrospun nanofibers is necessary. Gelatin can be cross-linked through either physical methods, such as dehydrothermal treatment and ultraviolet irradiation, or chemical agents, such as glutaraldehyde and D,L-glyceraldehyde.[14, 15] We chose genipin, a chemical agent with low cytotoxicity, to cross link the gelatin outer layer of coaxial electrospun nanofibers. Genipin (structure shown in Fig. 6.1) is a hydrolytic product of geniposide extracted from gardenia fruit[16]. It is soluble in ethanol, methanol and acetone, and cross-linking always occurs with vapor phase genipin. Although there are a lot of studies on the application of genipin as a natural cross linker for proteins in recent years[17, 18] as well as some assumptions[19] about the reactions during the cross linking process, the cross linking mechanism is still not well understood.

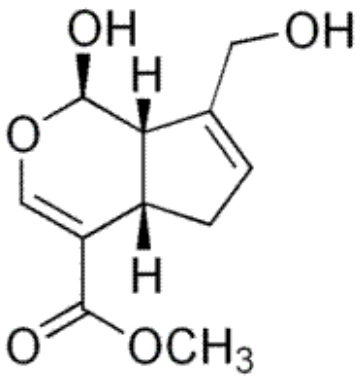

Figure 6.1 Structure of genipin

Our preliminary results show that there is no release of growth factors from the coaxial electrospun PCL/gelatin fibers after an initial burst release. According to the literature[20], the low degradation and compact internal structure of the PCL shell layer make it difficult for macromolecules to be released via diffusion. This explains our release results with PCL/gelatin fibers. There are two ways to overcome this obstacle, 1) use polymers with fast degradation rates to replace PCL as the shell material; or 2) mix PCL with porogens (water soluble material such as PEG, PVOH) to create open pores in the fibers[20].

As mentioned in Chapter 4, the degradation rate of PLGA is fast and controllable. Thus we designed experiments using PLGA to replace PCL in order to allow the growth factors to release with degradation of PLGA. PLGA is a synthetic polymer that is widely used in the biomedical area. However, most studies have only focused on the degradation of PLGA and its related release profile[21, 22 23]. The dimensional stability of PLGA based scaffolds in cell cultures has been mostly ignored in these studies. Significant

swelling and shrinkage of PLGA mats was observed in our study. The shrinkage is due to the relaxation of aligned PLGA chains which have a glass transition temperature lower than 37 ℃ in aqueous media[24]. The swelling and shrinkage make PLGA, with a fast degradation rate, unsuitable for cell culture studies. Finally, we decided to turn to the other method and use porogens to control the release of the incorporated molecules. In our study, PEG is chosen and added to the PCL solution to create pores within the PCL layer. The macromolecular release is controlled by varying the PEG percentage in the PCL layer.

6.2 Potential Application of Coaxial Electrospun PCL/Gelatin Nanofibers on Tissue Engineering

6.2.1 Design

To study the potential of coaxial electrospun gelatin/PCL/gelatin as a tissue engineering scaffold, we measured the mechanical properties of different electrospun fibrous mats by tensile testing on a Dynamic Mechanical Analyzer (DMA). The Young's modulus, ultimate tensile stress and breaking strain are derived from the stress-strain curve. Genipin was applied as a chemical agent to crosslink the gelatin layer of the tri-layer structured nanofibers. Experiments were designed and carried out to determine the optimum procedure and parameters for crosslinking of the gelatin layer. The morphology of cross linked nanofibers before and after exposure to the aqueous environment were imaged with SEM. Connective tissue growth factor (CTGF) was loaded into the coaxial PCL/gelatin nanofibers in order to study the release profile of the growth factor.

6.2.2 Experimental Section

Electrospinning: In order to study the effect of coaxial electrospinning on mechanical properties of nanofibers, three kind of nanofibrous mats were prepared: pure gelatin, pure PCL and coaxial tri-layered gelatin/PCL/gelatin. Gelatin solution (25% in TFE/H_2O) were electrospun using the regular electrospinning setup with a flow rate of 0.5 ml/h. The working distance was 25 cm and the applied voltage was 18 kV for the needle and -1 kV for the collector. To prepare single PCL nanofibers, PCL solution (11% in TFE) was electrospun at a flow rate 0.5 ml/h, with a working distance of 16 cm and applied voltages of 15 kV, -5 kV at the needle and collector respectively. The preparation of coaxial gelatin/PCL/gelatin was described in Chapter 3. CTGF (36-38 kDa) was purchased from BioVendor and loaded into the coaxial bi-layered nanofibers by mixing 40 µl CTGF (0.25 mg/ml) with the core solution at room temperature. The flow rates were kept at 0.7 ml/h and 0.15 ml/h for shell and core solutions, separately. The working distance was held at 15 cm. The applied voltage was 10 kV for the nozzle and -2 kV for the collector. SEM images were obtained to observe the morphology of the nanofibers.

Tensile testing: The tensile tests of fibrous mats were performed with a DMA. The samples were made in the form of a dog bone shape by die cutting from electrospun fibrous mats. Samples were stretched at room temperature under an extension rate of 0.05 mm/s until failure (as shown in Figure 6.2). Three different samples were tested for each kind of fibrous mat to obtain an average stress-strain behavior.

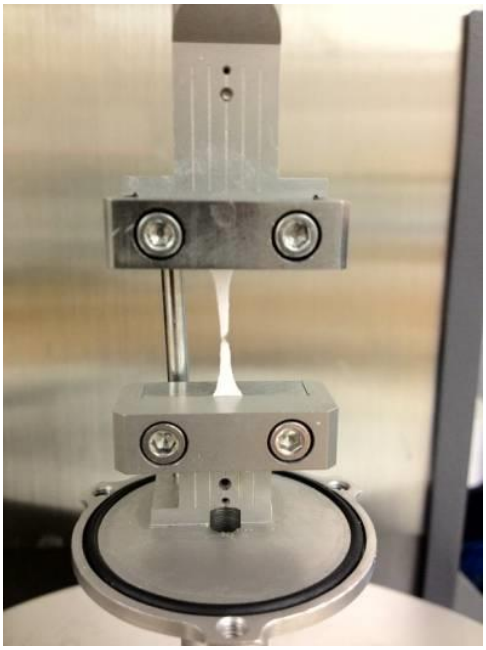

Figure 6.2 DMA test with nanofibrous sample

Crosslinking of gelatin and gelatin shell layer of coaxial nanofibers: Genipin was purchased from Challenge Bio Products Co., LTD and ethanol was purchased from Sigma Aldrich. The cross linking of gelatin occurred in two steps. Step one is the preparation of a gelatin–genipin solution: 0.2% genipin was added to the gelatin solution (17% in TFE/H_2O). The mixture was stirred for 30 min to allow preliminary crosslinking. The gelatin-genipin solution was then used as the shell solution for coaxial electrospinning of the gelatin/PCL/gelatin nanofibers. Step two is cross linking in the fibrous mat with genipin vapor: genipin was dissolved into 80% (V/V) ethanol/water to make a 1.5% wt solution. The genipin solution was poured into a 60 mm plastic Petri dish. The fiber mat was cut into 8 mm x 20 mm pieces and attached to the inside of the lid of the Petri dish and

exposed to the genipin vapor for 5 days at room temperature. After crosslinking, the samples were dried and rinsed in ethanol and dried again.

In vitro CTGF release study: CTGF release was measured and evaluated with an enzyme-linked immunosorbent assay (ELISA) kit (PeproTech). To prepare samples, the scaffolds were cut into square pieces, peeled off from the aluminum foil, weighed and numbered. The samples were submerged in the release buffer (PBS + 1 mg/ml BSA + 1 mg/ml NaN_3 + 1% Penicillin/Streptomycin) in the incubator (96 well plate). The supernatant PBS was collected for evaluation with ELISA every 3 hrs. The release test was done by Zhixiang Tong and Aidan Zerdoum.

6.2.3 Results and Discussion

6.2.3.1 Mechanical Property Studies

Three kinds of nanofibers were prepared for tensile behavior measurements. In order to exclude the effect of fiber diameter on the tensile behavior, the electrospinning parameters were optimized to get the diameters of different samples similar to each other. As shown in SEM images (Figure 6.3), the average diameters of gelatin (720 nm), PCL (790 nm) and coaxial electrospun fibers (730 nm) were very close to each other. Also, from the SEM images, one can observe that there is no particular macroscopic orientation of fibers and no trace of fiber-fiber bonding structures in each kind of sample.

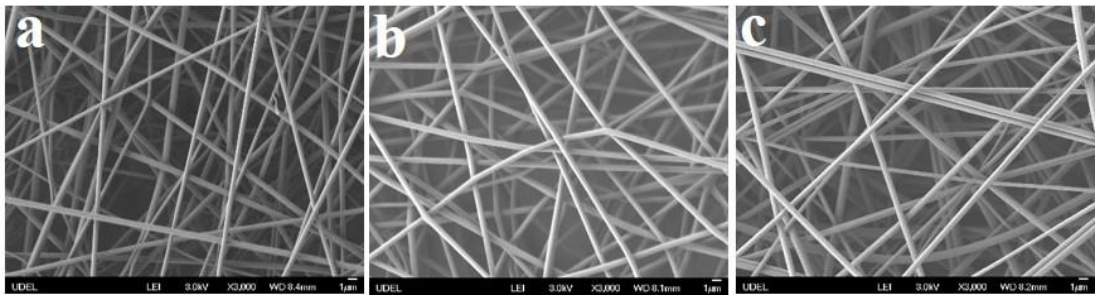

Figure 6.3 SEM images of gelatin, PCL and coaxial gelatin/PCL/gelatin electrospun nanofibers. a: gelatin nanofibers; b: PCL nanofibers; c: coaxial gelatin/PCL/gelatin nanofibers

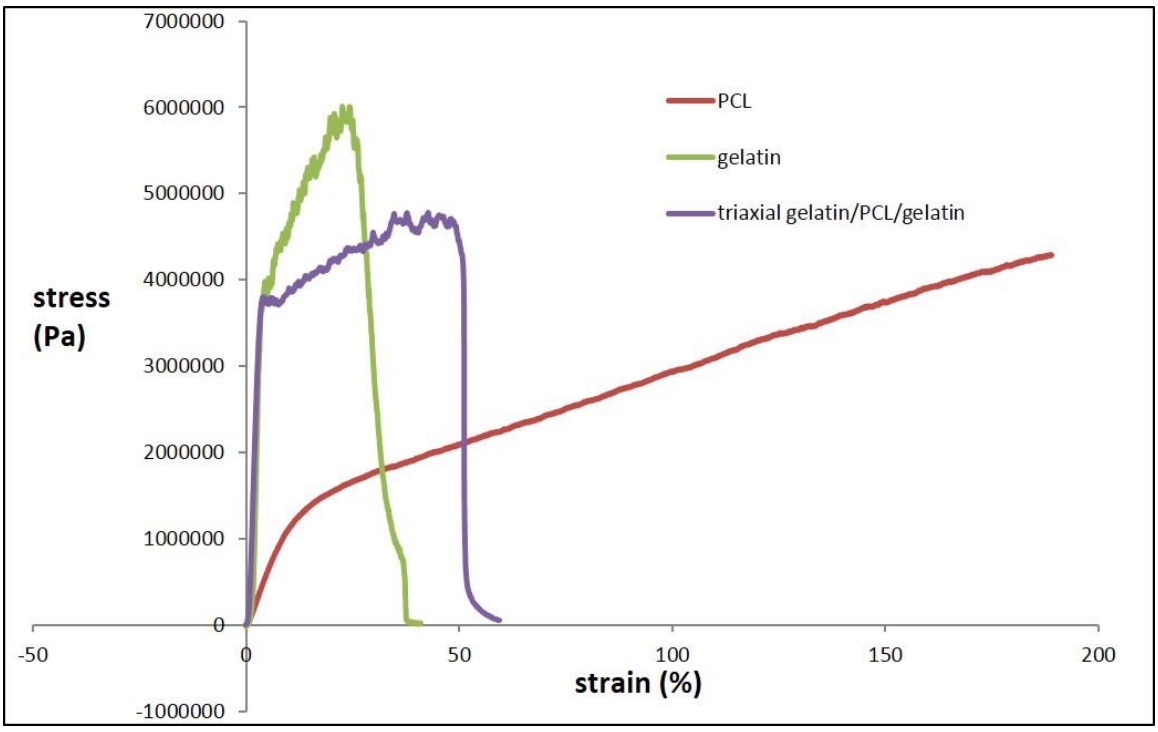

Figure 6.4 Stress-strain behavior of PCL fibrous mat, gelatin fibrous mat, and coaxial tri-layered gelatin/PCL/gelatin fibrous mat.

Table 6.1 Tensile properties of electrospun fibrous mats

Sample	Young's modulus (MPa)	Tensile stress (MPa)	Elongation at maximum stress (%)
PCL fibrous mesh	12.2 ±0.7	4.4 ±0.2	368.3 ±48.0
gelatin fibrous mesh	216.5 ±10.3	5.9 ±0.3	23.7 ±3.6
gelatin/PCL/gelatin fibrous mesh	153.9 ±7.0	4.7 ±0.3	46.5 ±4.5

Figure 6.4 presents the stress–strain curves of a pure gelatin fibrous mat, a pure PCL fibrous mat and a coaxial gelatin/PCL/gelatin fibrous mat. Various mechanical properties including tensile strength, Young's modulus and elongation to break were evaluated and are reported in Table 6.1. The mean values of the Young's modulus, tensile strength, and strain at break for the PCL fibrous mat are 12.2 ±0.7 MPa, 4.4 ±0.2 MPa and 368.3 ±48.0, respectively. These values for a PCL fibrous mat are not the same as values reported in previous literature[25, 26]. The differences in mechanical behavior are most likely due to the differences in fiber diameters, pore size and porosity between our samples and those previously reported. The mean values of the Young's modulus, tensile strength, and strain at break of gelatin fibrous mat are 216.5 ±10.3 MPa, 5.9 ±0.3 MPa and 23.7 ±3.6. These values are not the same but are consistent with those reported in literature[27]. Hence, PCL exhibits a much smaller modulus than gelatin, which indicates that PCL is elastic

while gelatin is brittle. The Young's modulus and tensile strength of the tri-layered coaxial electrospun nonwoven mats are highly improved compared to those of PCL nonwoven mats, while the elongation at break is larger than that of the gelatin nonwoven mats. From Fig. 6.4 and Table 6.1, it is clear that the mechanical properties, especially the modulus and yield stress, of electrospun fibrous PCL mats are improved through coaxial electrospinning of PCL and gelatin in a tri-layered configuration.

6.2.3.2 Cross-linking of Gelatin and Gelatin Shell Layer of the Coaxial Nanofibers.

Gelatin is soluble in water, and at room temperature, it swells and absorbs water to form a gel. When a drop of water is placed on the gelatin nanofibers, the nanofibrous structure is destroyed (Figure 6.5).

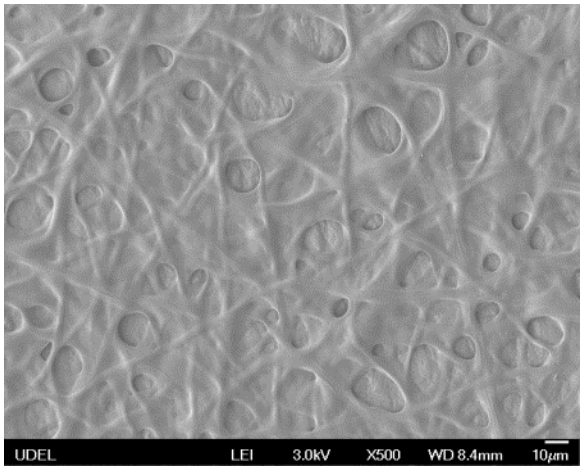

Figure 6.5 SEM image of gelatin fibers with a drop of water

To avoid the fast dissolution of gelatin in aqueous media, genipin was applied to crosslink the gelatin shell layer of coaxial tri-layered gelatin/PCL/gelatin nanofibers. The morphology of cross-linked nanofibers is shown in Figure 6.6. With crosslinking, the morphology of fibers is obviously changed, with fusion occurring at the fiber junctions, which may be the result of a water component in the genipin vapor.

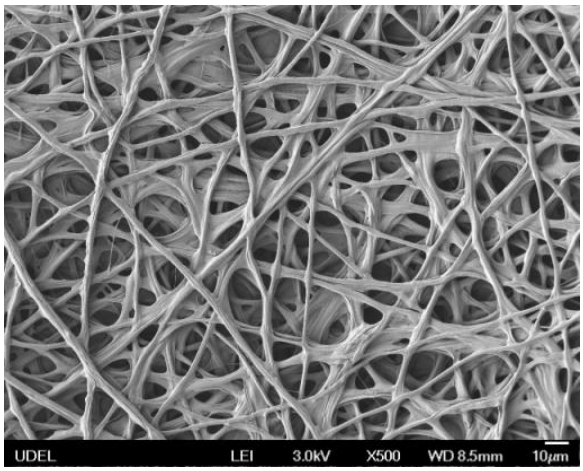

Figure 6.6 SEM image of coaxial tri-layered gelatin/PCL/gelatin nanofibers with cross linking

The cross linked mats were soaked in DI water at room temperature for a selected period of time to test the solubility of fibers in an aqueous environment. Figure 6.7 shows the morphology of the fibers after exposure to water for 2 days, 5 days, and 10 days. In Figure 6.7a, there are some fused zones and the pore structure is reduced. In Figure 6.7b, many junction zones fuse leaving smaller pores, and some fibers break into flat ribbons with the outflow of the gelatin core. In Figure 6.7c, the pores almost disappear; the

fibers fuse but do not dissolve. The cross linking indeed increases the water resistance of coaxial tri-layered electrospun fibers. However, the resistance time is not long enough and further studies are needed to achieve a better degree of crosslinking with genipin.

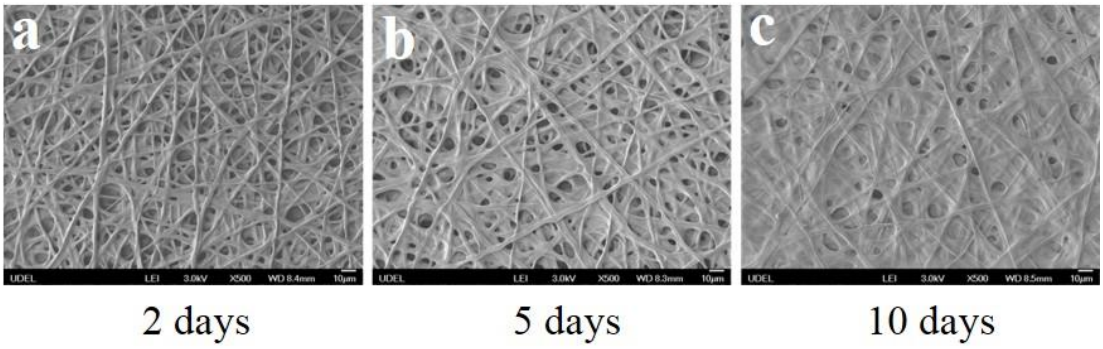

Figure 6.7 SEM images of cross linked coaxial gelatin/PCL/gelatin nanofibers with water treatment

6.2.3.3 Release of CTGF with Coaxial Gelatin/PCL Electrospun Nanofibers

Coaxial tri-layered gelatin/PCL/gelatin nanofibers have been fabricated previously. To study the growth factor release with this system, we started with the gelatin-PCL coaxial *bi-layered* system. Figure 6.8 shows the release results for CTFG from gelatin-PCL coaxial nanofibers. Only 20% of the CTGF was released over 5 hrs, which is characterized as a burst release. No release was observed after this initial release. As PCL has a compact internal structure, the remaining CTGF was probably trapped in the PCL shell. Also, the degradation rate of PCL is very low so it is difficult to realize complete

CTGF release with degradation of PCL. Hence we concluded that the design using PCL as the shell of the coaxial electrospun nanofiber to control the release of growth factor does not work because the PCL serves as a perfectly intact barrier and traps the CTGF in the shell permanently.

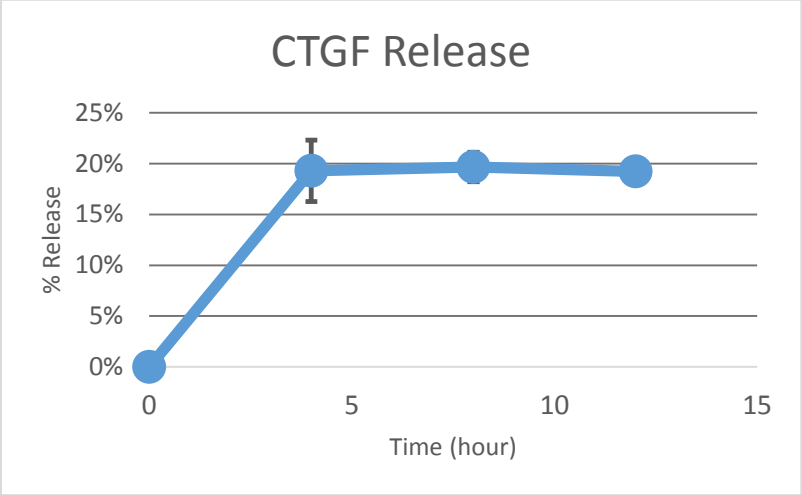

Figure 6.8 CTGF in vitro release with coaxial electrospun PCL/gelatin nanofibers

6.3 Electrospinning and Degradation of PLGA

6.3.1 Design

To overcome the poor release with PCL, polymers with faster degradation rates (such as PLGA) could be used to replace PCL as the shell material. In our study, release efficiency and magnitude could reach our performance requirements if the polymer serving as the barrier would degrade with a 50% mass loss in 3 weeks. In the PLGA

copolymers, PLGA (50:50) has the fastest degradation rate. The degradation rate of PGLA (50: 50) with high M_w (HW) results in about a 2 month lifetime, while the degradation rate of PLGA (50:50) with low M_w (LW) results in a 2 week lifetime. However, LW-PLGA is difficult to electrospin by itself, so we attempted to mix HW- and LW-PLGA together to get a solution that can be electrospun and that also has the desired degradation rate. The polymers we selected to work with are PLGA (50:50) with M_w of 54K-69K, and PLGA (50:50) with M_w of 7K-17K. Four mixture ratios were prepared with compositions as follows: LW: HW=0:10, 2:8, 4:6, and 6:4.

6.3.2 Experimental Section

Materials: PLGA (50:50) with Mw of 54k-69k and 7k-17k, PEO (Mw=300k), Dichloromethane (DCM) and heparin sodium salt from porcine intestinal mucosa ((18 KDa, 177 USP units mg-1) were all purchased from Sigma-Aldrich. Hepatocyte growth factor (HGF) was purchased from Sino Biological Inc.

Four distinct PLGA solutions were prepared: 12 wt% PLGA (0:10) in 30/70 w/w DCM/TFE, 14 wt% PLGA (2:8) in 30/70 w/w DCM/TFE and 16 wt% PLGA (4:6) in 30/70 w/w DCM/TFE, 18% PLGA (6:4) in 30/70 w/w DCM/TFE. 11 wt% gelatin in 80/20 w/w TFE/ water and 6 wt% PEO in H_2O were also prepared. In addition, 40 µl HGF (50 µg/ml) and 12 mg heparin were mixed with the PEO solutions at room temperature.

Electrospinning: The three-needle concentric nozzle was used to electrospin tri-layered nanofibers. The shell solution was gelatin, the middle solution was the different PLGA solutions and the core solution was a PEO solution with heparin & HGF. These three solutions were loaded independently into the coaxial concentric nozzle. Three syringe

pumps were used to keep the flow rates at approximately 0.5-0.7, 1 and 0.07-0.1 ml/h, for the shell/middle/core solutions. The working distance between the nozzle and the aluminum foil collector was held at 20 cm. In addition, the applied voltage was 18 kV for the nozzle and -2 kV for the collector.

Gelatin cross linking： After electrospinning, genipin vapor (5%) was employed to slightly cross link the outer layer of the nanofiber over a 24 hour period.

In vitro HGF release test and cell culture: The coaxial electrospun gelatin/PLGA/PEO scaffolds were cut into square samples for growth factor release and cell culture studies. HGF release from coaxial nanofibers was evaluated with an ELISA kit. The release and cell culture study was carried out by Tugba Ozdemir.

6.3.3 Results and Discussion

After three days of incubation, there were significant changes in the overall size for several of the samples. From Figure 6.9, it is seen that the shrinkage of samples varies with PLGA blend composition. For samples with PLGA (0:10), no shrinkage was observed. Samples with PLGA (2:8) had some degree of shrinkage. Significant shrinkage was observed for samples with PLGA (4:6) and PLGA (6:4). Hence, we conclude that the shrinkage becomes more significant with increasing proportion of LW-PLGA in the PLGA blend. From the literature[22, 28], similar compositions show that the T_g of PLGA decreases with a decrease in M_w. If the T_g of PLGA is lower than 37 ℃, the polymer chains in the fiber will relax to a random coil configuration leading to shrinkage of the nanofibrous mats during the incubation process[24].

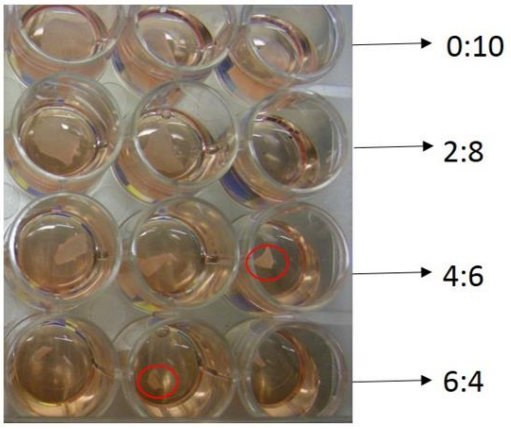

Figure 6.9 Photograph of coaxial tri-layered electrospun nanofibrous mats with different PLGA blend (after 3-day cell culture in incubator)

Figure 6.10 shows the SEM images of different coaxial nanofibrous scaffolds after incubation for three days. As shown in these images, the fibrous scaffolds are all partially covered by thin films, which may be the residual protein, gelatin or cells (scaffolds were dried without washing after removal from the medium). The nanofibrous structure and morphology are maintained for samples with PLGA blends of (0:10) and (2:8), while significant swelling and fusion of fibers along, with a decrease in the porosity of mats, are observed for samples with PLGA blends of (4:6) and (6:4). The shrinkage shown in Figure 6.9 and the swelling shown in the SEM images illustrate that coaxial electrospun nanofibers with LW-PLGA are not suitable for cell culture applications.

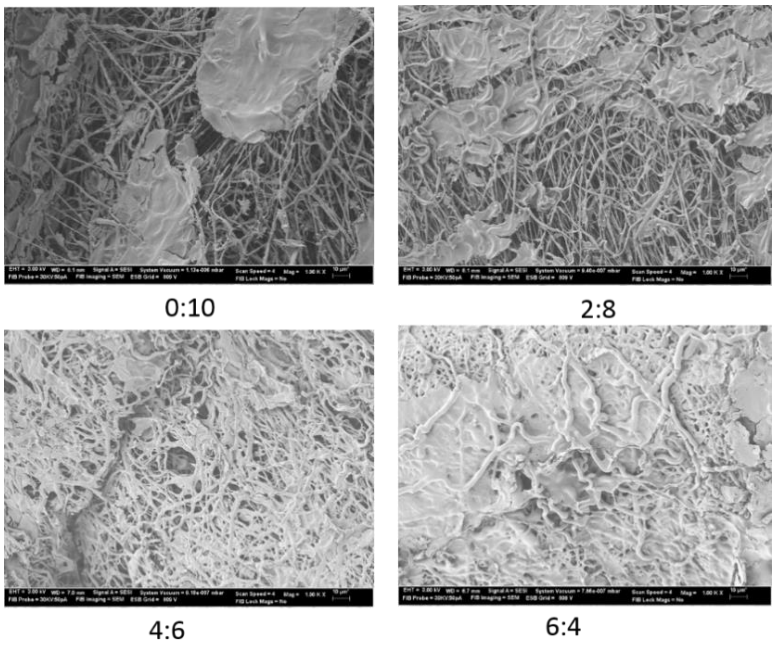

Figure 6. 10 SEM images of coaxial gelatin/PLGA/PEO fibers (3 days in cell culture)

The HGF release profiles are shown in Table 6.2. After 5 days, approximately 13% of HGF has been released from coaxial electrospun scaffolds with PLGA blends of (0:10) and (2:8); 20% of HGF is released from samples with PLGA blends of (4:6); and only 10% of HGF is released from samples with a PLGA blend of (6:4). Although HGF release efficiency is promising, the shrinkage of the scaffolds resulting from the relaxation of the polymer chains in the fibers makes this material system not suitable for cell culture and a new material system was required to replace PLGA in the coaxial nanofibers.

Table 6.2 Cumulative release results of HGF over 5 days

PLGA (LW:HW)	PLGA solution (%)	HGF/solution(ng/ml)	HGF/scaffold（ng/g）	Released amount (pg)	Release (%)
0:10	12	67	255	9.25	13.0
2:8	14	67	230	8.8	13.7
4:6	16	67	210	9.15	20.3
6:4	18	67	190	9.6	10.8

6.4 Preparation of PVOH/PCL-PEG Coaxial Electrospun Nanofibers and *in vitro* BSA Release Study

6.4.1 Design

PLGA was excluded in our study due to the shrinkage of PLGA scaffolds in aqueous media. A new material system was needed to control the release over a certain period of time. Although PCL could serve well as the shell material maintaining the physical structure in aqueous media, it could retain the small molecules in the fibers. To improve the control of the small molecule release rate, low molecular weight PEG was added to the PCL shell layer as the porogen to generate a porous structure in the shell layer

and allow the transport of small molecules through the PCL shell layer. In this design, bioactive small macromolecules (BSA or GF) would be incorporated into the core with PVOH as the carrier and released from the porous structured PCL as the bioactive agent leaches out of PEG (Figure 6.11). The release efficiency was controlled by varying PEG percentage in the PCL layer.

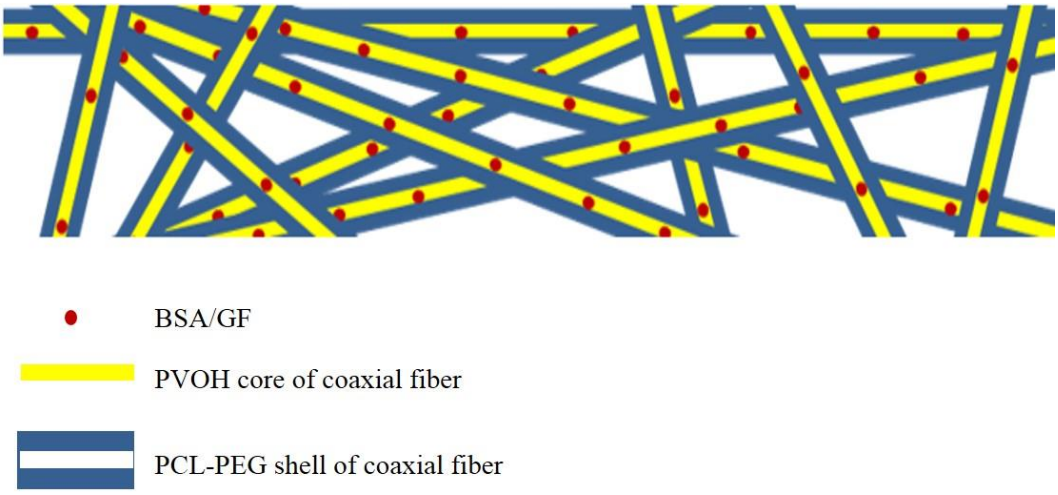

Figure 6.11 Schematic illustration of BSA/GF release from coaxial electrospun nanofibers

6.4.2 Experimental Section

Electrospinning: PCL 9% w/w in 30/70 chloroform/DMF was prepared as follows. PEG (M_w=2000) was mixed into the PCL solution to generate 1% and 5% PEG-PCL solutions. The mixed solution was stirred for 2 hrs to obtain uniformly dispersed PEG in the PCL solution. 4 % PVOH in H_2O was heated at 60 ℃ to get PVOH completely

dissolved. 2.54 mg of BSA was mixed with the PVOH solution at room temperature and stirred for 1 h.

A coaxial electrospinning setup was used with the PEG-PCL solution as the shell solution and BSA-PVOH solution as the core solution. The flow rate ratio was 1.8 ml/h and 0.1 ml/h for the shell and core solutions. The working distance was set at 18 cm and the applied voltage was set at 15 kV for the nozzle and -2 kV for the collector.

In vitro BSA release study: The BSA loading efficiency and release profile was assessed and evaluated by using a bicinchoninic acid (BCA) protein assay. To prepare samples, the scaffolds were cut into square pieces, peeled off from the aluminum foil, weighed and numbered. Each sample was placed in a 1.5 ml microfuge probe and washed three times with PBS containing antibiotic (Penicillin/Streptomycin) for 15 min to remove the BSA on the surface of the fibers. The samples were suspended in 1 ml PBS in the tubes and incubated at 37 ℃. 500 µl of PBS was collected for each sample and an equal amount of fresh PBS was added. The concentration of BSA released into the PBS was analyzed with a BCA assay. The release amount and cumulative release amount of BSA was calculated from a standard curve produced with standard BSA solutions.

6.4.3 Results and Discussion

Figure 6.12 are the SEM images of coaxial fibers which shows the evolution of a porous structure on the PEG-PCL shell (PEG 5%) after soaking in aqueous media for 0, 1, 3 and 7 days. At day 1, fibers exhibited significant swelling compared with the original fibers but no pores were formed. The SEM image (Figure 6.12c) shows a clear pore

formation on the fiber starting at day 3. The porous structure becomes clearer at day 7 (Figure 6.12d).

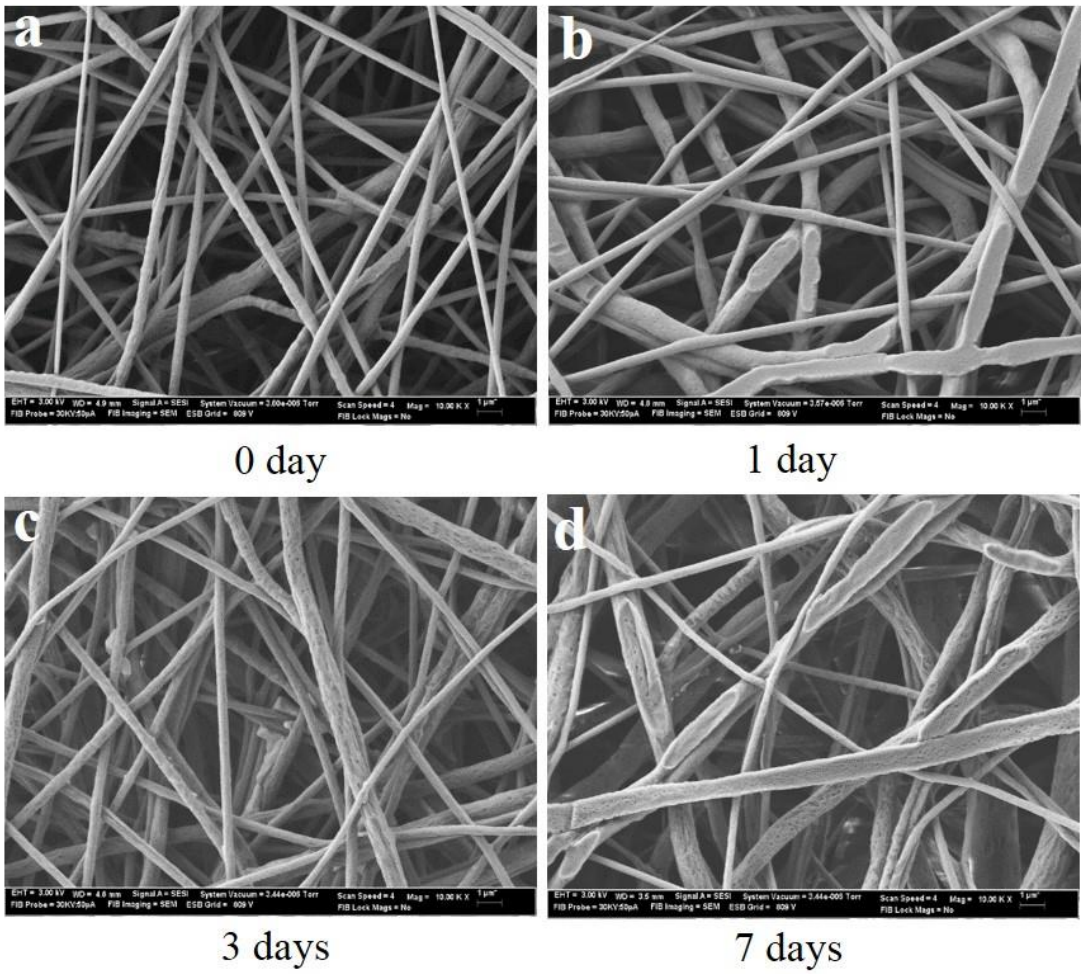

Figure 6.12 SEM images tracking pore formation on coaxial electrospun nanofibers

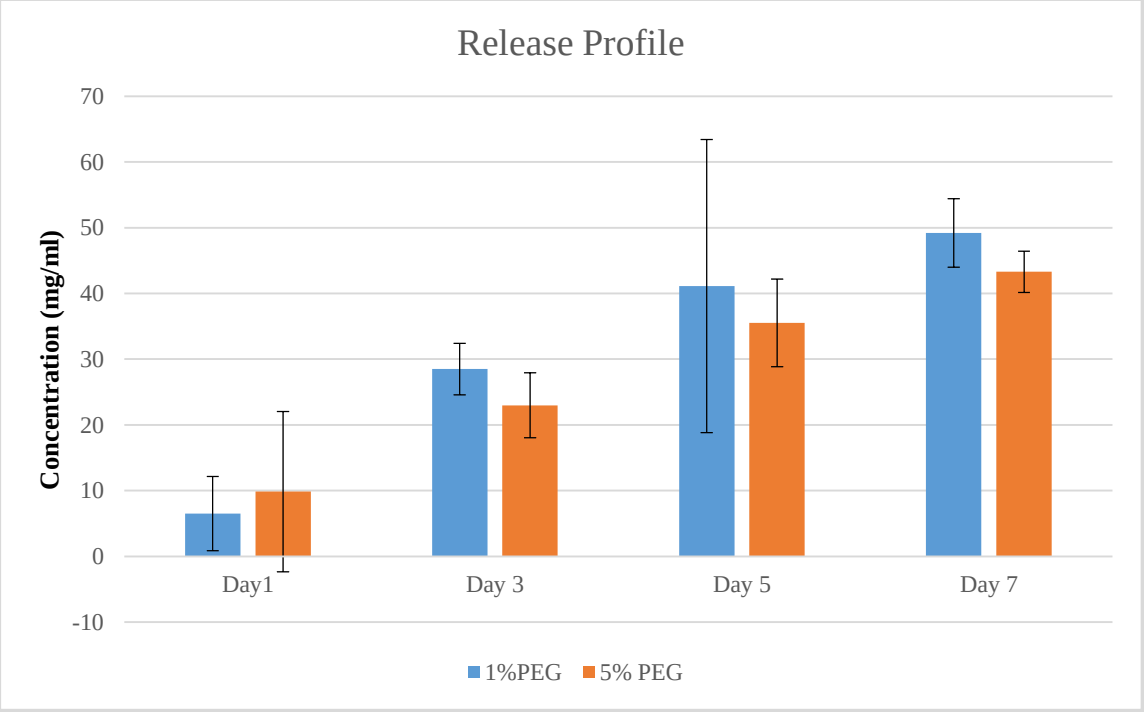

Figure 6.13 *In vitro* cumulative release of BSA from coaxial electrospun PVOH-BSA/PCL-PEG scaffolds

The cumulative release profiles of BSA from coaxial electrospun scaffolds with different PEG formulations (PEG-PCL 1%, PEG-PCL 5%) are shown in Figure 6.13. The preset interval is 2 days and the release period is 7 days. At day 1, less than 10% of BSA release was observed. Since the pore structure was not observed after day 1, the initial release of BSA at day 1 most likely was burst release, which is probably due to the imperfect morphology and structure of the nanofibers. By day 3, approximately 25% of the BSA was released. By day 7, almost 50 % release is observed from the 1% PEG-containing fibers and 44% release was observed from 5% PEG containing fibers. The release amounts gradually decrease from day 1 to day 7. These release results suggest that the BSA was

successfully encapsulated and exhibited a long-term release. Overall, the results show that coaxial electrospinning is an ideal approach to fabricating a small biomolecule delivery vehicle and it holds great promise for long term release. Further studies will be carried out on the controlled release of BSA and GF with coaxial electrospun fibers.

6.5 Conclusions

In this chapter, our preliminary results on the utilization of coaxial electrospinning in the fabrication of bioactive scaffolds for tissue engineering was summarized. Different kinds of coaxial nanofibers were fabricated in order to explore the potential for BSA and growth factor release. Some improvements were made to the original tri-layered coaxial gelatin/PCL/gelatin system. Pure PCL was shown to be unsuitable for serving as a barrier layer for biomolecules due to its absorption of the biomolecules. Although the fast degradation rate of PLGA make it a good choice for a release study, the swelling issues that occurred during degradation, usually ignored in others' work, has proven to be detrimental. Our study showed that pure PLGA with a fast degradation rate was also not suitable as a scaffold material due to its unstable structure. PEG was mixed with PCL serving as a porogen to allow the controlled release of biomolecules. These preliminary results suggest that the BSA was successfully encapsulated and had a long-term release. Overall, these results demonstrate that coaxial electrospinning could be used to fabricate a biomolecule delivery vehicle and holds great promise for long term release. Further studies will focus on the controlled release of growth factor from coaxial electrospun nanofibers with PEG-PCL as the sheath.

REFERENCES

1. Sill, T. J.; von Recum, H. A. *Biomaterials* **2008,** 29, (13), 1989-2006.
2. Agarwal, S.; Wendorff, J. H.; Greiner, A. *Polymer* **2008,** 49, (26), 5603-5621.
3. Ji, W.; Sun, Y.; Yang, F.; van den Beucken, J. J. J. P.; Fan, M.; Chen, Z.; Jansen, J. A. *Pharmaceutical Research* **2011,** 28, (6), 1259-1272.
4. Cantara, S. I.; Soscia, D. A.; Sequeira, S. J.; Jean-Gilles, R. P.; Castracane, J.; Larsen, M. *Biomaterials* **2012,** 33, (33), 8372-8382.
5. Amler, E.; Mickova, A.; Buzgo, M. *Nanomedicine* **2013,** 8, (4), 509-512.
6. Jiang, H. L.; Wang, L. Q.; Zhu, K. J. *Journal of Controlled Release* **2014,** 193, 296-303.
7. Chew, S. Y.; Wen, Y.; Dzenis, Y.; Leong, K. W. *Current Pharmaceutical Design* **2006,** 12, (36), 4751-4770.
8. Yang, Y.; Li, X.; Qi, M.; Zhou, S.; Weng, J. *European Journal of Pharmaceutics and Biopharmaceutics* **2008,** 69, (1), 106-116.
9. Lee, J.; Yoo, J. J.; Atala, A.; Lee, S. J. *Biomaterials* **2012,** 33, (28), 6709-6720.
10. Shen, H.; Hu, X.; Yang, F.; Bei, J.; Wang, S. *Biomaterials* **2011,** 32, (13), 3404-3412.
11. Srikar, R.; Yarin, A. L.; Megaridis, C. M.; Bazilevsky, A. V.; Kelley, E. *Langmuir* **2008,** 24, (3), 965-974.
12. Jia, X.; Zhao, C.; Li, P.; Zhang, H.; Huang, Y.; Li, H.; Fan, J.; Feng, W.; Yuan, X.; Fan, Y. *Journal of Biomaterials Science-Polymer Edition* **2011,** 22, (13), 1811-1827.

13. Sahoo, S.; Ang, L. T.; Goh, J. C.-H.; Toh, S.-L. *Journal of Biomedical Materials Research Part A* **2010,** 93A, (4), 1539-1550.

14. Sisson, K.; Zhang, C.; Farach-Carson, M. C.; Chase, D. B.; Rabolt, J. F. *Biomacromolecules* **2009,** 10, (7), 1675-1680.

15. Ozeki, M.; Tabata, Y. *Journal of Biomaterials Science-Polymer Edition* **2005,** 16, (5), 549-561.

16. Tsai, C. C.; Huang, R. N.; Sung, H. W.; Liang, H. C. *Journal of Biomedical Materials Research* **2000,** 52, (1), 58-65.

17. Panzavolta, S.; Gioffre, M.; Focarete, M. L.; Gualandi, C.; Foroni, L.; Bigi, A. *Acta Biomaterialia* **2011,** 7, (4), 1702-1709.

18. Lien, S. M.; Li, W. T.; Huang, T. J. *Materials Science & Engineering C-Biomimetic and Supramolecular Systems* **2008,** 28, (1), 36-43.

19. Butler, M. F.; Ng, Y. F.; Pudney, P. D. A. *Journal of Polymer Science Part a-Polymer Chemistry* **2003,** 41, (24), 3941-3953.

20. Liao, I. C.; Chen, S.; Liu, J. B.; Leong, K. W. *Journal of Controlled Release* **2009,** 139, (1), 48-55.

21. Loo, S. C. J.; Tan, Z. Y. S.; Chow, Y. J.; Lin, S. L. I. *Journal of Pharmaceutical Sciences* **2010,** 99, (7), 3060-3071.

22. Makadia, H. K.; Siegel, S. J. *Polymers* **2011,** 3, (3), 1377-1397.

23. Chen, M. L.; Gao, S.; Dong, M. D.; Song, J.; Yang, C. X.; Howard, K. A.; Kjems, J.; Besenbacher, F. *ACS Nano* **2012,** 6, (6), 4835-4844.

24. Liu, Y. J.; Jiang, H. L.; Li, Y.; Zhu, K. J. *Chinese Journal of Polymer Science* **2008,** 26, (1), 63-71.

25. Croisier, F.; Duwez, A. S.; Jerome, C.; Leonard, A. F.; van der Werf, K. O.; Dijkstra, P. J.; Bennink, M. L. *Acta Biomaterialia* **2012,** 8, (1), 218-224.

26. Wong, S.-C.; Baji, A.; Leng, S. *Polymer* **2008,** 49, (21), 4713-4722.

27. Huang, Z. M.; Zhang, Y. Z.; Ramakrishna, S.; Lim, C. T. *Polymer* **2004,** 45, (15), 5361-5368.

28. Passerini, N.; Craig, D. Q. M. *Journal of Controlled Release* **2001,** 73, (1), 111-115.

Chapter 7

CONCLUSION AND FUTURE WORK

7.1 Conclusions

Coaxial electrospinning has attracted much attention as a modified electrospinning technique to fabricate nanofibers with various structures. To develop biodegradable polymeric nanofibers with coaxial electrospinning, biodegradable natural polymer gelatin and synthetic polymer PCL were selected as the material system. Core-shell structured gelatin/PCL and PCL/gelatin nanofibers have been fabricated with a customized coaxial electrospinning apparatus. Subsequently, tri-layered coaxial gelatin/PCL/gelatin biodegradable nanofibers were successfully fabricated for the *first time* by electrospinning using a uniquely designed three needle concentric spinneret. The tensile test results of different fibrous mats showed that the Young's modulus and tensile strength of coaxial electrospun nonwoven mats are highly improved compared to those of PCL nonwoven mats.

To create tri-component, tri-layered polymeric ABC nanofibers with coaxial electrospinning, we built on the use of PCL and gelatin as two components of the material system and we added synthetic polymer PLGA as a third polymeric component. Initially, the core-shell structured gelatin/PLGA and PCL/PLGA nanofibers were fabricated using a customized coaxial electrospinning setup. Then, the tri-layer structured,

coaxial gelatin/PCL/PLGA biodegradable nanofibers were successfully fabricated with a three needle coaxial electrospinning setup.

To characterize the morphology of various nanofibers, the SEM was used to observe and measure the fiber diameters, diameter distribution, porosity, fiber orientation and surface roughness. Analyzing the inner structure in single polymeric electrospun fibers is challenging due to the low contrast of electron densities between polymer phases and the overlapping of different layers. The core-shell and tri-layered structures of electrospun nanofibers were characterized by several commonly used techniques, such as LSCM, TEM and cross-section TEM. Besides the conventional methods, we explored other newer techniques, including FIB-SEM, SR-SIM and nano-IR for the characterization of core-shell and tri-layered structure in single fibers. It was found that SR-SIM was the easiest way to characterize the inner layered structure of single nanofibers.

The potential application of coaxial electrospinning in the fabrication of bioactive scaffolds for tissue engineering has been studied. Different kinds of coaxial nanofibers were fabricated and studied to determine the potential for BSA and growth factor release and some preliminary results were obtained. Overall, these results demonstrate that coaxial electrospinning could be used to fabricate a biomolecule delivery vehicle holding great promise for long term release.

7.2 Future Work

Although the fabrication and characterization of tri-component, tri-layered biodegradable nanofibers derived from coaxial electrospinning has been successfully

carried out, there are still some challenges in the study of coaxial electrospinning and its application to tissue engineering.

First of all, alignment of three concentric needles is not easy and currently, there is no standard three needle coaxial electrospinning spinneret. Although the third generation of the spinneret used in our recent studies is a commercial one, it is still difficult to get the needles completely concentric. In addition, the setup for coaxial electrospinning is difficult to clean and requires perfect alignment each time for continuous and stable production of coaxial nanofibers. Difficulties associated with getting a well performing coaxial spinneret limit the long term development of this technique.

Secondly, nano-IR spectra and measurements on the cross section samples can be used to prove the core/shell structure of a single fiber. With nanoscale spatial resolution, the nano-IR technique will be very useful in chemically characterizing the inner structure of coaxial electrospun nanofibers. However, the preparation of thin and flat samples is critical for good nano-IR results. It is very difficult to prepare a useable cross section fiber sample with cryo-microtomy and thus more efforts are needed on sample preparation.

Thirdly, compared with traditional electrospinning, coaxial electrospinning is more complicated as it depends on many more individual parameters and interactions between each solution layer during the spinning process. A successful coaxial electrospinning process results from the correct balance between various solution parameters and processing parameters. Although many efforts have contributed to discover the rules[1] and build the solution selection model[2], there is still no universal agreement on

some issues, such as the effect of miscibility between different solvents and solutions, and the actual critical parameters (e.g., viscosity) of different solutions. The selection of materials/solvents and processing parameters for coaxial electrospinning are still mainly based on the experimental trials. For a better understanding of tri-layer coaxial electrospinning, a further systematic study is needed on the effect of different parameters on the electrospinning process.

Finally, coaxial core-shell structured electrospun fibrous scaffolds are very attractive for use in tissue engineering due to their similarity to natural ECM and its ability to incorporate controlled release growth factors. Recently, the study of potential applications of tri-layered coaxial electrospinning in tissue engineering has been initiated by D. Han et al.[3] By loading two model drugs into different layers of PCL (polycaprolactone) /PCL/PVP (polyvinylpyrrolidone) coaxial nanofibers, a novel dual drug delivery system with a different release profile was fabricated. Instead of using the tri-layered coaxial nanofiber as drug carrier, we believe that our approach to incorporating bioactive macromolecules, such as BSA and growth factors, into the coaxial tri-layered nanofibers for controlled release, is more effective. Based on our design and assumption, the coaxial tri-layered nanofibers would be ideal scaffolds for tissue engineering where the inner core could serve as a growth factor reservoir and the intermediate and outer shells could control growth factor release. Also, tri-layered nanofibers would have the potential for dual macromolecular release. Figure 7.1 shows a schematic diagram of a coaxial tri-layered nanofiber with a single bioactive molecule loaded into the core layer (left) and a coaxial tri-layered nanofiber with dual bioactive molecules loaded into different layers with

different release profiles (right). The diagram in Figure 7.2 shows the dual release of different macromolecules from the coaxial tri-layered nanofibers, in which the macromolecules would release with the dissolution and degradation of different layers.

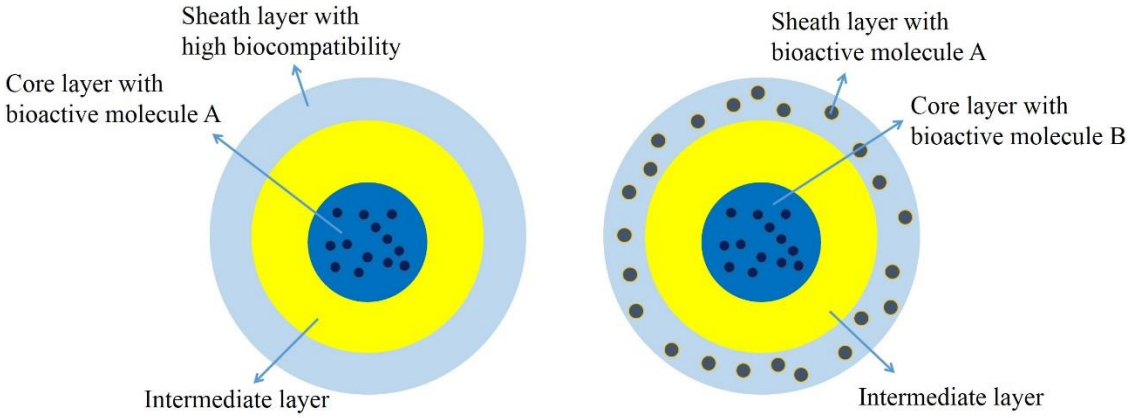

Figure 7.1 Schematic diagram of coaxial tri-layered nanofibers with bioactive molecules loaded

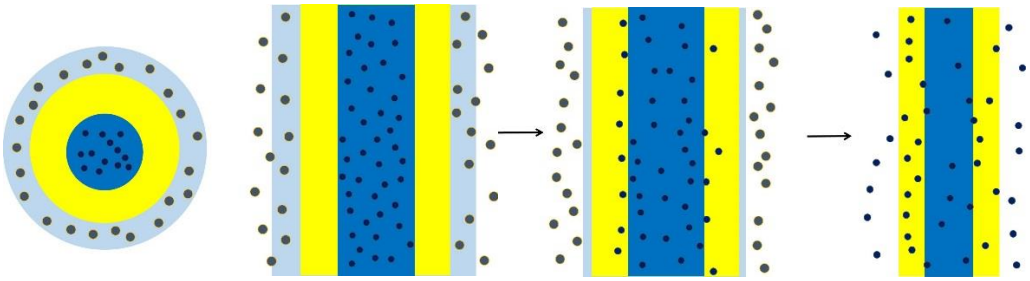

Figure 7.2 Schematic diagram of bioactive molecules released from coaxial tri-layered nanofibers

However, we did encounter issues in initially achieving this research goal for tissue engineering. Some improvements have been made to the originally designed tri-layered gelatin/PCL/gelatin system. For example, PLGA with a fast degradation rate was used to replace PCL in order to release BSA with PLGA degradation, and PEG-PCL has been used to replace PLGA to create a porous structure for BSA release. The preliminary results suggest that BSA was successfully encapsulated and observed to have a long-term release. This results are based on the core-shell structured PVOH-BSA/PEG-PCL nanofibers. Further efforts are needed to study the controlled release of growth factors from coaxial electrospun nanofibers with PEG-PCL as the nanofiber sheath.

In conclusion, there are two main challenges in realizing the controlled release of bioactive molecules with coaxial tri-layered electrospun nanofibers. They include: 1) the selection of a material and solvent system for encapsulation with an acceptable controlled release and profile; and 2) finding a polymer system with reasonable degradation rate for use as the barrier layer. Since tri-layer coaxial electrospinning offers a degree of freedom in the selection of the polymers and the controlled release basically depends on degradation and porosity of barrier layer, it is highly possible that tri-layer coaxial electrospinning will find its application in tissue engineering in the near future.

REFERENCES

1. Moghe, A. K.; Gupta, B. S. *Polymer Reviews* **2008,** 48, (2), 353-377.
2. Kurban, Z.; Lovell, A.; Bennington, S. M.; Jenkins, D. W. K.; Ryan, K. R.; Jones, M. O.; Skipper, N. T.; David, W. I. F. *Journal of Physical Chemistry C* **2010,** 114, (49), 21201-21213.
3. Han, D.; Steckl, A. J. *ACS Applied Materials & Interfaces* **2013,** 5, (16), 8241-8245.

Appendixs

PERMISSION FROM ACS PUBLICATIONS

Title: Preparation of Multilayer Biodegradable Nanofibers by Triaxial Electrospinning

Author: Wenwen Liu, Chaoying Ni, D. Bruce Chase, et al

Publication: ACS Macro Letters

Publisher: American Chemical Society

Date: Jun 1, 2013

Logged in as:

Wenwen Liu

LOGOUT

PERMISSION/LICENSE IS GRANTED FOR YOUR ORDER AT NO CHARGE

This type of permission/license, instead of the standard Terms & Conditions, is sent to you because no fee is being charged for your order. Please note the following:

- Permission is granted for your request in both print and electronic formats, and translations.
- If figures and/or tables were requested, they may be adapted or used in part.
- Please print this page for your records and send a copy of it to your publisher/graduate school.
- Appropriate credit for the requested material should be given as follows: "Reprinted (adapted) with permission from (COMPLETE REFERENCE CITATION). Copyright (YEAR) American Chemical Society." Insert appropriate information in place of the capitalized words.
- One-time permission is granted only for the use specified in your request. No additional uses are granted (such as derivative works or other editions). For any other uses, please submit a new request.